STRUCTURAL CHARACTERIZATION OF AUSTRALIAN COALS
BY FTIR AND SOLID-STATE ^{13}C NMR SPECTROSCOPIES

by

Supachai Supaluknari,

B. Sc., M.Sc. (Mahidol University, Bangkok)

in the Faculty of Science, Department of Chemistry

submitted in fulfilment of the requirements

for the degree of

Doctor of Philosophy

University of Tasmania

October, 1989

STATEMENT

This thesis contains no material which has been accepted for the award of any other higher degree or graduate diploma in any tertiary institution and to the best of my knowledge and belief, the thesis contains no material previously published or written by another person, except when due reference is made in the text of the thesis.

S.Supaluknari

October 1989

ABSTRACT

The structural characteristics of twenty-nine Australian coals and their hydroliquefaction products have been investigated by Fourier Transform Infrared (FTIR) and solid-state ^{13}C nmr spectroscopies. The coal samples were selected to cover a wide range of rank from semianthracite to brown coals. Chemical compositions of the coals varies from 66.4 to 90.6 wt.% C, 3.8 to 7.2 wt.% H and 3.1 to 28.0 wt.% O (by difference).

The FTIR techniques were used to measure the structural parameters associated with aliphatic and aromatic structures and oxygen-functional groups, namely, hydroxyl and carbonyl groups.

The solid-state ^{13}C nmr measuements were carried out at a high-field of 7.05 T by using standard CP/MAS/HPPD techniques in conjunction with a TOSS pulse technique. Modifications of the TOSS sequence have been made for dipolar-dephasing analyses of the samples. Cross-polarization dynamics in the coals were also studied by means of variable contact time experiments.

The structural parameters derived from the FTIR and solid-state ^{13}C nmr data were compared and their relationships with the elemental compositions and liquefaction data were examined. It has been demonstrated that the FTIR techniques are more useful in the elucidation of oxygen-containing structures while the solid-state ^{13}C nmr methods are more effective in obtaining structural data related to the aliphatic and aromatic structures. However, as complementary techniques, both methods have been proved to be very useful in elucidating the structures of coals studied. The results demonstrated the dissimilarity between the general structural features of the brown coals and those of the higher-rank coals. It has been found that the brown coals have uniform aliphatic and aromatic structures with a high variability in the oxygen-functional groups. In contrast, the variations in the aliphatic and aromatic structures of the higher-rank coals are more pronounced with less diverse oxygen-containing groups being observed in these coals.

ACKNOWLEDGEMENT

TABLE OF CONTENTS

CHAPTER ONE

CHAPTER THREE

FTIR STUDIES OF AUSTRALIAN COALS   42

CHAPTER FOUR

SOLID-STATE ^{13}C NMR STUDIES of AUSTRALIAN COALS   95

CHAPTER FIVE

COMPARISON of FTIR and SOLID-STATE ^{13}C NMR DATA 151

CHAPTER SIX

CONCLUSIONS 171

REFERENCES 179

APPENDICES 191

CHAPTER ONE

INTRODUCTION

1.1 THE PROJECT AIM

Knowledge of the chemical structure of coal is essential to an understanding of its properties and use. To understand the chemical structure of coal, however, requires detailed information on the chemical functional groups in the coal. As a naturally occurring material, having a long and diverse geological history, coal is highly complex, heterogeneous and diverse. Its complexity and heterogeneity make coal difficult to study by conventional chemical methods while its diversity imposes limitations on any generalizations made about its properties and structural features. Before 1980, information on the chemical structures of coals was mainly derived from studies of coal extracts and the degradation products from various reactions on coals. These studies have been extensively reviewed by Davidson [1980], Given [1984] and Berkowitz [1985]. It has been questioned as to what extent the structural information derived from the indirect studies of coal extracts or coal degradations may represent the structural features of the original coals. Moreover, in many studies the problems related to the methods used, such as the contamination of solvents in the extracts, and the incorporation of the reactants into coal structures, have been identified. In many cases, even the chemistry involved was not completely known or was uncertain.

Direct measurements of chemical functional groups in the coals, especially those associated with oxygens, were also carried out by chemical methods or so-called wet techniques [Attar and Hendrickson, 1982; Zhou et al., 1984; Given, 1984]. The uncertainty in the data obtained is widely recognized. The problems were related to the reactions used, namely, the incompleteness and the lack of specificity for particular functional groups, giving rise to the unreliability and irreproducibility of the results.

Since the beginning of this decade, with the advent of new instrumentation and computer technologies, coal studies have relied increasingly on instrumental techniques. Among the techniques are Fourier Transform Infrared and solid-state ^{13}C nmr spectroscopies which are probably the only two techniques that can be applied directly to analyse coal or its solid products in a non-destructive way. Both techniques may be used as complementary methods and have become the essential tools in studying coal chemistry.

While the potentials of the two techniques are well recognized, most previous studies on coal analyses have concentrated on some particular functional groups such as those related to aromatic structures. Much of the work using the FTIR technique has aimed at qualitative interpretations. Moreover, most previous studies were mainly on northern-hemisphere coals with the emphasis being on coals of high rank. Very few detailed studies, using the two techniques on Australian coals or coals from other regions, have been reported in the literature .

It is thus the objective of this project to investigate the chemical structures of Australian coals by using the FTIR and solid-state ^{13}C nmr

techniques. Because of the diversity of coals, the samples used have been selected to cover a wide range of rank and chemical composition (see Chapter 2). The study has been concentrated on the main chemical structures and functional groups in the coals, namely, the aromatic and aliphatic structures and the oxygen functional groups. The FTIR results are based on a preliminary study carried out by Mr. N. Brookes for his honours degree [Brookes, 1984].

The solid-state ^{13}C nmr experiments were carried out on a high-magnetic-field of 7.05 T . The technique of total suppression of spinning sidebands (TOSS) was used with the high-field spectrometer to obtain the high-resolution spectra of the coals. The pulse technique of dipolar dephasing has been implemented with the TOSS technique in this study. Cross-polarization dynamics in the coals have also been investigated.

To elucidate the general structural features of the coals, the relationships between the structural data obtained from the two techniques and the chemical compositions of the coals were examined. Furthermore, for a better understanding of some coal properties including their hydroliquefaction behaviours, the relationships between the relevant data and the structural parameters were investigated.

1.2   FTIR STUDIES of COALS - A Literature Review

Fourier Transform Infrared Spectroscopy (FTIR) has been recognized as one of the most promising techniques for the study of coals and related materials. A computerized data-acquisition system greatly enhances the performance of the instrument and provides facilities for analysing and manipulating the spectral data. Spectrometric techniques, such as diffuse reflectance [Fuller et al., 1982] and photoacoustic spectroscopy [Chien et al., 1985], have also been used in coal studies. These new developments of infrared techniques have led to a resurgence of interest in the infrared analysis of coal.

This review will focus on the quantitative measurements of organic functional groups in the coals by the FTIR techniques. Some previous relevant studies, using the conventional dispersive IR systems, also will be outlined.

1.2.1   Identification of the Functional Groups in Coals

With dispersive IR spectrophotometers, various organic functional groups in coals have already been identified in the earlier studies [van Krevelen and Schuyer, 1957a; Speight, 1978; Berkowitz, 1985a]. The principal achievements of the FTIR techniques, in recent studies, have been to confirm the general interpretations in the earlier works. The band assignments for the IR spectra of coals reported in previous studies are summarized in **Table 1.1**.

Some detailed studies have been reported for three IR regions, namely, the aliphatic **C-H** stretching (3000 cm^{-1} - 2750 cm^{-1}) [Painter et al.,1981], the aromatic **C-H** bending (900 cm^{-1} - 700 cm^{-1}) [Kuehn et al., 1982] and the carbonyl stretching (1800 cm^{-1}-1500 cm^{-1}) [Brookes, 1984] regions. In all of these studies the techniques of least-squares curve-fitting were used to resolve the composite bands in the regions.

In the IR spectra of coals, two prominent bands were usually observed at approximately 1600 cm^{-1} and between 1300 cm^{-1} and 1000 cm^{-1}. The assignments for the two bands, however, are still uncertain.

Solomon [1979] maintained that the band in 1300 cm^{-1} - 1000 cm^{-1} region can be ascribed to **C-O** stretching modes while Painter et al. [1981] indicated that vibrational modes of other structures such as **C-C** stretching, **O-H** bending and **-CH$_2$-** bending modes can also have IR absorptions in this region.

The most probable assignments that can be given to the 1600 cm^{-1} band in the coal spectra are the aromatic ring **C=C** stretching vibrations or the hydrogen-bonded and highly conjugated carbonyl stretching modes [Berkowitz, 1985a]. More recently, Painter et al. [1981,1983a] demonstrated that the 1600 cm^{-1} absorption should be ascribed to the aromatic ring vibrations and pointed out that the enhancement of the band intensity arises from the effect of oxygenated substituents on the aromatic structure.

By using the curve-fitting techniques to resolve the band between 1800 cm^{-1} and 1500 cm^{-1} in the spectra of Australian coals, Brookes [1984] observed that there was no increase in the areas of 1600 cm^{-1} band with

coal aromaticities or carbon contents but the data showed reverse trends. It was suggested that the absorptivity of 1600 cm^{-1} band may be related to the variability in polyaromatic structures of the coals.

Since there is still no conclusive evidence to support the interpretations of the spectral data in the two regions, the assignments for them are still an open question.

Recently, Painter et al.[1987] reported an interesting study on the hydrogen bonding in coal. The samples studied were the pyridine extracts of coals and the techniques used were the cast-film method and the diffuse reflectance technique. The shoulders in the broad **O-H** stretching band (3600 cm^{-1} -2800 cm^{-1}) were ascribed to a number of hydrogen-bonded **OH** structures. In the order of increasing hydrogen-bond strength, the four general structures are **OH--π** bonds, self-associated **OH--O** bonds, **OH--O** ether bonds and **OH--N** bonds. All of these H-bonded structures were considered to be of intermediate strength.

Table 1.1 Band assignments in the IR spectra of coals

Band Position(cm⁻¹)	Assignment	Reference
3500-3200	Hydrogen-bonded O-H stretch	Cannon and Sutherland [1945] Painter et al. [1987]
3030	Aromatic C-H stretch	Brown [1955]
2956-2850	Aliphatic C-H stretch (CH_3, CH_2, CH)	Painter et al. [1981] Brookes [1984]
1770	Phenolic ester, C=O stretch	Brookes [1984]
1735	Aliphatic ester, C=O stretch	Brookes [1984]
1700	Carboxylic acid, C=O stretch	Starsinic et al. [1984]
1650	Highly conjugated carbonyl, C=O stretch	Painter et al. [1983a]
1600	Aromatic ring C=C stretch	Cannon and Sutherland [1945] Painter et al. [1981]
1650	Highly conjugated carbonyl, C=O stretch	Fujii [1963]
1575	Carboxylate, C=O stretch	Starsinic et al. [1984]
1400-1375	Aliphatic C-H bending	Cannon and Sutherland [1945]
1300-1000	C-O stretch C-C stretch, O-H bending	Brown [1955] Painter et al. [1981]
860,820, 750	Aromatic C-H bending	Brown [1955] Kuehn et al. [1982]
830,785	Aliphatic CH_2 rocking	Kuehn et al. [1982]

1.2.2 Quantitative Measurements of the Functional Groups

The potential of the FTIR technique as a tool for quantitative analysis has not been much appreciated by coal researchers. So far, much of the work reported for coal related problems has been concerned with qualitative interpretations. The exceptions relate principally to studies by two groups [Solomon et al. and Painter et al.] who have been working on U.S. coals. In particular, they have focussed on the structural parameters related to hydrogen-containing groups, namely the hydroxyl, the aromatic and the aliphatic groups. In their studies, the **KBr** disc technique was normally used with the method of baseline correction for the removal of scattering background absorption [Solomon and Carangelo, 1982; Painter et al., 1981].

a) Determination of hydroxyl groups

In an early study, Osawa and Shih [1971] used the intensity at 3450 cm^{-1} as a direct measurement of **OH** groups in the coal. They observed a good correlation between the specific extinction coefficient and the hydroxyl content in the coal, determined by the acetylation method. By using a similar approach but with the FTIR technique, Solomon and Carangelo [1982] demonstrated that a better correlation was obtained when the intensities at 3200 cm^{-1} of coal spectra were used in the calibration with the hydroxyl contents. However the accuracy of this procedure has been questioned by Painter et al. [1981], as regards the interferences from the IR absorptions of water **O-H** and **N-H** vibrations in the 3500 cm^{-1}-3200 cm^{-1} region. They suggested a combined method of coal acetylation and FTIR measurement. From the FTIR spectrum of acetylated coal, the

intensity or area of the ester carbonyl band (1770 cm^{-1} - 1700 cm^{-1}) were used to measure the **OH** groups in the original coal [Kuehn et al., 1982]. The extinction coefficients related to the intensity and the area of the ester band were determined by calibrating the spectral data to the **OH** contents in the original coals reported by Yarzabs et al. [1979]. In a later study, instead of using the calibration method, the extinction coefficients of the ester band, derived from the spectra of model compounds, were used to estimate the **OH** content in the coals [Snyder et al., 1983].

b)   Determination of carboxylic groups

Starsinic et al. [1984] combined the FTIR technique with the ion-exchange method developed by Schafer [1970] to determine carboxyl contents in demineralized lignites. The extinction coefficients associated with the intensity and the area of the band at 1710 cm^{-1} were determined in order to calculate the amount of carboxyl groups in the coal as a percentage of total oxygen. They also demonstrated that by using the standard method of ion-exchange alone, the carboxyl content can be underestimated owing to the incomplete exchange of the **COOH** groups.

c)   Determination of aromatic and aliphatic hydrogens

Brown [1955] was the first to report the use of IR data to estimate the aromatic and aliphatic hydrogens in the coal. The ratios of aromatic **C-H** intensity (3020 cm^{-1}) to aliphatic **C-H** intensity (2920 cm^{-1}) were found to increase markedly for coals having a carbon content greater than 90 wt. %. The intensity ratio was used with the extinction coefficients derived

from some model compounds to estimate the relative aromatic and aliphatic hydrogen contents in the coals. Durie et al. [1966] measured the hydrogen distributions in the coal extracts by ^1H nmr and used the data to calibrate the ratio of the area of aromatic **CH**-to-aliphatic **CH** for the extinction coefficient ratio of the two bands.

In a more recent study, by using the FTIR technique Solomon [1979] developed a method to determine the aromatic and aliphatic hydrogen contents in the coal. The integrated intensities of aromatic **C-H** bending (~ 800 cm^{-1}), **A$_{ar}$**, and aliphatic **C-H** stretching (~2900 cm^{-1}), **A$_{al}$**, were graphically calibrated according to the equation :

$$a \cdot [\, A_{al} \,/\, (H_{tot} - H_{OH})\,] \,=\, 1 - b \cdot [\, A_{ar} \,/\, (H_{tot} - H_{OH})\,] \qquad (1.1)$$

where **H$_{tot}$** is the total hydrogen content, **H$_{OH}$** is the hydroxyl hydrogen content and **a** and **b** are the constants related to the aliphatic and aromatic absorptivities respectively. Recently a full account of the method has been published [Solomon and Carangelo, 1988]. They also demonstrated that the absorptivities were rank dependent. The results were compared with those reported by others for coals having the carbon content in the range 80-85 wt. %, by using a ratio of aromatic hydrogen-to-aliphatic hydrogen, **H$_{ar}$/H$_{al}$**, as a parameter. The average value of **H$_{ar}$/H$_{al}$** from their study was 0.52, 16 % higher than the average value derived from the other works.

Instead of the graphical method, Kuehn et al. [1982] used a procedure of error minimization to solve a set of simultaneous equations, wherein each equation is for each sample, for the values of absorptivities or the conversion factors (by their definition).

The equation is in the form :

$$H_{tot} - H_{OH} = \varepsilon_{ar} \cdot A_{ar} + \varepsilon_{al} \cdot A_{al} \qquad (1.2)$$

where ε_{ar} and ε_{ar} are the conversion factors related to the absorptivities of aromatic **C-H** and aliphatic **C-H** stretching vibrations respectively. The procedures, initially applied to the U.S. vitrinites, were then used to study coal extracts [Sobkowiak et al., 1984] and whole coals [Riesser et al., 1984]. The results also showed the rank dependence of the conversion factors. The average H_{ar}/H_{al} value for the coals (80-85 wt. % **C**) was 0.35 as opposed to Solomon's value of 0.52.

d)   Determination of coal structural parameters

With the knowledge of hydrogen distribution, some parameters related to the aromatic structure of coal can be estimated by using the Brown-Ladner equations [Brown and Ladner, 1960]. These parameters are the carbon aromaticity, f_a, the degree of aromatic substitution, σ, and the atomic **H/C** of the hypothetical unsubstituted aromatic ring, H_{aru}/C_{ar}.

Although the three parameters, in particular the carbon aromaticity, can be obtained from the solid-state ^{13}C measurement, the Brown-Ladner calculations are still useful since they are the only alternative methods for the estimation of the parameters. However, they may be found to be in a limited application as the formulations are based on the assumptions that **(i)** all oxygens are in the form of phenolic groups and none of them is shared between aromatic rings and **(ii)** there is no aryl-aryl linkage. At least for the low-rank coals where other oxygen-functional groups were

found in substantial amounts [Attar and Hendrickson, 1982], the first assumption is obviously invalid.

Originally the data of hydrogen distribution were derived from ^{1}H nmr analyses and the methods were widely applied to coal liquids or soluble products [Retcofsky et al., 1977 and references therein]. Painter et al. [1983b] and Gerstein et al. [1982] used the data obtained from the FTIR measurements to calculated the f_a values for the solid coal samples, according to the Brown-Ladner equation :

$$f_a = [(C / H) - (H_{al}/H) / (H_{al}/C_{al})] / (C/H) \qquad (1.3)$$

where **C/H** is the atomic ratio from elemental analysis data, **Hal/H** is the aliphatic hydrogen fraction and H_{al}/C_{al} is atomic ratio of aliphatic hydrogen-to-carbon. The H_{al}/C_{al} value was assumed to equal to 2 by Painter et al. while Gerstein et al. used the value of 1.8. From both studies, the calculated values of f_a were found to be in a reasonable agreement with the values obtained from solid-state ^{13}C nmr measurements. However, Painter et al. suggested that the discrepancy between the two values was due to the the variation in the assumed value of H_{al}/C_{al} . They estimated the H_{al}/C_{al} value varying from 2.58 to 1.66. Gerstein et al. also reported the values of H_{al}/C_{al} ranging from 2.42 to 1.32 . In both studies, the combined FTIR and solid-state ^{13}C state nmr data were also used to calculate the atomic ratio of aromatic hydrogen-to-carbon.

e) Concluding remarks

The problem in quantitative IR measurement of functional groups in the coal is principally related to the determination of the absorptivities of the IR bands associated with those groups. Direct measurements of the absorptivities from the coal spectra cannot be reliably obtained. The methods, thus, require a calibration of the coal spectral data to the quantity of interest measured by other means such as chemical analysis or ^{13}C nmr spectrometry. In some studies the absorptivities used for coal samples were derived from the spectra of model compounds or coal products. This is the limitation of the IR technique to coal study. With the reliability in the measurement of the spectral data, however, the FTIR technique can provide semiquantitative data in coal analysis.

1.3 SOLID-STATE ^{13}C NMR STUDIES of COALS
- A Literature Review

Solid-state ^{13}C nmr techniques have made possible a direct measurement of carbon distribution in coal and related materials. Over the past decade, since the first report on ^{13}C NMR spectra of coal was published [Van der Hart and Retcofsky, 1976], solid state ^{13}C nmr techniques have been widely used in coal characterization [Davidson, 1986a; Wilson, 1987a]. ^{1}H-^{13}C cross-polarization (CP), high-power proton-decoupling (HPPD) and magic-angle spinning (MAS) are the commonly used techniques for the measurements. The CP technique enhances the sensitivity of the ^{13}C nuclei [Pines et al., 1973] while the HPPD and MAS techniques improve the resolution of the ^{13}C signals by removing the broadening effects, resulting from ^{1}H-^{13}C dipolar interaction [Pines et al., 1973] and chemical-shift anisotropy [Schaefer and Stejskal, 1976] respectively.

Although the solid-state ^{13}C nmr techniques have been proved to be very useful in coal studies, the analytical accuracy of the methods has been a great concern among the researchers [Davidson, 1986b; Wilson, 1987b; Snape et al.,1989]. In fact, most of the quantitative solid-state ^{13}C nmr studies were mainly related to coal samples or coal-related materials.

Many studies have also been carried out to improve the resolution of coal spectra with the aim that more structural information can be obtained. The most widely used method for this purpose is the dipolar dephasing (DD) techniques which allow discrimination between strongly proton-coupled carbons and weakly coupled or non-protonated carbons. Several workers have used a high-magnetic-field spectrometer (50-75 MHz ^{13}C frequency) for coal studies and have demonstrated that the

improvements in spectral resolution and sensitivity can be achieved [Ohtsuka et al., 1984; Newman and Davenport, 1986 and Axelson, 1987a, 1987b]. However the CP/MAS ^{13}C nmr spectra obtained at high field, with the sample spinning speed of 3-5 kHz are usually obscured with spinning sidebands which render difficulties in spectral interpretation and quantitative measurement. The obvious solution to the problem is to use a special spinning-sideband suppression technique, namely the TOSS pulse sequence proposed by Dixon [1982]. Although a number of problems associated with the technique have been reported, it has been shown that the data from TOSS measurements were comparable to those obtained from normal CP/MAS experiment [Axelson, 1987b].

In this section, a summary of the important studies in the literature, regarding the above-outlined topics, will be given. An extensive review on the solid-state ^{13}C nmr studies of coals including solution-state ^{1}H and ^{13}C nmr measurements of coal-derived materials has been given by Davidson [1986]. The review covered the previous studies upto 1985.

1.3.1 Solid-state ^{13}C nmr spectra of coals

In general, the CP/MAS ^{13}C nmr spectrum of coal showed only broad resonances of aromatic and aliphatic structures. Sullivan and Maciel [1982a] have demonstrated that the broad features in a coal spectrum are due to the overlapping of the chemical shifts of various carbon functionalities in the coal structures. In other words, the broad spectrum of coal reflects the inherent complexity of the coal structures. Having a wider range of carbon types, the low-rank coals showed greater spectral details than the higher-rank coals [Maciel and Sullivan,1982; Russell et

al.,1983; Yoshida and Maekawa,1987 and Axelson, 1987a]. In most studies the assignments given to the resonances observed in the solid-state ^{13}C nmr spectra were based on the chemical-shift data derived from the solution-state ^{13}C nmr studies of model compounds or coal-derived liquids. Snape et al. [1979] have provided an extensive survey study on the chemical-shift data of ^{13}C nmr for the application to coal-derived materials. However, as the solid-state ^{13}C nmr spectra of coals were relatively poorly resolved, it was difficult to determine accurately the chemical-shift ranges of the resonances in the broad aromatic or aliphatic region. To enhance the resolution of the coal spectrum, several groups have used the methods of mathematical manipulations of the ^{13}C FID signals [Hagaman and Woody, 1982; Sullivan and Maceil,1982a; Newman and Davenport, 1986]. In general the methods involved a removal of the broad background by multiplying the FID signal with some filtering functions of the Gaussian or Lorenzian form, resulting in sharp features of the frequency-domain spectrum [Sullivan and Maciel, 1982a]. With a high-field spectrometer of ~ 4.7 T (50.3 MHz ^{13}C frequency) and using the mathematical manipulation method for the resolution enhancement, Newman and Davenport [1986] were able to observe many more fine structures in the spectra of low-rank coals. In particular the resolved signals in the region of oxygenated aromatic carbons, at 145 ppm and 155 ppm have been assigned to diphenolic structures and isolated phenolic groups respectively.

The pulse technique of dipolar dephasing have been used by many workers to assist in assigning the chemical shifts in coal spectra [Davidson, 1986c]. The technique has been also applied extensively to other solid materials [Alemany et al. 1983 and references therein]. In this technique the ^{1}H decoupling field in the standard CP/HPPD pulse

sequence is gated off for a sufficiently long period (normally > 40 μs) after the cross polarization to allow strongly proton-coupled ^{13}C resonances to dephase before data acquisition [Alla and Lippmaa, 1976; Opella and Frey, 1979]. As a result, the DD spectrum contains mainly the signals of weakly coupled or non-protonated carbons. By comparing the DD spectrum with the normal CP/MAS spectrum the chemical-shift ranges of the protonated carbons and non-protonated carbons can be determined. Particularly, in the aliphatic region of the DD spectrum, the ^{13}C signals observed also include those of **-CH$_3$** groups which experience a weak dipolar-coupling field as a consequence of a free motion of the groups [Alemany et al., 1983]. In the aliphatic region of coal DD spectra, apart from the signals of methyl carbons, intense signals in the region of methylenic carbons (~ 30 ppm) were usually observed, especially in the DD spectra of coal having a high aliphatic content [Wilson et al.,1984; Sfihi et al., 1986; Soderquist et al, 1987]. It was suggested that the resonances are probably associated with mobile **-CH$_2$-** groups. In particular, Soderquist et al.[1987] have proposed that these mobile **-CH$_2$-** groups can be considered as parts of the coal structures having segmental motion. The observation of the mobile aliphatic groups seems to be consistent with the ^{1}H nmr studies and has been claimed to support the two-component model for the coal structure [Given and Marzec,1988]. The highly mobile aliphatics may be seen as associated with the small molecules trapped in the macromolecular networks of the coal structure. However, as pointed out by Wilson et al. [1988] in their ^{13}C nmr study of torbanite and its precursors, the mobile **-CH$_2$-** groups, as observed from the solid-state ^{13}C nmr spectra, can be also considered as part of the coal macromolecular network.

To illustrate the carbon functionalities that may be identified from the

solid-state ^{13}C nmr spectra of coals, a diagram reported by Pugmire et al. [1981] is reproduced in **Figure 1.1**.

1.3.2 Quantitative solid-state ^{13}C nmr Measurement

a) Quantitative reliability of the techniques

As noted earlier, the quantitative reliability of the solid-state ^{13}C nmr techniques in coal analyses has been the problem of great concern in the literature.   Recently, the problems regarding the accuracy of the techniques have been addressed by a group of workers who can be considered as experts in the field [Snape et al., 1989]. Previous studies associated with quantitative reliability have been reviewed.   In this section, a summary of the main points discussed in that paper will be given.

It was accepted that some ^{13}C nuclei in the coals may not be observed in a typical CP/MAS experiment. Two factors related to the heterogeneity of coal, the presence of paramagnetic centers and the nonuniform distribution of the ^{1}H-^{13}C dipolar couplings, are the main sources of the inaccuracy of the CP measurement.

In the CP process, an effective ^{1}H-^{13}C polarization transfer requires a condition that the cross-polarization rate, $1/T_{CH}$, must be faster than the rate of ^{1}H spin-lattice relaxation in the rotating frame, $1/T_{1\rho}{}^{H}$. The quantitative CP measurement, in turn, depends on a requirement that the ^{1}H-^{13}C cross-polarization is equally effective i.e., with common T_{CH} and $T_{1\rho}{}^{H}$ for all ^{13}C nuclei in the sample. The results from a number of

studies on the cross-polarization dynamics in the coals have demonstrated that such requirement may not be met as a result of the nonuniform distribution of the ^1H-^{13}C dipolar couplings in the sample [Botto et al.,1987; Solum et al., 1989]. In particular, it was found that the T_{CH} values of the aromatic carbons were generally larger than those of the aliphatic carbons. Thus it was demonstrated that in some cases, where the differences between the aromatic and aliphatic T_{CH} and $T_{1\rho}^H$ values were very large, a variable contact time measurement is necessary.

By means of electron-^1H spin interaction, the paramagnetic species in the form of organic or inorganic free radicals may affect the relaxation of ^1H spins to a substantial extent that $T_{1\rho}^H < T_{CH}$. This problem also discriminates against the aromatic carbons since the paramagnetic centers are most likely to be found in a close proximity to the aromatic structure [Botto et al.,1987; Snape et al.,1989]. Moreover, further loss in the ^{13}C signals, resulting from the effect of paramagnetic shift and broadening effect, were also observed even in the single-pulse experiment [Botto et al., 1987]. These paramagnetic effects, however, can be minimized by the method of demineralization of the coal sample or by a radical quenching method [Muntean et al., 1988].

Another experimental condition that may affect the accuracy of the CP/MAS experiment is the spinning speed at the magic angle. The effect of MAS speed on the CP process is well documented [Stejskal et al.,1977; Sardashti and Maciel, 1987; Jacobsen et al., 1988]. Gerstein and Pruski [in Snape et al., 1989] have found that the amount of carbon detected in a coal sample spun at spinning frequencies of 4 kHz and 8 kHz was reduced to 64 % and 45 % respectively, compared to that measured under a condition of static sample. The value of the carbon aromaticity measured at the above

spinning speeds was also reduced to 74 % and 71 % respectively.

The problem of MAS speed is more important in a measurement carried out on a high-magnetic-field spectrometer since to remove the broadening effect associated with the chemical-shift anisotropy (CSA) which is field dependent, the spinning frequency must be greater than the magnitude of the chemical-shift anisotropies (up to 15 kHz at a field of 7.05 T). Spinning the sample at a frequency lower than that of the largest CSA results in an appearance of spinning sidebands which can overlap with other spectral bands [Yannoni, 1982]. Theoretically, the sideband intensities can be calculated as they are related to the CSA [Maricq and Waugh, 1979; Herzfeld and Berger,1980], however, the method may not be practical in coal analyses. Other approaches have been proposed as discussed by Axelson [1987b]. Among them is a pulse technique of total suppression of spinning sidebands (TOSS) proposed by Dixon [1982]. The technique involves introducing additional four 180° pulses into the ^{13}C channel at predefined times for a removal of all rotational echoes and thus the spinning sidebands. In his original paper, Dixon[1982] has noted several problems that may be associated with the technique. The most serious one is probably the possible loss of signals as a result of the extra time required in the refocus of the ^{13}C spins. Olejniczak et al. [1984] have shown that such an intensity loss increases as a function of $\Delta\sigma/v_r$ where $\Delta\sigma$ is the magnitude of CSA and v_r is the MAS speed. Furthermore, the loss of the signals of some carbon types having a spin-spin relaxation time comparable to the waiting period can be more substantial. In spite of the problems and scepticisms [Snape et al., 1989] there have been reports of some success in the application of the technique to coal analyses [Dixon et al., 1982; Painter et al., 1983b; Axelson, 1987a, 1987b]. In particular, Axelson [1987b] has demonstrated that the

TOSS values of carbon aromaticity are in a reasonable agreement with the values derived from the normal CP/MAS spectra. It is therefore possible that with a careful attention to the experimental conditions used and to the nature of the samples studied the application of the TOSS technique with a high-field spectrometer can provide useful information on chemical functionalities in the coal. Such a view, however, may not be appreciated by some researchers who still maintain that there is no advantage of using a high-field instrument in the solid-state ^{13}C nmr study of coal [Snape et al.,1989].

b)   Determination of coal structural parameters

In the earlier solid-state ^{13}C nmr studies of coals, the carbon aromaticity, f_a, is the only parameter that was commonly reported [Wilson, 1987c]. In most studies the f_a value was measured directly from the integrated area of the aromatic envelope as a fraction of total area of the entire spectrum. Generally the trend of increase in the f_a value was found as the rank of coal increases [Maciel and Sullivan,1982; Painter et al., 1983b; Wilson et al., 1984].

With arbitrarily defined chemical-shift ranges for various carbon types, the relevant carbon fractions have been determined by Yoshida and Maekawa [1987]. The parameters included those associated with oxygen functional groups, namely, the carbonyl, phenolic, methoxy and ether groups.

Newman and Davenport [1986] used the ratios of signal-height relative to the aromatic signal at approximately 129 ppm to estimate the relative

contents of methyl groups (15 ppm), methylene carbons (31 ppm), methoxy (56 ppm), cellulose-like structures (74 ppm) and phenolic groups (155 ppm and 144-147 ppm for isolated phenolic and diphenolic structures respectively) in Australian and New Zealand coals.

Many groups have reported the calculation of the atomic **H/C** ratios for hypothetical unsubstituted aromatic carbons (the fraction of aromatic carbons that is not of the bridgehead aromatics), H_{aru}/C_{ar}, using the combined f_a values and elemental analyses data [Retcofsky and Van der Hart, 1978; Painter et al., 1983b; Furimsky and Ripmeester, 1983; Yoshida and Maekawa, 1987]. The calculation was based on assumptions related to aromatic ring substitutions. The value of H_{aru}/C_{ar} can be considered as a parameter for the size of aromatic cluster [Painter et al.,1983b]. Furimsky and Ripmeester [1983] reported the trend of decreasing in H_{aru}/C_{ar} value with the increase in carbon aromaticity for a series of Canadian coals. The observation was considered as an indication of the increase in ring condensation accompanying the decrease in ring substitution as the rank of coal increases.

As mentioned in **section 1.2.2**, Gerstein et al. [1982] and Painter et al. [1983b] derived additional structural parameters related to the aromatic and aliphatic structures, H_{ar}/C_{ar} and H_{al}/C_{al} by using the f_a values and the hydrogen-distribution data obtained from the FTIR measurements.

The techniques of dipolar dephasing (DD) outlined in **section 1.3.1** have been used by many workers to estimate the amount of non-protonated carbons and protonated carbons in coal. Among the early studies on the application of the technique to coals was that reported by Murphy et al. [1982] on an anthracite sample. Based on the detailed DD analyses of two model compounds, which showed that all tertiary carbons were

eliminated with a DD time, T_{DD}, of 60 µs, the DD spectrum of the anthracite was acquired with T_{DD} = 60 µs. The DD spectrum was extrapolated to T_{DD} = 0 by multiplying the 60 µs DD spectrum with a term $\exp(60/T'_2)$ where T'_2 is the decay constant (in µs) for the non-protonated aromatic carbons, having a value of 192. With an assumption that the anthracite contained only aromatic carbons (f_a= 0.97 $\pm$ 0.03), the atomic H/C ratio of the coal was estimated from the quaternary-to-tertiary aromatic ratio, $f_{Q/T}$, to be 0.35 $\pm$ 0.07 as opposed to the value from elemental analysis of 0.26 $\pm$ 0.03. The discrepancy between the two values was explained as being due to the unobservable quarternary aromatic carbons in the CP/MAS measurement, leading to an underestimation of the $f_{Q/T}$ value. However the amount of measurable quarternary aromatic carbons was approximated to be 66 %. By using a model of pericondensed two-dimensional aromatic cluster for the anthracite and using the average diameter of the cluster of 160 nm, in accordance with the estimates from X-ray scattering experiment reported by Hirsch [1954], Murphy et al. [1982] also estimated the number of condensed aromatic rings in the anthracite. The value was in the range 33-54.

Schmitt and Sheppard [1984] applied the DD technique in order to determine the methyl, quaternary aliphatic and aromatic and other protonated carbons in a sample of coal and three oil shales. They found that the DD time of 41 µs was adequate for the measurement according to the study of 13 model compounds. No correction was made for the quarternary carbons but a calibration factor for methyl suppression was used. Five simultaneous equations, relating the mole fractions of the carbon types including the total H/C ratio from elemental analysis, were solved for the values of the mole fractions of the carbon types. A Monte Carlo error analysis of the calculation was performed to determine the

influences of the parameters used on the results. The result of the analysis was claimed to be acceptable.

A more extensive study on the application of DD technique to coal analyses was carried out by Wilson et al. [1984]. Of the 63 coals samples, including some maceral concentrates, six samples were subjected to a full DD analysis with varying DD times. They observed that the decrease of the intensity of aromatic carbons as a function of DD time followed a double exponential decays while that of aliphatic carbons showed a single decay. The fast and slow decay components for the aromatic carbons were related to the loss of protonated and non-protonated carbons respectively. By extrapolating the data for the slow component to the initial DD time of 0 μs, the amount of non-protonated aromatic carbons as well as that of the protonated aromatics in the coals were estimated. As the multiple DD time experiment is time consuming , for other coal samples Wilson et al.[1984] used just two spectra, a normal CP/MAS and 40 μs DD spectra, to estimate the proportion of protonated aromatic carbon. The intensity of the aromatic carbons measured from the 40 μs DD spectrum of each sample was corrected for the loss of non-protonated aromatic carbons by using an averaged factor derived from the full DD analyses of five samples. The amount of protonated and non-protonated aromatic carbon expressed as a fraction of total carbon were then readily estimated. The protonated aromatic fraction was combined with atomic carbon-to-hydrogen ratio, **C/H**, to calculate the aromatic hydrogen fraction. The trends of increases in protonated aromatic carbon and hydrogen fractions with the f_a values were observed. Furthermore, the protonated aromatic carbon fraction also showed a trend of increasing value with %**C**. The results were interpreted as demonstrating evidence for the coalification process in which the protonation of the aromatic rings accompanying

losses in aromatic substituents is more favourable than the cross-linking process. However, as noted by Wilson [1987d], the observation may simply showed the trend for the carbon aromaticities since when the proportion of protonated aromatic carbons (expressed as a fraction of aromatic carbons) was plotted with carbon content no clear trend was observed. A detailed discussion on possible pathways in the coalification process has been also given by Wilson [1987d]. In addition to the parameters related to the aromatic structure of coal, Wilson et al. [1984] also reported the estimated range for the methyl carbon fraction in the coals. The estimation procedure was similar to the method used by Murphy et al. [1982] for non-protonated-aromatic carbons. The range of the decay constant, T'_2, were taken to be 120 μs and 50 μs as for non-tert-butyl methyl carbons.

Following Wilson et al. [1984], Theriault and Axelson [1988] carried out a solid-state ^{13}C nmr DD study on 19 Canadian coals. The multiple DD time analyses were used to estimate the parameters for all coals studied. They also reported a trend of relationship between the T'_2 value for the non-protonated carbon and carbon content, particularly for coals with %C greater than 73 %. The finding thus suggested that the method of applying a single DD time and a common T'_2 value, in the quantification of protonated and non-protonated carbons, to different coal samples may not be accurate.

More recently, Solum et al. [1989] reported a full DD study on a set of Argonne Premium coals. Apart from the parameters reported previously, they estimated the fractions for bridgehead, alkyl-substituted and oxygenated-aromatic carbons. The aliphatic carbon fractions were divided further into oxygenated aliphatics, **CH** or **CH$_2$**, **CH$_3$** and non-protonated

aliphatics. They also devised a method to calculate the number of carbons per aromatic cluster. The calculation was based on a hyperbolic tangent function relating the proportion of bridgehead carbons to the number of carbons in the aromatic cluster. The equation was a result of fitting the theoretical values derived from a number of polyaromatic models. The results showed an increase in the aromatic cluster size as the rank of coal increases. Additional structural parameters of the number of attachments per cluster and the molecular weight of the cluster were also reported. Interestingly, the variation in the value of the number of attachments per cluster was rather small compared to the difference in the value of the aromatic cluster size. The interpretation for the finding was that as the rank increases, the aromatic cluster size grows thus the site for the attachment increases, but the aliphatic content decreases therefore fewer sites are used.

Carbon distributions in maceral types have been also reported in many studies [Pugmire et al., 1984; Wilson et al., 1984; Soderquist et al., 1987]. In general there is a trend for the variation in f_a value with maceral type in the order inertinite > vitrinite > exinite. A similar trend was also observed for the aromatic hydrogen content measured as a fraction of total hydrogen [Wilson et al, 1984; Soderquist et al., 1987].

1.3.3   Concluding Remarks.

It is obvious that the solid-state CP/MAS ^{13}C nmr is a powerful technique for the elucidation of coal structure. However, as regards the quantitative aspect of the CP/MAS measurement, care must be taken in the choice of experimental conditions and some prior knowledge of the properties of the samples studied may be necessary. A similar approach is also required in using the TOSS technique, since a number of problems associated with the method have been identified. The pulse method of dipolar dephasing has been used to extend the capability of the solid-state CP/MAS ^{13}C nmr spectroscopy in coal analyses. Results from the DD technique coupled with the knowledge of chemical-shift data can provide many more structural parameters than the normal CP/MAS ^{13}C nmr measurement.
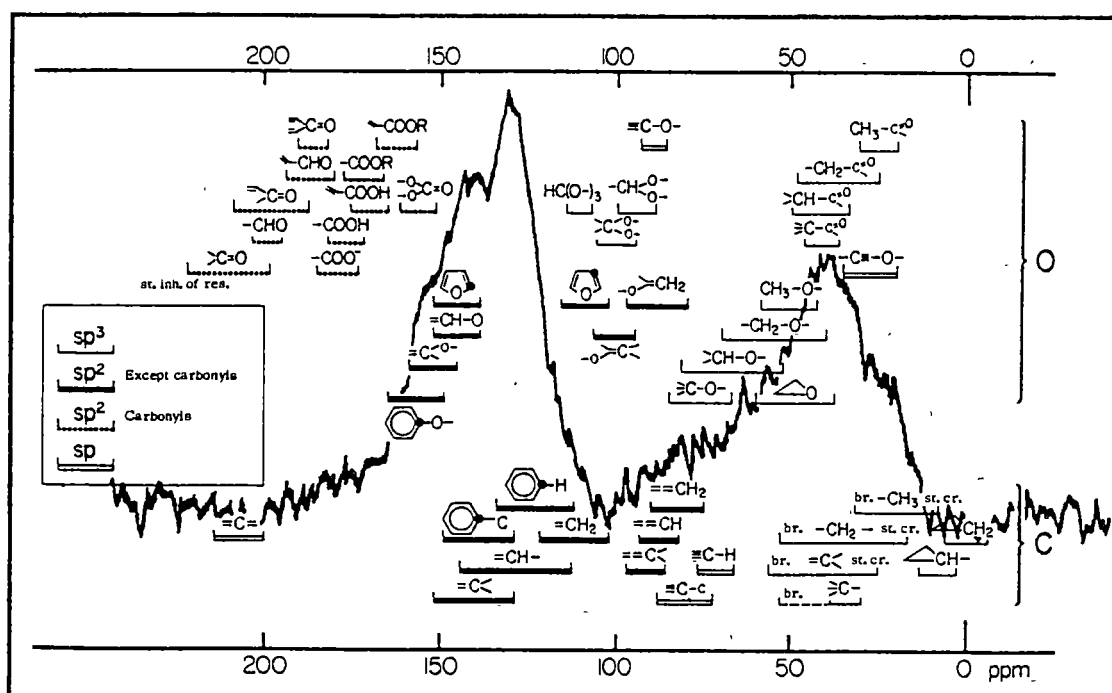
Figure 1.1 ^{13}C nmr correlation chart and coal spectrum. (After Pugmire et al.,1981).

CHAPTER TWO

CHEMICAL COMPOSITION and LIQUEFACTION DATA
of
AUSTRALIAN COALS

2.1   INTRODUCTION

The suite of Australian coals selected for this study is composed of one semianthracite, seven bituminous coals, seven subbituminous coals and fourteen brown coals (see **Table 2.1**). Originally the samples were received in an as mined condition. The brown coals were core samples obtained by the State Electricity Commission of Victoria with the exception of the Bacchus Marsh Pale sample which was hand mined [Redlich, 1987]. All higher-rank coals were obtained from commercial mines. The sources of the samples have been reported elsewhere [Redlich et al., 1989a] (see also Appendix A). The pretreated coal samples were obtained from the Coal Research Group, Monash University (Professor W.R. Jackson).

Initially, the coals were chosen for a detailed hydroliquefaction study. The aim was to investigate the relationship between the chemical characteristics of coals and their liquefaction reactivities in order to gain a better understanding of coal structure and the mechanism of coal liquefaction [Redlich, 1987]. Samples were selected to cover a wide ranges of atomic **H/C** ratio and carbon content and have a low organic sulphur and nitrogen content and also a low mineral content.

In this chapter the chemical compositions of the samples are reported. The interrelationships between the elemental compositions and related parameters are examined. These fundamental parameters will be used later to evaluate the structural data derived from FTIR and solid-state ^{13}C nmr results. Furthermore, their relationships with the FTIR and solid-state ^{13}C nmr data will be investigated regarding the structural features of coals studied. Finally, some important liquefaction data, that will be examined in relation to the structural data, are reported.

2.2 COAL PRETREATMENT.

Details concerning coal pretreatment are available in the literature [Redlich et al., 1989a]. A brief account of the method is given here.

The brown coals were predried at 25 °C (1 mm Hg), in order to reduce the moisture content from 50-70 % to 10-20 %. All coals were ground to less than 60 mesh (250 μm). To remove the mineral matter, the ground sample was then washed with 0.1 M H_2SO_4 by stirring the slurry of coal and acid (in a ratio of 1:20, coal : acid) for 24 h. The slurry was filtered and washed with distilled water until the pH of the filtrate was constant. The acid-washed coal was then kept under water to prevent air oxidation of the sample.

The ash contents of the acid-washed brown coals are in the range 0.1-0.2 wt. % db while those of the higher-rank coals ranging from 3.3 to 18.8 wt. % db (see **Table 2.1**). The ashes of brown coals are dominated by inorganic materials whereas the mineral matter is the major constituent of the

While the acid-wash treatment does, in general, not remove the mineral matter, it is assumed that this material would not unduly perturb the ^{13}C nmr measurement. This is because the mineral matter is in a separate phase whereas the inorganic ions are bound to the coal matrix.

ashes of the higher-rank coals. However, the brown coals contain very little **Fe, Ca, Mg** and **Na** (less than 0.02 wt.% db in most cases) [Redlich, 1987].

The presence of these inorganic materials may affect the FTIR and solid-state ^{13}C nmr measurements of coal. The inorganic cations can associate with tightly bound water molecules in the coal [Hippo, 1987], which may interfere with the measurement of hydroxyl groups in the coal by FTIR method. As discussed in **section 1.3.2**, the effect of paramagnetic species on the loss of ^{13}C signals in solid-state ^{13}C nmr measurement is well documented. For the coal studied herein, such effects can be considered to be minimal because the samples contain a small amount of inorganic materials.

2.3   ELEMENTAL COMPOSITIONS of AUSTRALIAN COALS

The elemental compositions of the Australian coals are given in **Table 2.1**. The coal samples are coded (in **column 2**) to facilitate the presentation and discussion of the results throughout this thesis. For Australian brown coals the code is ABRX while ABLX denotes Australian higher-rank coals.

All brown coals in this study were deposited during the Tertiary Period. The depositional age of all bituminous coals and the semianthracite ABL1 is Permian. Two subbituminous coals, ABL4 and ABL7 are also Permian while ABL2 and ABL8 are Triassic and the remaining subbituminous coals, ABL13-ABL15, were deposited in Jurassic Period.

Table 2.1 Elemental composition of Australian coals

Coal	Code	C	H	O	N	S	Ash[f]
		wt. % dmif coal					wt. %db
Yarrabee[a]	ABL1	90.6	3.85	3.1	1.76	0.71	7.0
Callide[b]	ABL2	79.3	3.78	15.4	1.18	0.34	7.6
Bulli[c]	ABL3	88.4	4.74	4.8	1.68	0.36	11.8
Oaklands[b]	ABL4	76.2	4.19	17.9	1.42	0.51	18.8
Pikes Gully Inertinite[d]	ABL5	84.3	4.72	8.7	1.77	0.51	13.4
Wongawilli[d]	ABL6	87.0	5.08	5.4	1.95	0.61	12.8
Collie[b]	ABL7	73.6	4.31	20.2	1.28	0.63	3.3
Leigh Creek[b]	ABL8	72.7	4.31	21.1	1.60	0.27	11.7
Young Wallsend[d]	ABL9	83.2	5.55	8.8	1.95	0.50	7.2
Pikes Gully Vitrinite[d]	ABL10	82.3	5.46	9.7	1.98	0.61	4.4
Liddell[d]	ABL11	82.7	5.60	9.1	2.10	0.51	7.8
Greta[d]	ABL12	83.0	5.88	8.2	2.09	0.77	3.9
Wandoan[e]	ABL13	77.4	5.99	15.1	1.08	0.48	9.4
Taroom[e]	ABL14	76.2	5.94	16.4	1.17	0.43	7.4
Millmerran[e]	ABL15	79.1	6.32	12.6	1.26	0.73	14.0
Loy Yang 1276	ABR1	68.4	4.50	26.2	0.50	0.39	0.7
Rosedale 29	ABR2	68.9	4.54	25.7	0.59	0.31	0.2
Rosedale 7	ABR3	67.4	4.64	27.1	0.55	0.28	0.1
Rosedale 18	ABR4	66.4	4.77	28.0	0.53	0.28	0.4
Rosedale 30	ABR5	69.5	5.14	24.5	0.57	0.38	0.3
Rosedale 17	ABR6	67.0	5.20	27.0	0.52	0.36	0.4
Rosedale 25	ABR7	68.5	5.30	25.4	0.57	0.51	0.2
Morwell No.46	ABR8	72.6	5.80	20.8	0.60	0.24	0.2
Rosedale 22	ABR9	69.0	5.60	24.4	0.49	0.44	0.7
Hazelwood 1317	ABR10	71.4	5.90	22.0	0.50	0.18	0.4
Rosedale 28	ABR11	70.8	5.96	22.5	0.54	0.29	0.2
Loy Yang 1279	ABR12	70.1	6.20	23.0	0.50	0.31	2.0
Rosedale 5	ABR13	70.9	6.40	21.8	0.45	0.46	0.6
Bacchus March Pale	ABR14	70.5	7.18	20.6	0.41	1.24	0.6

ABLX, Higher-rank-coal; **ABRX**, Brown coal.

[a]Semianthracite; [b]Medium volatile subbituminous (oxygen-rich); [c]Low volatile bituminous; [d]High volatile bituminous; [e]High volatile subbituminous. [f]Acid-washed coals (see text for details).

As can be seen in **Table 2.1,** the coals were chosen to cover a range of carbon contents from 66.4 to 90.6 wt. % and the oxygen contents, 3.1 to 28.0 wt. % on a dry mineral and inorganic free (dmif) basis. In most coal samples the sulphur content was less than 1 wt.% while the nitrogen content was well below 2 wt.%.

The diversity of the coals in the suite is well illustrated by the van Krevelen plot as shown in **Figure 2.1.** The diagram has been shown to demonstrate the chemical changes occurring during the course of the coalification process [van Krevelen and Schuyer, 1957b]. The plot has been also used to illustrate the coalification tracks for maceral types [van Krevelan and Schuyer, 1957c; Teichmuller and Teichmuller, 1982]. For this suite of coals, the diagram shows three distinctive trends, i.e., **(i)** the trend for the brown coals, showing an increase in atomic **H/C** ratios with a decrease in atomic **O/C** ratios (△), **(ii)** the trend for a group of four oxygen-rich subbituminous coals (●) and **(iii)** the trend for other higher-rank coals, showing an increase in the **H/C** values with **O/C** values (■ ,◆). It should be noted that the oxygen-rich subbituminous coals are inertinite-rich samples, while other higher-rank coals, except ABL5 which is an inertinite concentrate, contain predominantly a vitrinite maceral (see **Appendix A.**). The trend observed here for the higher-rank coals is consistent with those reported for other coals [Neavel et al., 1986]. As the suite of coals in this study can be classified further according to the three distinctive trends observed in the van Krevelen diagram, the results in this study will be presented and discussed accordingly .

The carbon content of coal is one of the many parameters that have been used widely as a rank parameter. For this suite the carbon contents in the coals strongly correlate with the oxygen contents as shown in **Figure 2.2.**

The inverse relationship is also found between the carbon contents and O/C ratios. It can be expected that the trends similar to those in the van Krevelen plot, but in a reverse manner, can be observed when the carbon content is plotted against coal H/C ratio. The diagram is shown in **Figure 2.3**. The carbon content, **O/C** and **H/C** will be used extensively as primary parameters in a later discussion of the FTIR and solid-state ^{13}C nmr results.
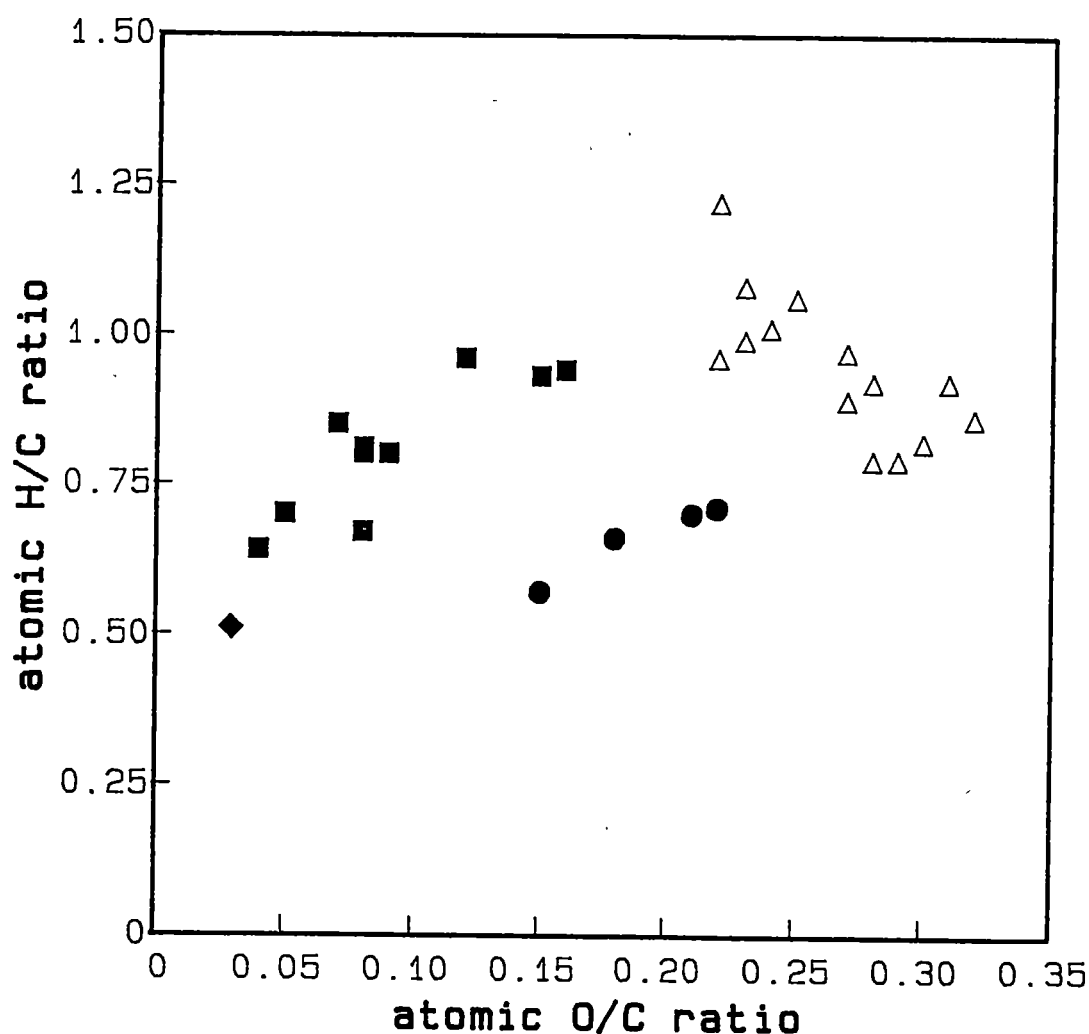
Figure 2.1 Plot of atomic O/C ratio against atomic H/C ratio for Australian coals: ▵, brown coals; ■, higher-rank coals ; ●, oxygen-rich subbituminous coals ; ◆, semianthracite.
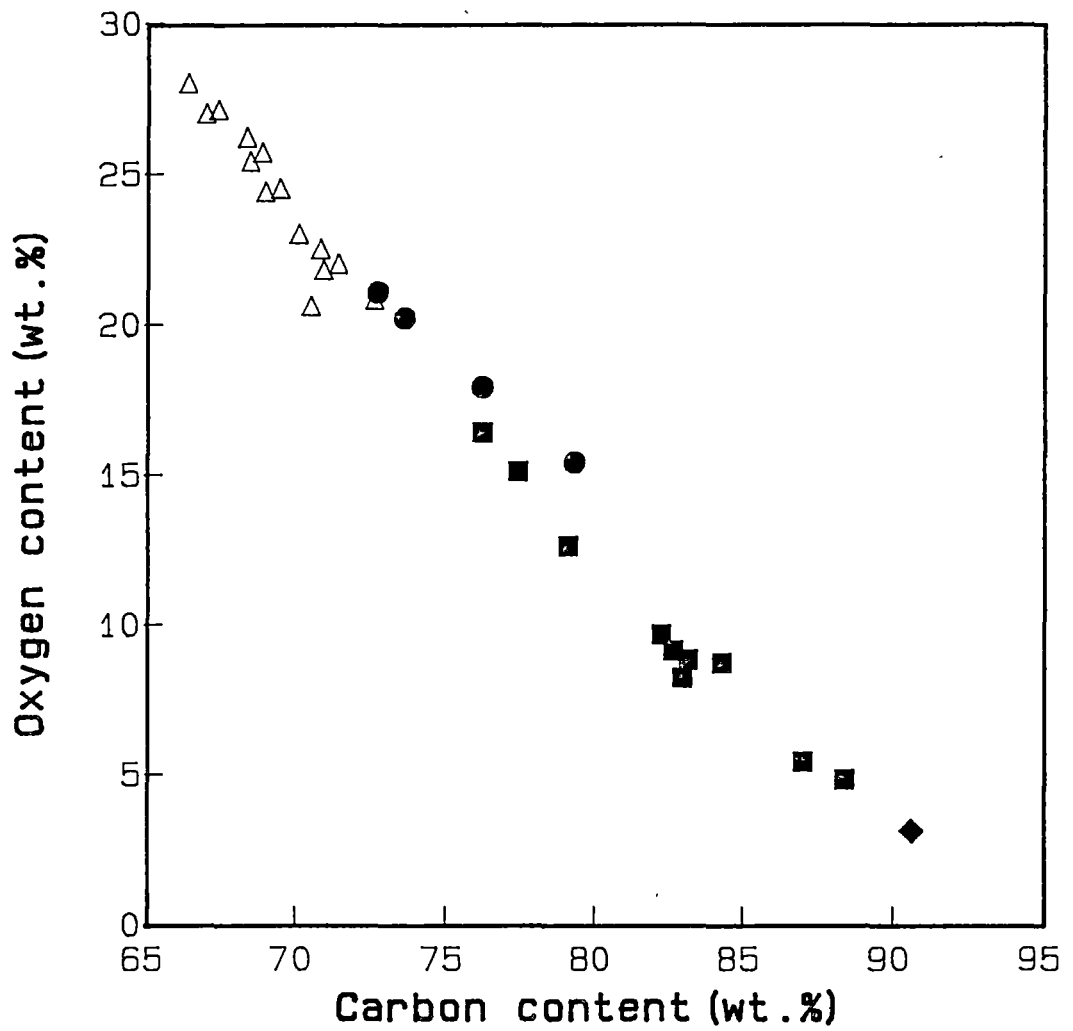
Figure 2.2 Correlation between carbon contents and oxygen contents for Australian coals (see **Figure 2.1** for symbols).
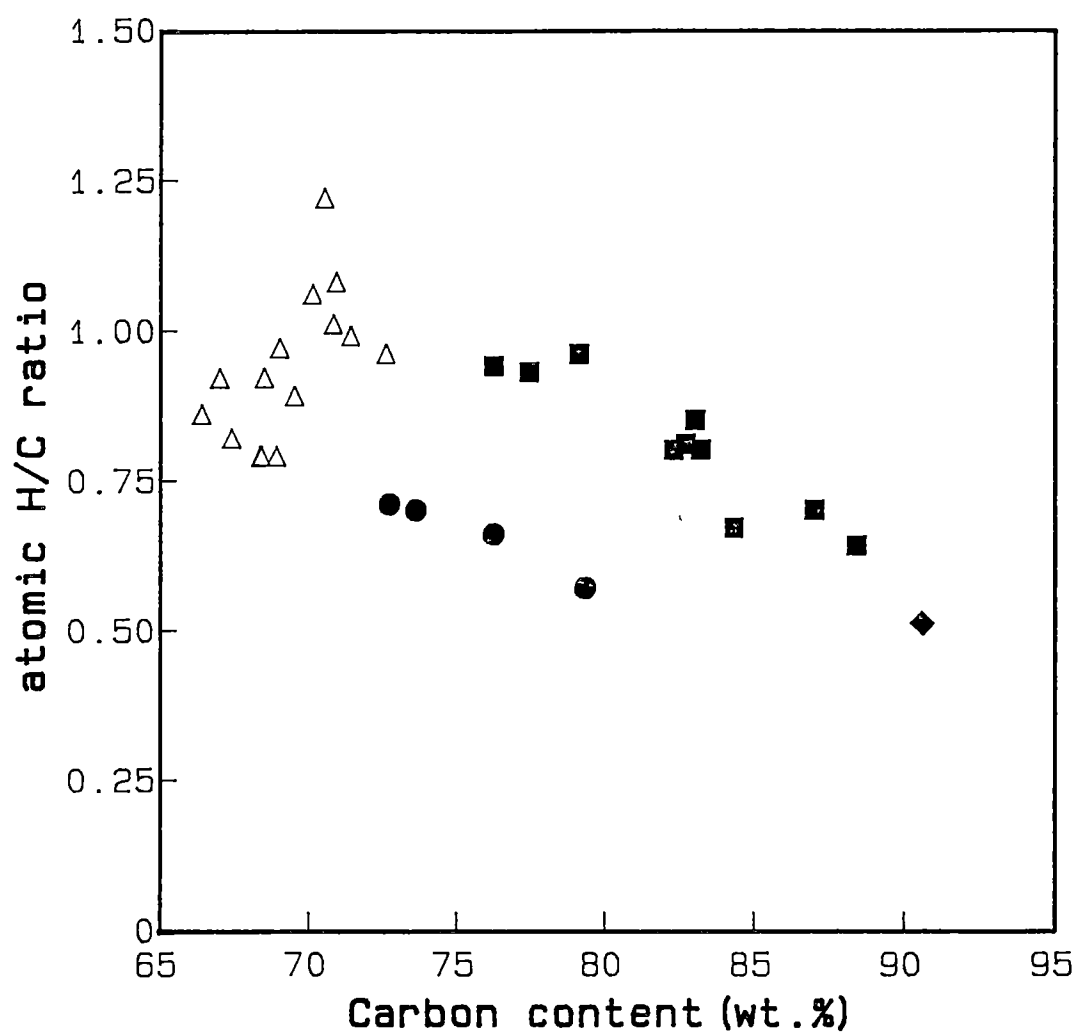
Figure 2.3 Plot of carbon content versus atomic **H/C** ratio for Australian coals (see **Figure 2.1** for symbols).

2.4 HYDROLIQUEFACTION STUDY of AUSTRALIAN COALS

The hydroliquefaction behaviour of the coals in this suite has been studied by Redlich [1987], [Redlich et al.,1985; Redlich et al., 1989b]. In this section a summary of the important findings is presented including some conversion data.

It was found that the liquefaction reactivities of Australian coals in this suite have a strong relationship with coal **H/C** ratios. (Redlich et al. have used the "CO_2 free" H/C ratio) / **Figure 2.4** illustrates a strong correlation between the **H/C** values and the oil yields obtained from the hydro liquefaction reaction of the coal in **tetralin** (3:1 by weight) at 405 °C for 1 h under initial hydrogen pressure of 6 MPa. The relationship between the yield of total hydrocarbon products (oil + asphaltene + hydrocarbon gases) and **H/C** ratios is also shown in **Figure 2.4**. With a similar **H/C** value the higher-rank coals have a higher asphaltene yield than do the brown coals, therefore a trend of higher yield of the total hydrocarbon products was observed for the higher-rank coals.

GC-MS analyses of the oils from the brown coals (reaction without solvent but with tin oxide as a catalyst) and from some of the higher-rank coals with a high **H/C** ratio (> 0.8) revealed a distribution of long chain hydrocarbons in a similar pattern. It was suggested that for the brown coals studied these long chain aliphatics are probably the main contributors to the variation in brown coal **H/C** ratios and oil yields. It was proposed that the structure of these brown coals is well described by a two-component model – a predominantly aliphatic-rich material, known as the guest, entrapped within a macromolecular polycyclic network of aromatic-type material, known as the host.
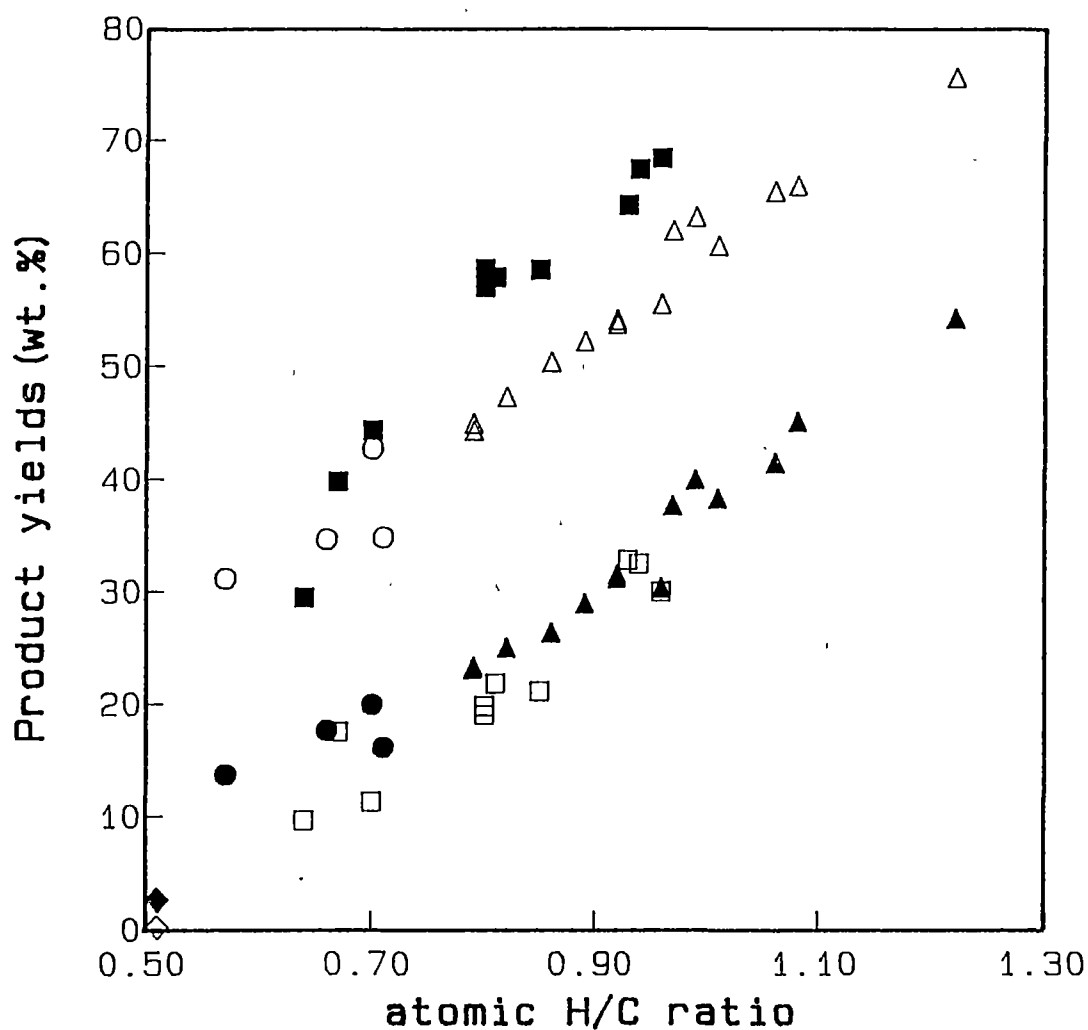
Figure 2.4 The relationships between the yields of liquefaction products and atomic **H/C** ratios for Australian coals.

Oil yield : ▲ , brown coals ; □ , higher-rank coals ; ● , oxygen-rich subbituminous ; ◇ , semianthracite

Total hydrocarbon products : △ , brown coals ; ■ , higher-rank coals ; O , oxygen-rich subbituminous ; ◆ , semianthracite

It has been shown that most of the guest components can be removed from the macromolecular host under a mild reaction condition at 320 °C in **decalin** and a nitrogen atmosphere.

Although some higher-rank coals, having **H/C** greater than 0.8, also have the oil yields similar to the brown coals (see **Figure 2.4**) and the analyses of their oils showed a similar distribution of long chain hydrocarbons to those of brown coals, it was observed that the long alkyl chains in the higher-rank coals were more strongly bound to the coal macromolecular matrix. To remove this type of aliphatic materials from the coal, a higher reaction temperature of 350 °C was required.

Other liquefaction data that show a good relationship with coal chemical compositions is the yield of carbon oxide gases. The correlation between coal **O/C** ratios and the total amount of carbon oxide gases (CO_2 + **CO**) is shown in **Figure 2.5**. Under the hydroliquefaction condition at 405 °C in **tetralin** the major carbon oxide gas produced from the coals is carbon dioxide. The CO_2 gas is probably the product of the decarboxylation of carboxyl groups whereas the decomposition of ketonic structures in the coals gives rise to the production of **CO** gas. At the reaction temperature of 405 °C, the redistribution of the two gases, as a result of water-gas-shift reaction, is also possible [Attar and Hendrickson, 1982]. According to the studies reported by Yost [1985] and Stray et al.[1986], the carbon oxide gases may be also derived from methoxyl groups in the coals. However, by assuming that the CO_2 mainly originated from carboxylic groups, the amount of the CO_2 gas has been used as a measurement of the carboxylic content in the coal [Redlich et al., 1989a].

The liquefaction data related to the above discussion are given in

Table 2.2. This data provide the basis for comparison with the structural data obtained during the present investigation.

The conversion and products yields are expressed as follows :

$$\% \text{ Conversion} = 100 - \{(\text{wt. } CH_2Cl_2 \text{ insoluble} - \text{wt. ash})/\text{wt. coal}\} \cdot 100$$

$$\% \text{ Asphaltene} = \{(\text{wt.} CH_2Cl_2 \text{ soluble} - \text{wt. n-hexane soluble})/\text{wt. coal}\} \cdot 100$$

$$\% \text{ Oil} = \{(\text{wt. n-hexane soluble})/\text{wt. coal}\} \cdot 100$$

$$\text{Total hydrocarbon products} = \% \text{ Oil} + \% \text{ Asphaltene} + \% \text{ Hydrocarbongases}$$
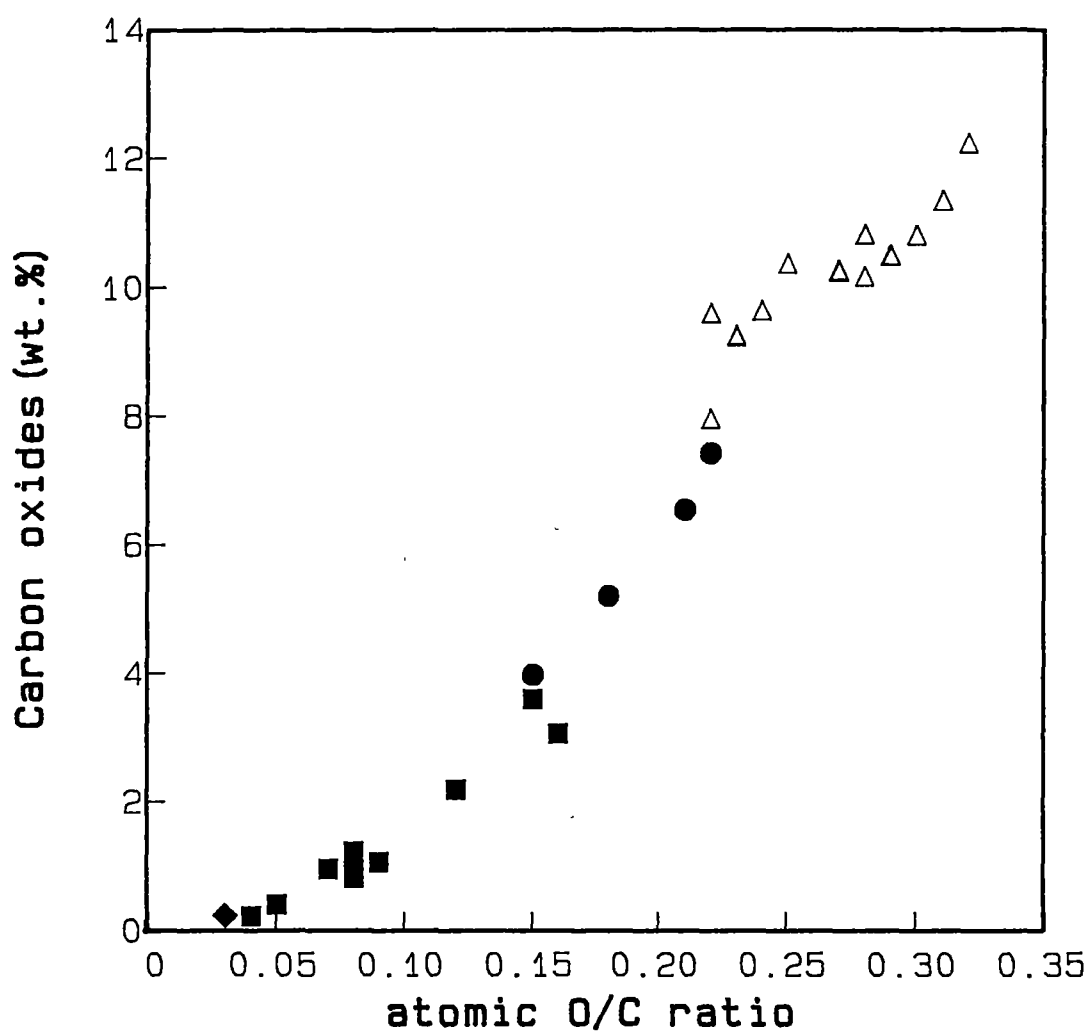
Figure 2.5 Correlation between atomic **O/C** ratios and the amounts of carbon oxides (CO_2+CO) measured from the liquefaction reaction at 405 °C in **tetralin** for Australian coals (see **Figure 2.1** for symbols).

Table 2.2 Hydroliquefaction data Australian coals[a] (405 °C for 1 h in **tetralin** and under initial H_2 pressure of 6 MPa).

Coal	H/C	O/C	Total conversion	Oil yield	[b]Total hydrocarbons	[c]Carbon oxides
			wt. % dmif coal			
ABL1	0.51	0.03	2.8	0.2	2.64	0.12
ABL2	0.57	0.15	38.5	13.65	31.11	3.97
ABL3	0.64	0.04	28.0	9.60	29.43	0.22
ABL4	0.66	0.18	44.5	17.63	34.60	5.20
ABL5	0.67	0.08	40.1	17.50	39.76	0.94
ABL6	0.70	0.05	44.2	11.25	44.28	0.40
ABL7	0.70	0.21	55.0	19.91	42.66	6.54
ABL8	0.71	0.22	47.3	16.12	34.81	7.42
ABL9	0.80	0.08	57.7	19.00	56.92	0.81
ABL10	0.80	0.09	58.5	19.80	58.52	1.06
ABL11	0.81	0.08	59.0	21.80	57.78	1.22
ABL12	0.85	0.07	60.6	21.10	58.45	0.95
ABL13	0.93	0.15	70.5	32.75	64.13	3.59
ABL14	0.94	0.16	71.7	32.41	67.27	3.05
ABL15	0.96	0.12	73.1	29.93	68.26	2.18
ABR1	0.79	0.29	62.9	23.08	44.88	10.48
ABR2	0.79	0.28	62.9	23.33	44.25	10.16
ABR3	0.82	0.30	67.3	24.98	47.22	10.80
ABR4	0.86	0.32	71.4	26.31	50.29	12.22
ABR5	0.89	0.27	69.9	28.87	52.11	10.24
ABR6	0.92	0.31	73.0	31.12	54.03	11.33
ABR7	0.92	0.28	71.9	31.47	53.66	10.81
ABR8	0.96	0.22	72.4	30.28	55.39	9.59
ABR9	0.97	0.27	79.4	37.60	61.87	10.26
ABR10	0.99	0.23	77.0	39.89	63.07	9.23
ABR11	1.01	0.24	75.9	38.23	60.58	9.63
ABR12	1.06	0.25	82.8	41.38	65.29	10.36
ABR13	1.08	0.23	81.5	45.01	65.80	9.25
ABR14	1.22	0.22	88.9	54.10	75.49	7.95

[a]Data from Redlich [1987]; [b]**Oil +Asphaltene + Hydrocarbon gases**; [c]CO_2+CO

CHAPTER THREE

FTIR STUDIES of AUSTRALIAN COALS

3.1   INTRODUCTION

In the IR spectra of coals studied the two most informative regions are the C-H stretching region between 3100 cm^{-1} and 2750 cm^{-1} and the C=O stretching region between 1850 cm^{-1} and 1450 cm^{-1}. In other regions where many different functional groups can have the IR absorption in the region such as the bands between 1300 cm^{-1} and 1000 cm^{-1} or where the interferences of the mineral matter are substantial such as the region between 900 cm^{-1}-500 cm^{-1}, very little useful information can be obtained (see **Figure 3.1**).

In this study the spectral data in three regions, namely the hydroxyl O-H bending, the aromatic and aliphatic C-H stretching and carbonyl C=O stretching regions have been investigated. The areas of the aromatic and aliphatic CH bands were used to calculate the aromatic and aliphatic hydrogen contents in the sample while the intensity of the OH band and the areas in C=O stretching region were used as a measure of the relative amount of the relevant functional groups. The measurements were carried out for the coals and their hydroliquefaction products, asphaltenes and residues.
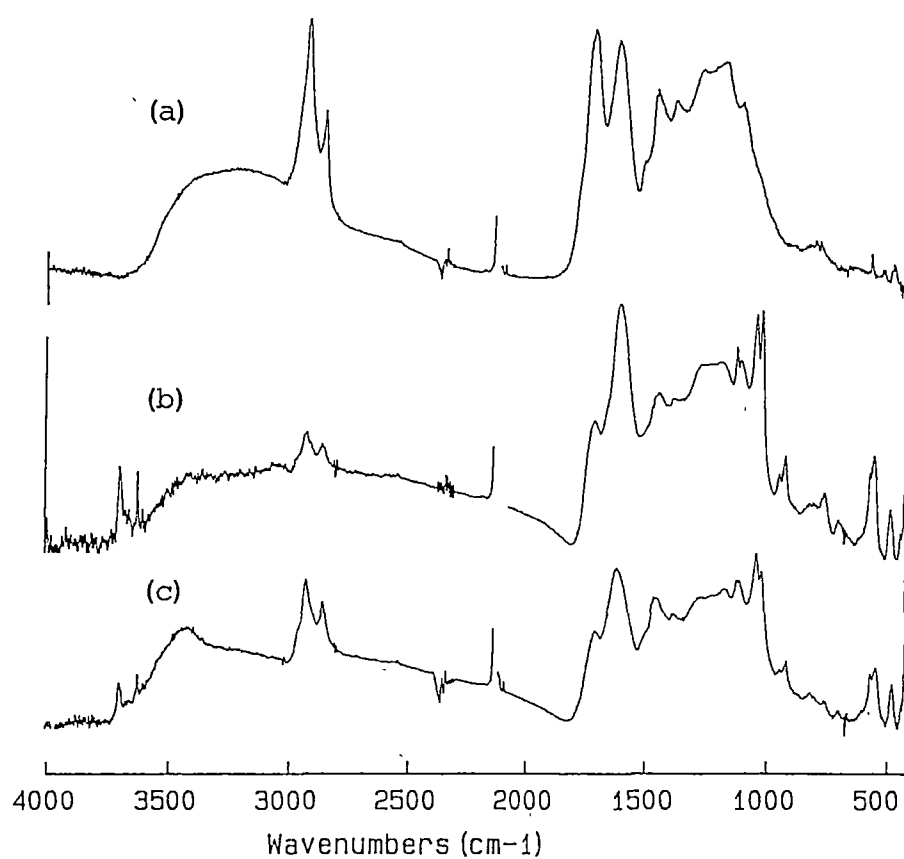
Figure 3.1 Typical spectra of Australian coals; **(a)** brown coal, ABR12, **(b)** oxygen-rich subbituminous, ABL2 and **(c)** high volatile subbituminous, ABL13 .

3.2   EXPERIMENTAL DETAILS

3.2.1   Samples for Analyses

The coal samples and their hydroliquefaction products were obtained from Monash University [Redlich, 1987]. The details of experimental procedures for liquefaction reactions and product separations have been reported previously in the literature [Redlich et al.,1989b]. Briefly, the reactions were carried out in a 70 ml rocking autoclave under either of two sets of reaction conditions :

(i)   3 g of coal in 9 g of tetralin under 6 MPa initial hydrogen pressure at 405 °C for 1 h and

(ii)   6 g of coal in 12 g of decalin under 6 MPa initial pressure of nitrogen at 320 °C for 1 h.

The products were separated into CH_2Cl_2 insoluble components, **residue**, CH_2Cl_2 soluble but **n-hexane** insoluble product, **asphaltene**, and CH_2Cl_2 soluble and **n-hexane** soluble components, **oil**.

The sample for FTIR analysis was dried at 105 °C under a nitrogen atmosphere (13.3 kPa) until a constant weight was obtained.

3.2.2 FTIR Measurement.

The **KBr** disc techniques were used in the FTIR measurements. A sample of 0.8 to 1.2 mg (± 0.01 mg) was mixed with 95-105 mg (± 0.01 mg) of **KBr**, finely ground for at least 15 minutes to ensure the optimum

measurement [Painter et al., 1981; Brookes, 1984] and then pressed under vacuum in a 13 mm die with a load of 8000 kg. The pellet was dried at 105 °C under a nitrogen atmosphere (13.3 kPa) for 24 h and analysed immediately thereafter. Inert atmosphere conditions were used at elevated temperature to minimize air oxidation. No evidence was obtained that air oxidation was a problem under the low severity conditions used for our studies.

All FTIR spectra were recorded on a **Digilab FTS-20E** system at a resolution of 2 cm^{-1} with one hundred co-adding interferograms. All spectra were adjusted for baseline drift [Painter et al.,1981] and normalized to 1.00 mg of sample in 100.00 mg of KBr on a dry-ash-free basis [Solomon and Carangelo, 1982]. Standard software packages on the **Digilab** system were used to analyse spectral data.

The method of baseline correction involves subtraction of the sloping baseline at approximately 3700–1850 cm^{-1} and 1850–400 cm^{-1} to produce a spectrum with flat baseline

3.3   RESULTS AND DISCUSSION

3.3.1   The oxygen-hydrogen stretching region

The broad absorption band associated with oxygen-hydrogen stretching modes in the region between 3500 cm^{-1} and 3100 cm^{-1} have been used by many workers to measure the hydroxyl contents in coals [Painter et al., 1981]. Recently, Painter et al. [1987] discussed the nature of this broad band in relation to several types of hydrogen-bonded **OH** structures. Questions have been raised regarding the accuracy of the measurement as there may be an interference of water molecules which also have an IR absorption in the region. However, Solomon and Carangelo [1982] have demonstrated that by using the intensity at 3200 cm^{-1} to determine the hydroxyl

contents, an improvement in the accuracy of the results can be obtained.

In this study the intensity of the band at 3200 cm^{-1} in the coal spectra was found to correlate with coal atomic **O/C** values as shown in **Figure 3.2.** The results indicate an increase in hydroxyl content as a function of **O/C** values. The scatter in the data is to be expected since coals, in particular brown coals, can contain varying amounts of other oxygen-containing groups. The contribution from hydrogen-bonded water in the region of 3200 cm^{-1} is expected to be small since the main absorption for such a species is usually near 3400 cm^{-1}. In most of the previous studies the IR absorption in this region has been assigned as being associated with the hydroxyl groups of phenolic structure by assuming that there were insignificant contributions from the hydroxyl groups of other structures, namely, carboxylic acids and alcohols. For the coals studied in this work, the spectral data in the carbonyl stretching region, which will be discussed later, reveal the presence of a substantial amount of carboxylic acids. Therefore the absorption at 3200 cm^{-1} for the coals investigated here has to be ascribed at least to the hydroxyl groups of both phenolic and carboxylic structures. The IR absorbance at 3200 cm^{-1} is therefore compared to the total acidic oxygen contents (phenolic + carboxylic) as determined by non-aqueous titration [Redlich et al.,1989a]. A good correlation between the two parameters is evident for the results presented in **Figure 3.3.** Uncertainty in the measurements of both parameters contributes to the scatter in the data. While coals in this suite have a low nitrogen content (0.41-2.10 wt.% dmif), a contribution from the **NH** stretching vibration to the 3200 cm^{-1} intensity is possible, although the main absorption is usually at higher wavenumber (typically 3500-3300 cm^{-1}) [Bellamy, 1975].
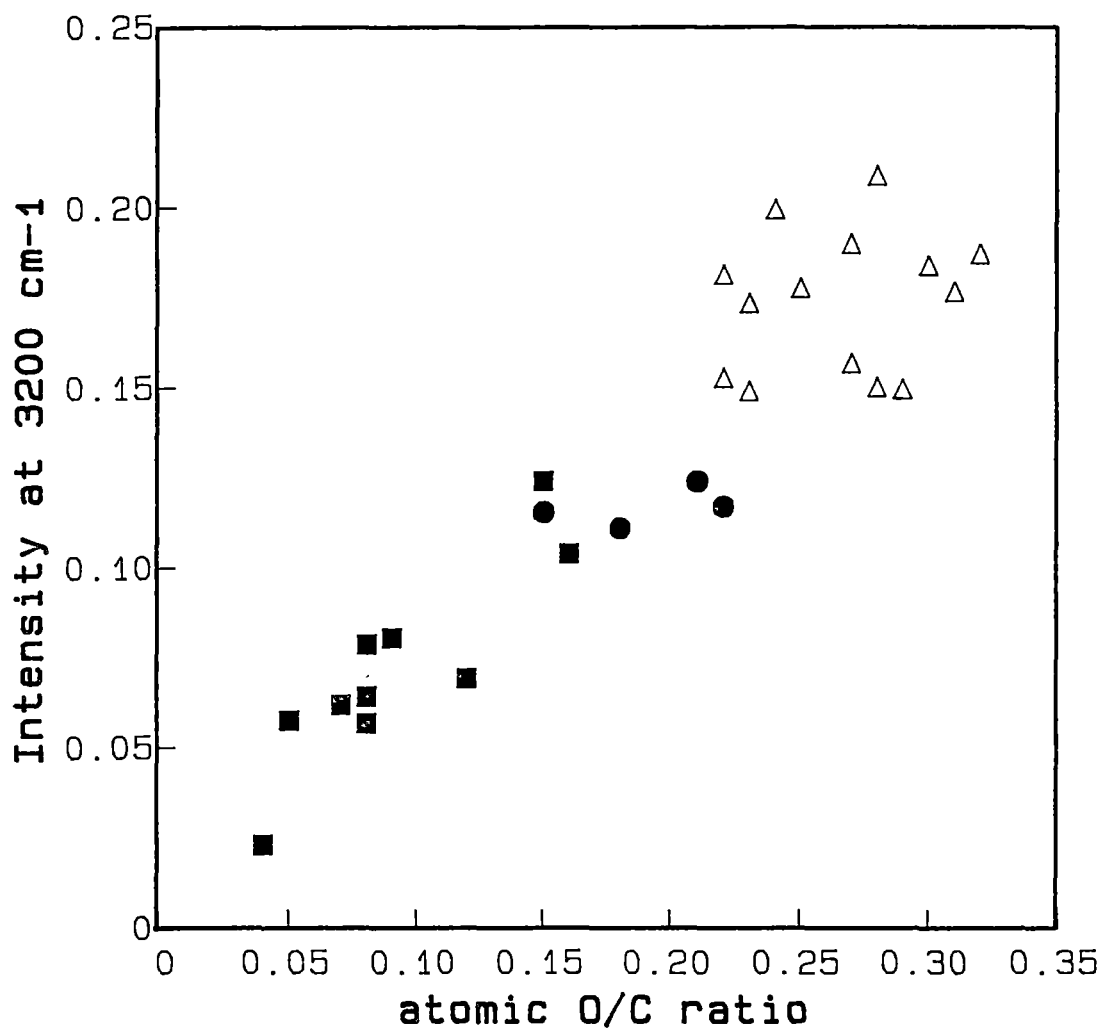
Figure 3.2 Comparison of the IR absorbance (intensity) at 3200 cm^{-1} with atomic **O/C** value for Australian coals : $\triangle$, brown coals ; $\blacksquare$,higher-rank coals ; $\bullet$, oxygen-rich subbituminous coals.
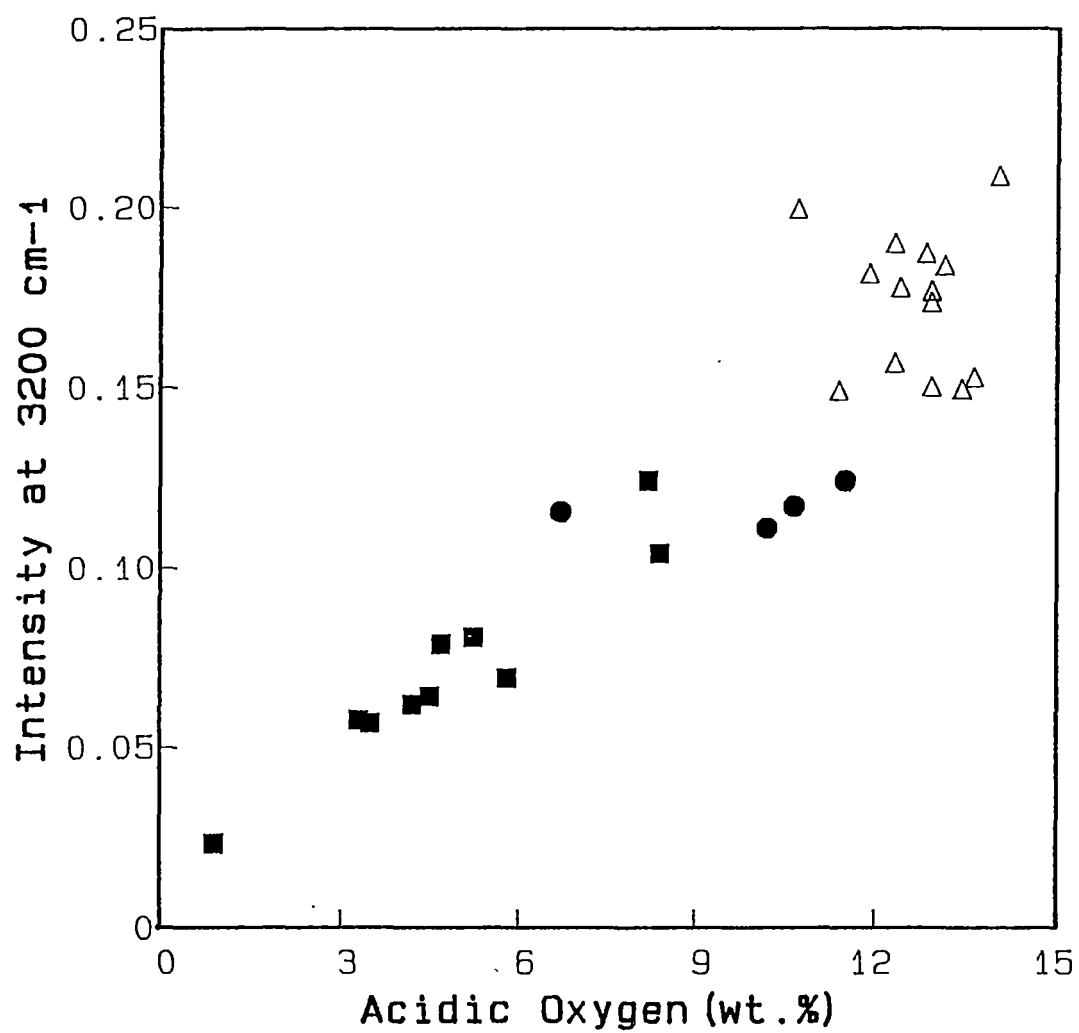
Figure 3.3 Plot of the IR absorbance (intensity) at 3200 cm^{-1} versus acidic oxygen content for Australian coals (see **Figure** 3.2 for symbols).

In addition, strongly bound water molecules could also contribute to this absorption. It has been reported that the tightly bound water molecules in the coal can be extracted by methanol refluxing and that the water content is related to the amount of cations present [Hippo et al., 1987]. For the coals in this study the reported extracting method is inapplicable, since more than 10 wt. % of hydrocarbons from a typical brown coal (**H/C** = 0.99, **O** wt.% = 22) was extractable using methanol. A comparison of the IR spectrum of the acid washed coal with that of the residue after methanol refluxing shows no detectable evidence of a spectral change in the 3500 cm^{-1}-3100 cm^{-1} region corresponding to the removal of water molecules. It should be noted that the acid-washed brown coals used contained very little **Fe, Ca, Mg, Na** (less than 0.02 % d.b. in most cases) [Redlich, 1987]. The acid washing (0.1M H_2SO_4, acid: coal, 20:1), was more severe than the citric acid treatment used by Hippo et al. [1987]. Since it has been demonstrated [Hippo et al., 1987] that bound water is removed by acid washing , the coal samples in this study probably contain little, if any, tightly held water molecules. The source of scatter in the acidic-oxygen content data is probably due to the presence of esters in coals. These groups do not contribute to the 3200 cm^{-1} intensity, however ester groups in coals can be hydrolysed by reacting with titration solvent to give titratable groups [Redlich et al.,1989a]. Hence they contribute to the acidic oxygen values. The correlation as shown in **Figure 3.3** may be useful for an estimation of acidic hydrogen content especially in a higher-rank coal, which is required in the determination of aliphatic and aromatic hydrogen contents from IR data (see **section 3.3.3**).

Correlations of the absorbance at 3200 cm^{-1} with the acidic oxygen contents and with the **O/C** values were also examined for the asphaltene samples. For the asphaltenes, which have a low carboxyl content as

observed from their IR spectra in the carbonyl region, the absorption at $3200\,cm^{-1}$ mainly arises from the oxygen-hydrogen stretching modes of phenolic groups. The relationship between the absorbance at $3200\ cm^{-1}$ and the acidic oxygen contents for some asphaltene samples is shown in **Figure 3.4**. Interestingly, it was also found that the absorbance at $3200\ cm^{-1}$ for the asphaltenes have a strong relationship with coal **O/C** values as seen in **Figure 3.5**. Since the non-acidic oxygen contents of coals were also found to show a strong relationship with coal **O/C** [Redlich et al., 1989a], the correlation in **Figure 3.5** is consistent with a model in which the phenolic groups in the asphaltene have been mainly derived from the non-acidic oxygen groups in the coal. This conclusion is based on the proposal that under the liquefaction condition a significant amount of phenolic ethers may be reduced to phenols which are subsequently stabilized and found in the asphaltenes [Attar and Hendrickson, 1982].

The data of intensity at $3200\ cm^{-1}$ and the acidic-oxygen contents for the coals and asphaltenes are summarized in **Table 3.1**.

Figure 3.4 Plot of the IR absorbance at 3200 cm^{-1} versus acidic oxygen content for asphaltene samples (see **Figure 3.2** for symbols).
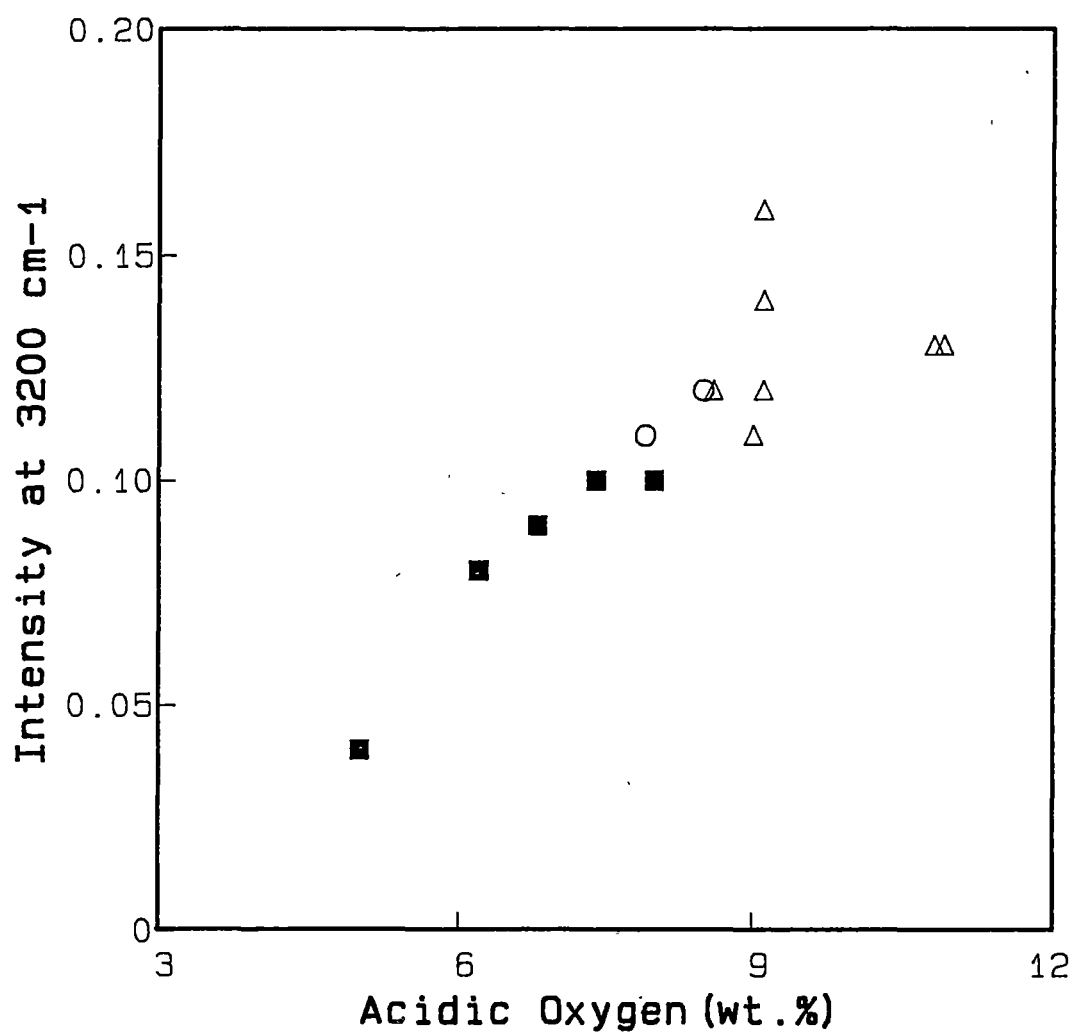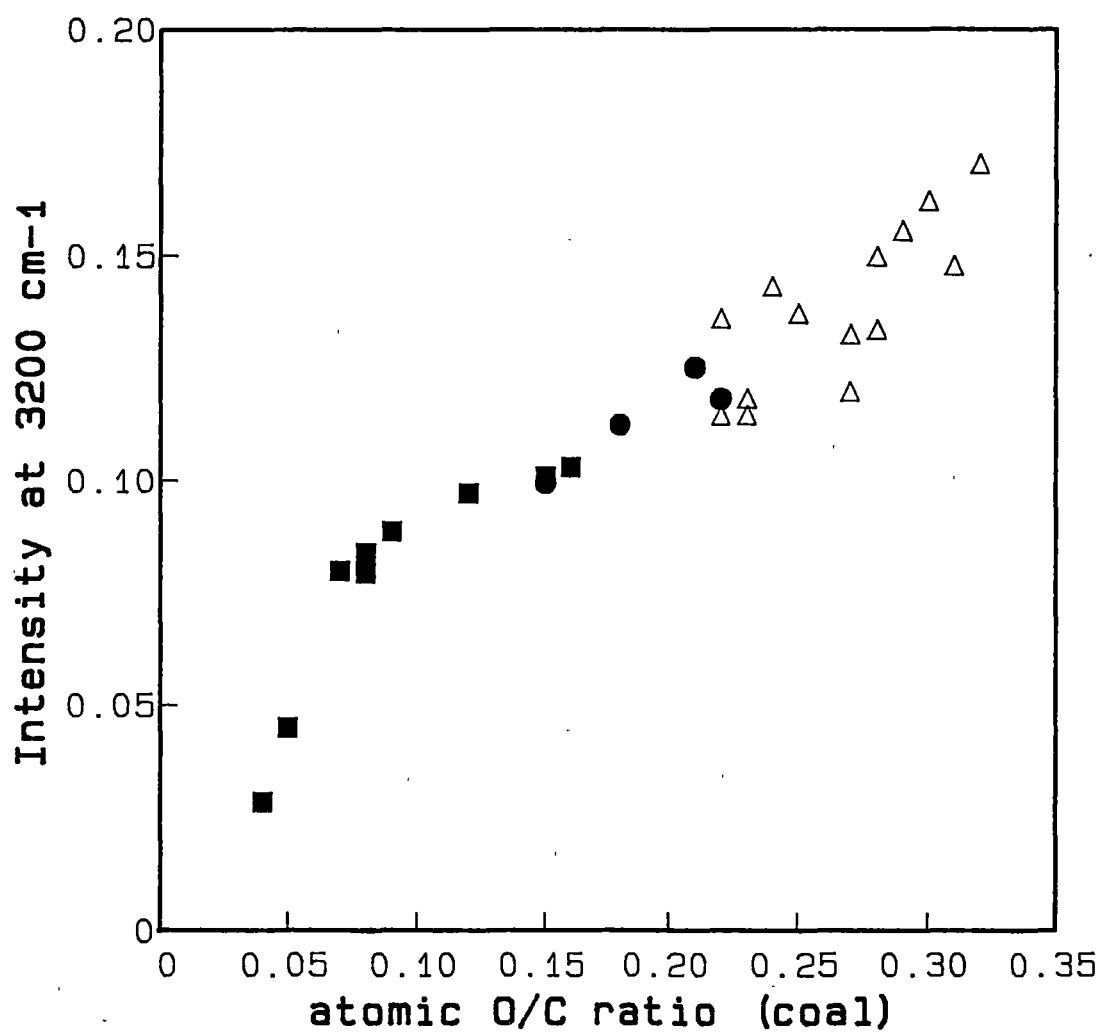
Figure 3.5 Relationship between IR absorbances at 3200 cm⁻¹ in asphaltene spectra and atomic **O/C** ratios of the parent coals (see **Figure 3.2** for symbols).

Table 3.1 Acidic-oxygen content and IR intensity at 3200 cm^{-1} for Australian coals and their asphaltenes (405 °C reaction).

Sample	Coal		Asphaltene	
	Acidic oxygen[a]	intensity[c]	Acidic oxygen	Intensity[c]
ABL2	6.70	0.12	7.80[b]	0.10
ABL3	0.90	0.02	4.30[b]	0.03
ABL4	10.20	0.11	7.90[a]	0.11
ABL5	3.50	0.06	6.80[b]	0.08
ABL6	3.30	0.06	5.00[a]	0.04
ABL7	11.50	0.12	9.10[b]	0.13
ABL8	10.65	0.12	8.50[a]	0.12
ABL9	4.50	0.06	-	-
ABL10	5.25	0.08	6.80[a]	0.09
ABL11	4.70	0.08	7.00[b]	0.08
ABL12	4.20	0.06	6.20[a]	0.08
ABL13	8.20	0.12	8.00[a]	0.10
ABL14	8.40	0.10	8.00[b]	0.10
ABL15	5.80	0.07	7.40[a]	0.10
ABR1	13.40	0.15	10.60[b]	0.16
ABR2	12.90	0.15	10.80[a]	0.13
ABR3	13.10	0.18	9.10[a]	0.16
ABR4	12.80	0.19	11.30[b]	0.17
ABR5	12.30	0.16	10.90[a]	0.13
ABR6	12.90	0.18	10.20[b]	0.15
ABR7	14.00	0.21	10.20[b]	0.15
ABR8	11.90	0.18	9.10[a]	0.14
ABR9	12.30	0.19	8.60[a]	0.12
ABR10	11.40	0.15	9.00[a]	0.11
ABR11	10.70	0.20	10.00[b]	0.14
ABR12	12.40	0.18	9.70[b]	0.14
ABR13	12.90	0.17	9.10[a]	0.12
ABL14	13.60	0.15	8.50[b]	0.11

[a]From non-aqueous titration in wt. % dmif coal [Redlich, 1987]. [b]Estimated from the calibration line in **Figure 3.4**. [c]In absorbance unit.

3.3.2   The carbonyl stretching region

The spectra of brown coals and oxygen-rich subbituminous coals show two prominent peaks which centre approximately at 1720 cm^{-1} and 1610 cm^{-1}. For the higher-rank coals with a low oxygen content the absorption at 1720 cm^{-1} appear as a shoulder on the 1610 cm^{-1} band.

The least-square curve-fitting techniques were applied to resolve the spectrum in the carbonyl stretching region (1850 cm^{-1}-1500 cm^{-1}). No baseline correction beyond that outlined in section 3.2.2 was made. Initial approximations of the number of bands, peak positions and full width at half heights were obtained by examining second derivatives of the spectral data. **Figure 3.6** illustrates the FTIR spectra and second derivative data in the carbonyl stretching region for a brown coal and a higher-rank coal . With the initial estimation and a criterion of minimum number of bands with the best fit, seven bands at approximately 1760, 1735, 1700, 1670, 1620, 1570 and 1500 cm^{-1} were used to fit the spectral profile. A mixed Gaussian -Lorenzian function was used as a mathematical function for band shapes [Fraser and Suzuki, 1969]. The initial set of peak parameters including a Gaussian fraction was left optimized until convergence of the data was achieved. For all spectra, the goodness of fit between the calculated data and the experimental spectra satisfied a discrepancy factor of < 0.025 [Maddams, 1980].

The integrated area of each component band was used as a measure of the amount of the relevant functional group by assuming that extinction coefficients for the absorption band are uniform across the samples studied. Since a variability in the coal structures is to be expected, the assumption is not rigorous. For a complex heterogeneous material such as coal, direct measurement of extinction coefficients cannot be reliably

obtained. This is a limitation of the application of FTIR techniques to coal studies. Often one may have to be content with the semiquantitative quality of the FTIR data.
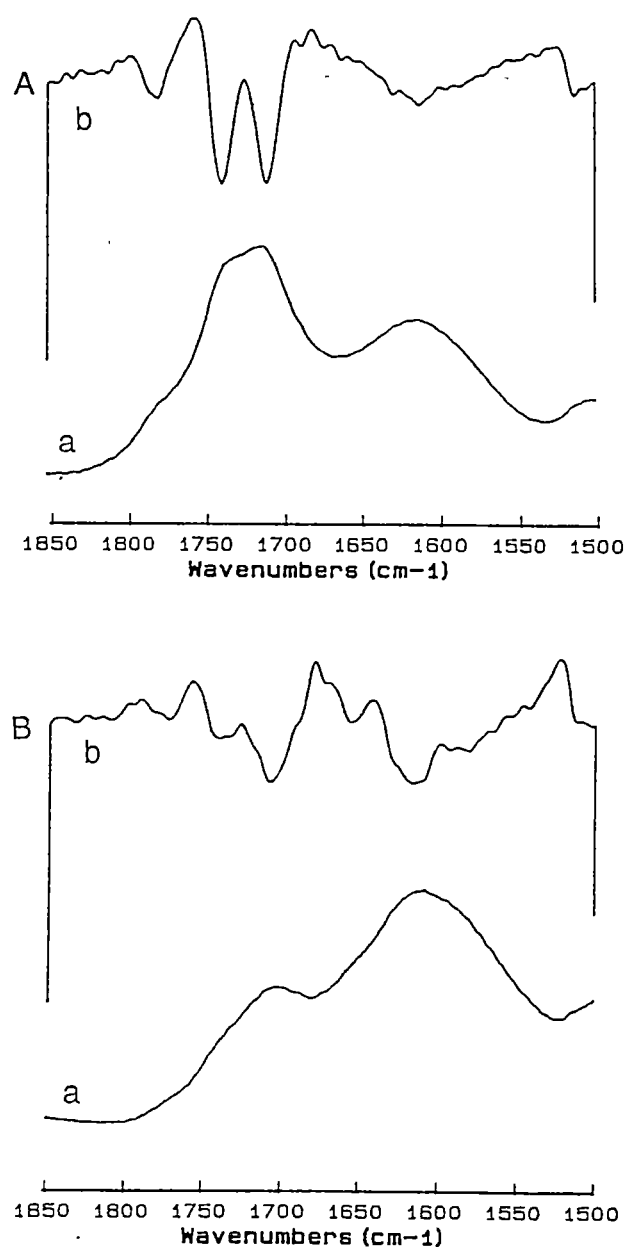
Figure 3.6 IR spectra in the carbonyl stretching region for ; **A.** a brown coal, Bacchus March Pale (ABR14), and **B.** a higher-rank coal, Wandoan (ABL13) : (a) the spectra , (b) the second derivative of the spectra.

The least-squares bands resolved for the region are shown in **Figure 3.7** for a brown coal and a higher-rank coal. Four bands at approximately 1760, 1735, 1700 and 1670 cm^{-1} can be ascribed to carbonyl functional groups while the bands at 1610, 1570 and 1470 cm^{-1} are all associated with the aromatic ring stretching vibrations [Bellamy, 1975]. The intensity of the 1610 cm^{-1} band has been thought to be enhanced by the oxygen-containing substituents of the aromatic structures [Painter et al., 1981]. Because of the heterogeneous nature of coals and the fact that various carbonyl structures can have infrared absorptions in the region between 1800 and 1610 cm^{-1}, there is a difficulty in giving unique assignments to the bands deconvoluted in the region. However, by comparing the spectral data to those reported for coal samples [Berkowitz, 1985a; Painter et al., 1981] and to characteristic group-frequencies [Bellamy, 1975; Rao, 1963], the most probable assignments may be given. The band assignments for the region are summarized in **Table 3.2**.

A predominant functional group associated with the band at 1760 cm^{-1} is probably a phenolic ester, **RCOOAr**, while the absorption at 1735 cm^{-1} is assigned mainly to aliphatic esters, **RCOOR'**, and phenol esters of aromatic acids, **ArCOOAr,** with a contribution from alkyl esters of aromatic acids, **ArCOOR**. The strong absorption near 1700 cm^{-1} is attributed predominantly to carboxylic acids but a contribution from alkyl esters of aromatic acids, **ArCOOR** is also probable. A relatively weak band at 1670 cm^{-1} is assigned to ketonic structures.

Table 3.2 Band assignments for the carbonyl region of coal spectra.

Band position (cm⁻¹)	Assignment
1760	Phenolic ester, **RCOOAr**
1735	Aliphatic ester, **RCOOR'**
	Phenol ester of aromatic acid, **ArCOOAr'**
	Alkyl ester of aromatic acid, **ArCOOR**
1700	Carboxylic acid, **Ar(R)COOH**
	Alkyl ester of aromatic acid, **ArCOOR**
1670	Ketonic structures
1610,1570,1470	Aromatic ring **C=C** stretching modes
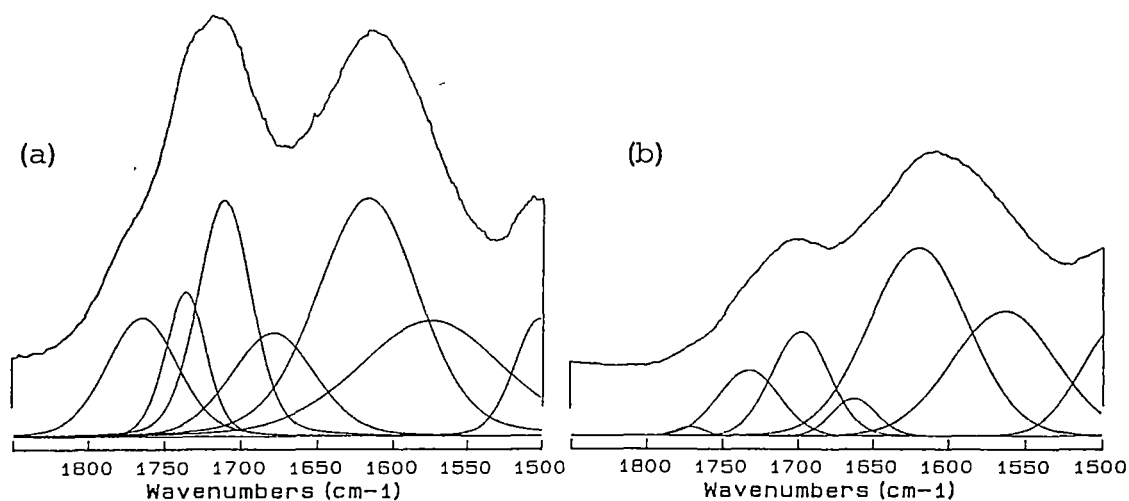
Figure 3.7 Curve-fitting bands in the carbonyl stretching region of the IR spectrum for **a)** a brown coal, Loy Yang 1279 (ABL12) and **b)** a higher-rank coal, Wandoan (ABL13).

In general, the total absorbance of all the carbonyl bands for the brown coals is greater than those for the higher-rank coals. This observation is consistent with conclusions from other analyses that the brown coals contain higher concentrations of carbonyl groups than do the higher-rank coals [Zhou et al., 1984]. The integrated intensities of the the curve-resolved bands are given in **Table 3.3**. Evidently, the higher-rank coals contain an insignificant amount of phenolic esters but a considerable amount of other carbonyl functional groups in many cases. In particular, the oxygen-rich subbituminous coals contain a high concentration of carboxylic acids and phenol esters of aromatic acids or aliphatic esters as shown by the strong absorbances associated with the 1700 cm ^{1} and 1735 cm ^{1} bands for these coals.

Because of the variability in the carbonyl structures in coals, there is no simple relationship between the carbonyl contents and other coal parameters. However, trends of increasing carbonyl functional group concentrations as a function of coal rank can be observed. The plots of the area of 1700 cm $^{-1}$ band which is predominantly carboxylic acids and of the total area for the ester groups (1760 cm $^{-1}$ band + 1735 cm $^{-1}$ band) against atomic **O/C** values of the coals are shown in **Figure 3.8** and **Figure 3.9** respectively. For the higher-rank coals the plot of total area of the carbonyl bands in **Figure 3.10** shows a similar trend of increasing total carbonyl contents with **O/C** values as do the components in **Figures 3.8** and **Figure 3.9**. However, there is a considerable scatter in the data for the brown coals. These results underline the complexity of these materials. The variations of carbonyl contents for the brown coals appear to form two trends. For most brown coals having a high oxygen content (▲ in **Figures 3.8 - 3.10**, **O/C** > 0.26, wt. % **O** > 24) the data are on a trend of having a lower carbonyl contents consistent with the higher-rank coals.

Table 3.3 Areas of the component bands in the carbonyl region[a] of the IR spectra of Australian coals.

Coal	Band position (cm^{-1})						
	1760	1735	1700	1670	1610	1570	1470
ABL2	0.09	3.55	10.63	1.77	22.09	23.56	7.87
ABL3	0.00	0.39	1.76	2.60	10.26	9.84	4.50
ABL4	0.44	4.93	8.54	1.46	18.91	15.48	9.23
ABL5	0.00	0.33	1.89	1.73	9.53	10.77	2.85
ABL6	0.00	0.48	1.63	1.79	11.72	13.71	3.05
ABL7	0.87	5.39	8.82	2.83	21.92	17.25	10.72
ABL8	0.63	5.68	10.40	1.66	19.88	20.65	5.68
ABL9	0.00	0.11	2.99	0.80	18.86	23.30	4.88
ABL10	0.07	3.14	3.06	1.39	16.85	23.66	4.87
ABL11	0.06	2.47	3.03	1.27	18.92	22.78	4.73
ABL12	0.61	0.59	1.71	0.47	10.35	12.81	2.59
ABL13	0.18	4.92	4.02	3.86	21.22	26.51	4.36
ABL14	1.80	2.25	4.26	0.78	16.00	8.54	6.14
ABL15	0.27	2.54	3.22	1.38	13.21	6.40	5.70
ABR1	4.04	3.98	7.62	2.64	17.54	14.90	4.79
ABR2	6.60	3.39	6.39	1.80	19.92	17.08	5.25
ABR3	10.59	3.37	9.93	5.73	22.81	20.20	6.29
ABR4	7.81	6.44	11.98	5.89	21.48	17.92	6.71
ABR5	9.97	1.37	7.90	2.50	19.74	22.52	4.50
ABR6	9.59	2.60	10.71	4.41	22.44	28.48	5.12
ABR7	8.26	6.41	14.19	11.86	26.97	9.11	18.10
ABR8	8.71	4.49	11.90	8.44	29.01	17.42	12.39
ABR9	8.33	5.99	13.98	10.55	26.61	16.74	7.85
ABR10	8.18	5.64	11.94	7.32	25.22	13.51	8.51
ABR11	7.67	9.07	14.15	11.83	28.54	17.65	9.50
ABR12	8.68	6.45	13.36	8.94	25.51	17.98	6.40
ABR13	6.20	11.22	13.53	9.54	26.59	16.10	8.53
ABR14	7.34	9.49	12.72	9.29	22.49	10.36	6.27

[a] In absorbance cm^{-1}.
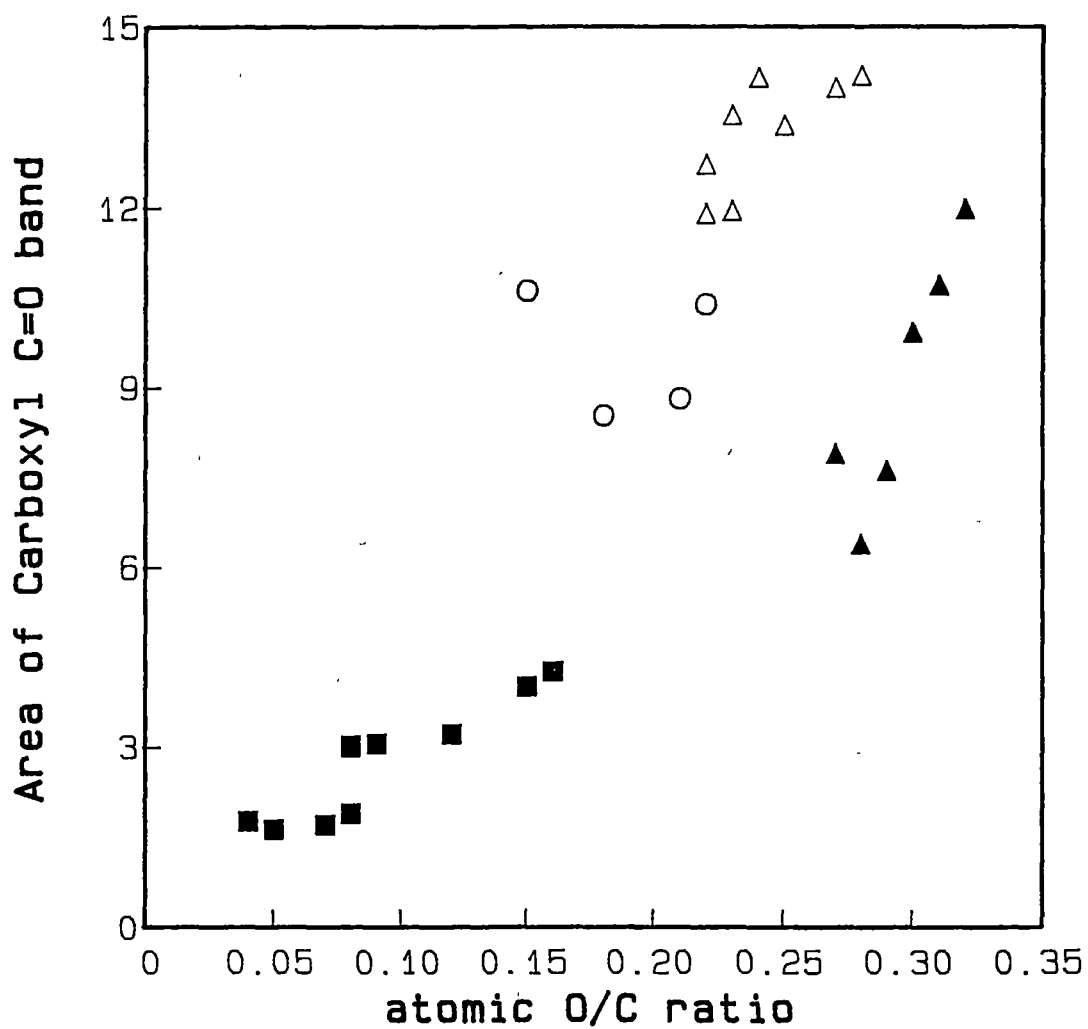
Figure 3.8 Plot of the area of carboxylic acid **C=O** band (1700 cm⁻¹) versus coal **O/C** value : △ , brown coals having a low oxygen content ; ▲ , brown coals having a high oxygen content ; ■ , higher-rank coals ; o , oxygen-rich subbituminous coals.
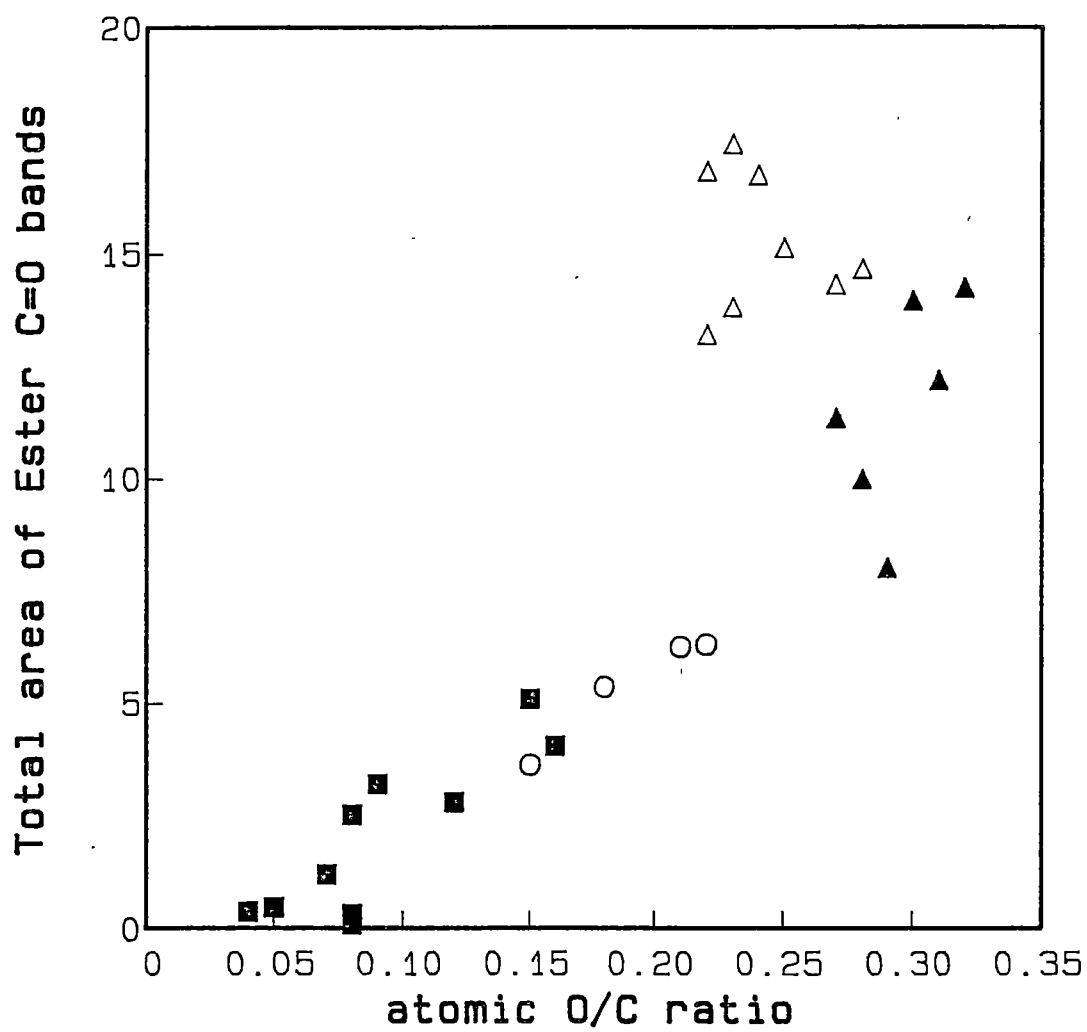
Figure 3.9 Plot of the total area of the ester **C=O** bands (1760 cm^{-1} + 1735 cm^{-1}) versus coal **O/C** value (see **Figure 3.8** for symbols).
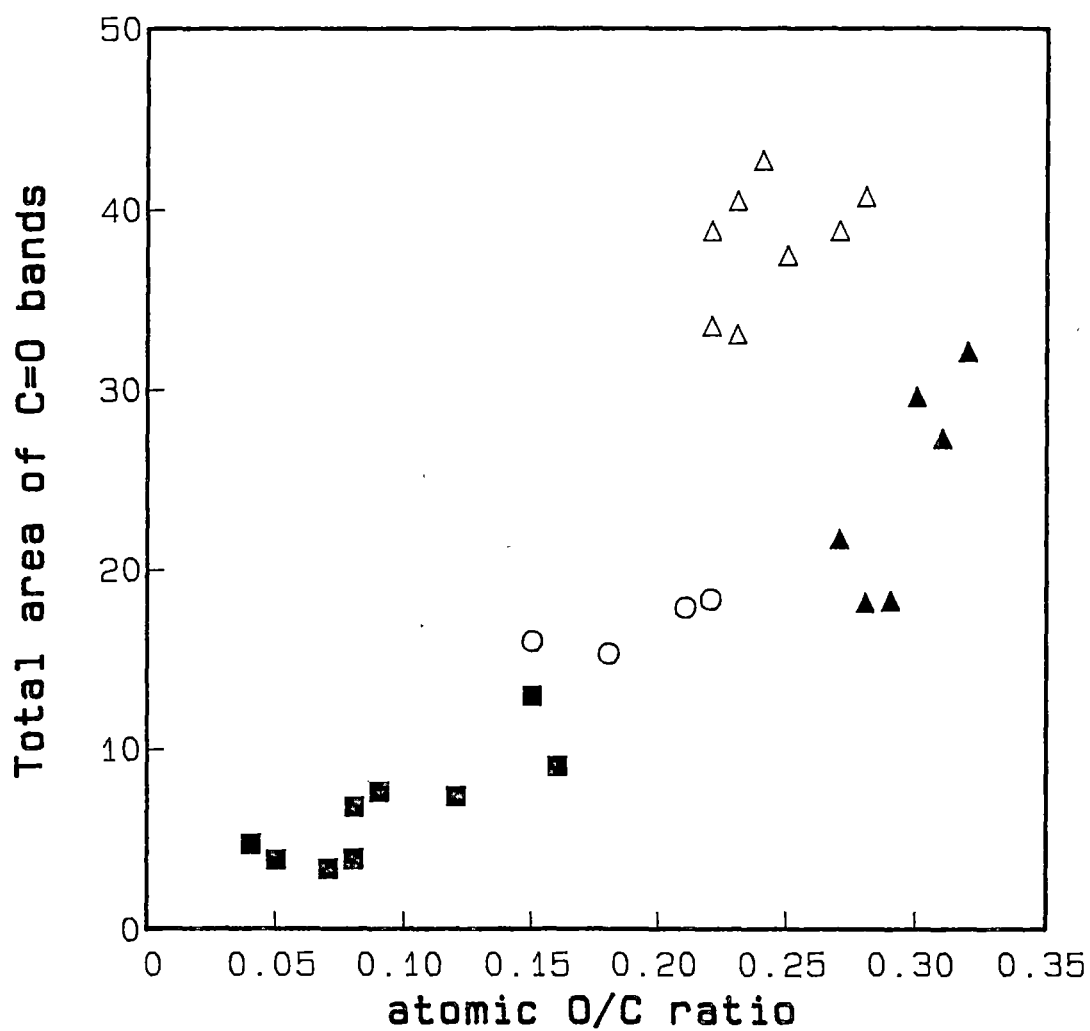
Figure 3.10   Plot of total area of carbonyl bands (1760 cm^{-1}-1670 cm^{-1}) versus coal **O/C** value (see **Figure 3.8** for symbols).

These brown coals have been shown to have higher non-acidic oxygen contents than do the coals in the other group ($\triangle$ in **Figures 3.8 - 3.10**) [Redlich et al., 1989a]. Examination of other properties of the brown coals revealed that those coals having high carbonyl contents also have a high concentration of aliphatic groups. The distribution of oxygen-containing groups in brown coals is central to elucidating their structures.

A guest-host model has been proposed for the structure of brown coals in order to explain their liquefaction behaviour [Redlich et al., 1985, 1989b]. It has been shown that most of the guest material can be removed from the macromolecular host by a mild reaction at 320 °C in **decalin** under a nitrogen atmosphere. IR analyses of asphaltenes from the guest (**CH$_2$Cl$_2$** soluble, **n-hexane** insoluble product) revealed that they are highly aliphatic products containing larger carbonyl concentrations than the parent coals. This can be seen from **Figure 3.11** where the spectra in the carbonyl region for the coal ABR12 (Loy Yang 1279) and its asphaltene are compared. The spectra also indicate that the 320 °C asphaltene has a low concentration of phenols and/or phenolic ethers, because of the relatively weak absorption of the 1610 cm^{-1} band, compared with the parent coal. This finding is in accordance with an observation of weak absorbance in the oxygen-hydrogen stretching region (3500-3100 cm^{-1}) in the asphaltene spectrum.

Since the amount of guest material in brown coals is found to increase with coal **H/C** values, as the material is predominantly aliphatic ($\mathbf{f_{ar}}$ = 0.2 to 0.3), there should be a similar relationship for the carbonyl contents. Indeed, the plot of total area of the carbonyl stretching region (1850 cm^{-1} - 1675 cm^{-1}) for the brown coals as shown in **Figure 3.12** exhibits the trend of increasing carbonyl contents with **H/C** values.
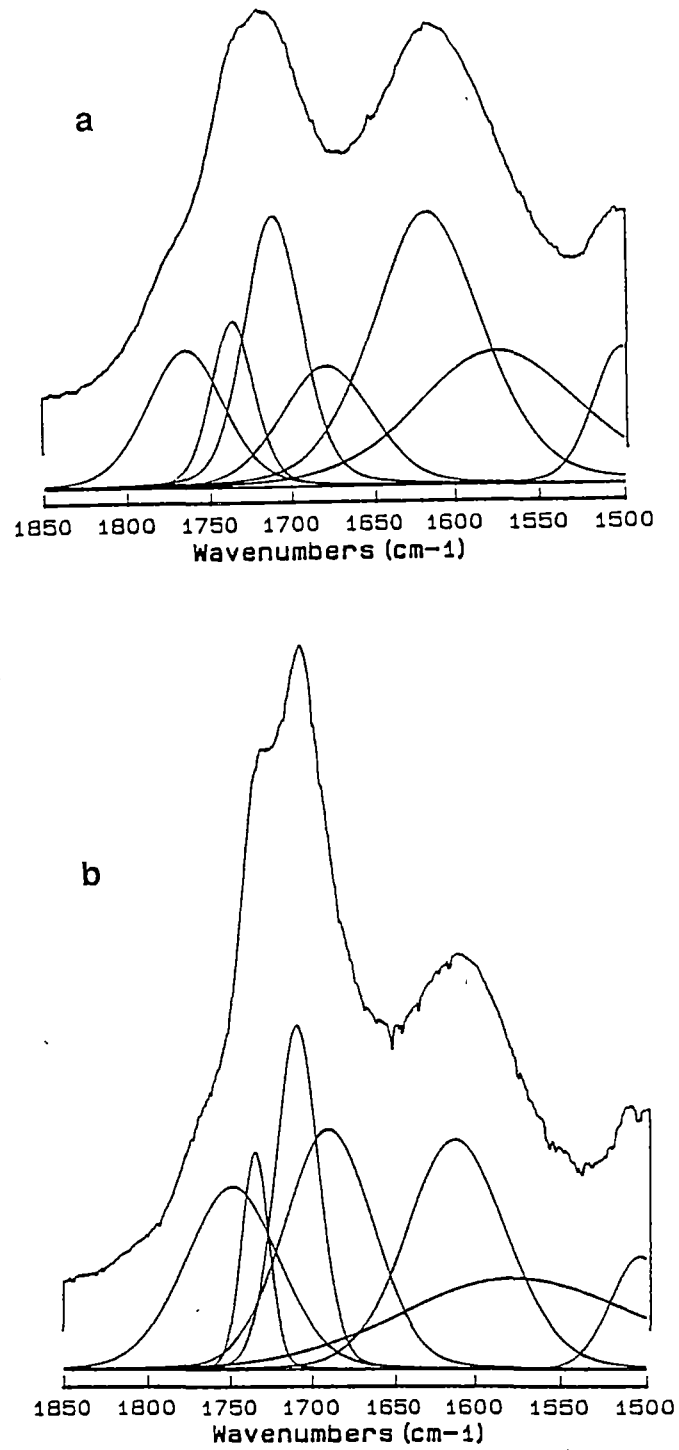
Figure 3.11 Comparison of the spectra of **a.** the brown coal, Loy Yang 1279 (ABR12) and **b.** its asphaltene from 320 °C liquefaction reaction.
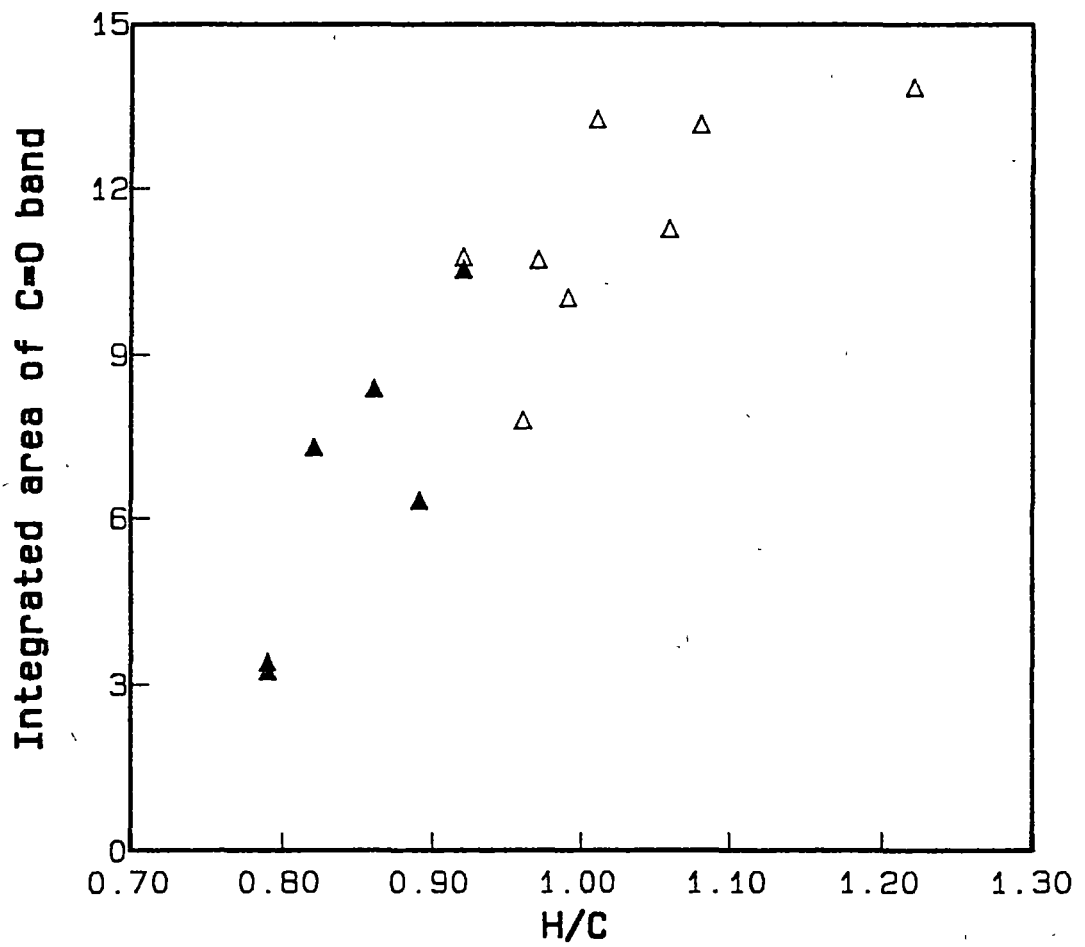
Figure 3.12 Relationship between the integrated areas of the carbonyl band and coal atomic **H/C** ratios for Australian brown coals: ▲, brown coals having high oxygen contents; △, brown coals having low oxygen contents.

This result indicates that the brown coals that have lower **H/C** values contain less guest material and have lower carbonyl contents. However, these brown coals contain a higher total oxygen content. This fact was established earlier in **Chapter 2** , from the inverse relationship between the atomic **O/C** values and **H/C** ratio in the van Krevelen plot.

From a consideration of the data in **Figure 3.8 - Figure 3.10**, it is evident that no clear relationship exists between the carbonyl contents and the **O/C** values for the brown coals, however a direct correlation has been shown to exist between the non-acidic-oxygen contents and the **O/C** values [Redlich et al., 1989a].

Under the standard hydrogenation reaction conditions at 405 °C in tetralin, the major portions of carbonyl groups were found to be removed from the coal structure as observed from the comparison of the spectra of asphaltenes and residues with the spectra of the parent coals (**Figure 3.13** for samples from a typical brown coal). These carbonyl groups in the coals may be removed by the decarboxylation of carboxylic acids producing CO_2 gas, and the decomposition of the ketonic structures forming **CO** gas. A redistribution of CO_2 and **CO** gas concentrations could arise from the water-gas shift reaction [Attar and Hendrickson, 1982]. Moreover, under the reaction condition used, the ester groups may be cleaved and then decarboxylate, yielding CO_2. The total carbon oxide yield correlates well with the coal **O/C** value as shown in **Chapter 2** , **Figure 2.5** , however, the overall correlation between the total carbon oxides and the total area of the carbonyl bands is not as good (**Figure 3.14**). Nevertheless, for the higher-rank coals there is a good correspondence between the two values.

brown coal

a

1850 1800 1750 1700 1650 1600 1550 1500
Wavenumbers (cm-1)

asphaltene

b

1850 1800 1750 1700 1650 1600 1550 1500
Wavenumbers (cm-1)

residue

c

1850 1800 1750 1700 1650 1600 1550 1500
Wavenumbers (cm-1)
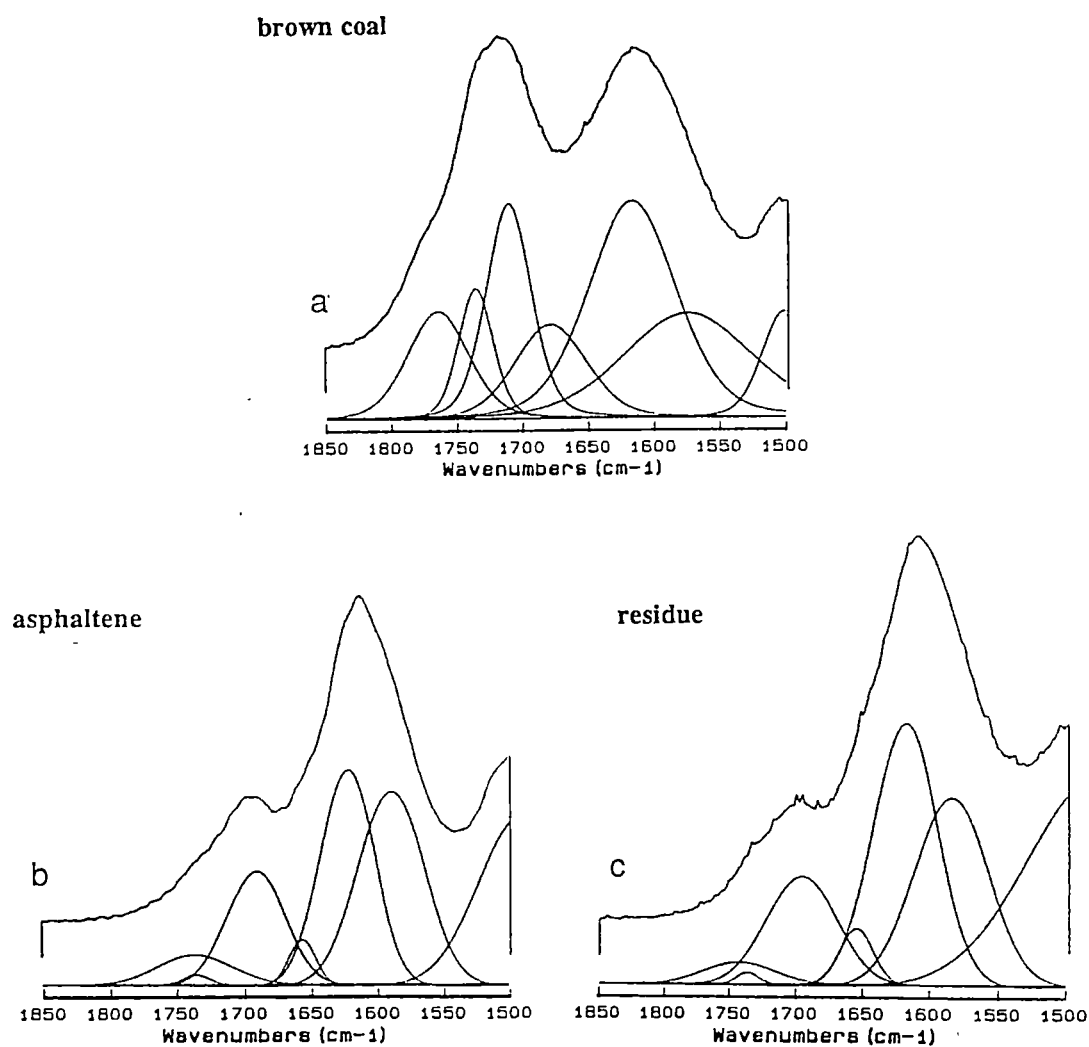
Figure 3.13   Comparison of the IR spectra of **(a)** the brown coal, Loy Yang 1279 (ABR12) and **(b)** its asphaltene and **(c)** residue, from the reaction at 405 °C.
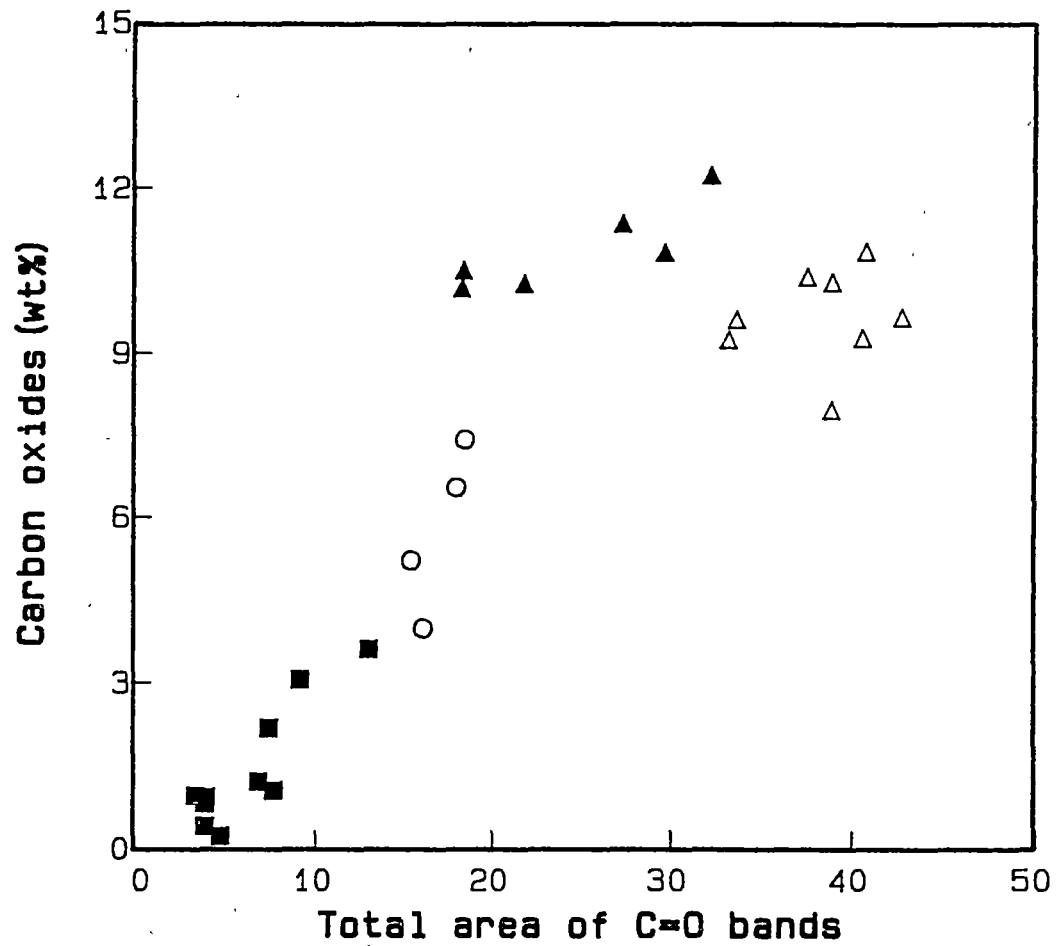
Figure 3.14 Relationship between the amounts of carbon oxide gases (CO_2+CO) from the liquefaction reaction at 405 °C and the total area of carbonyl bands for the Australian coals (see **Figure 3.8** for symbols).

For all the brown coals, the carbon oxides display a small variation over the range of carbonyl band areas, with some coals below and the others above the trend line. An explanation, especially for the brown coals with mainly lower oxygen contents ($\triangle$) below the trend line (**Figure 3.14**), is that the carbonyl band area includes a contribution from ester groups which do not significantly decarboxylate or decarbonylate under the reaction conditions [Brown, 1980]. For the brown coals with higher oxygen contents ($\blacktriangle$) which are above the trend line in **Figure 3.14**, decomposition of methoxyl groups may contribute to carbon oxide gases. This conclusion is based upon the findings from the studies of the hydrogenation of lignin [Yost, 1985; Stray et al., 1986].

3.3.3   The aromatic and aliphatic C-H stretching region

Figure 3.15 shows the spectra in the aromatic and aliphatic C-H stretching region for a representative brown coal (ABR12, Loy Yang 1279) and a higher-rank coal (ABL10, Pikes Gully Vitrinite), compared to those of the liquefaction products, asphaltene and residue. A relatively strong and sharp band in the vicinity of 2922 cm^{-1} in the spectrum of the brown coal indicates the abundance of -CH$_2$- alkyl groups. The spectral feature of the band is a characteristic of the IR absorption of long chain -CH$_2$- groups (Bellamy, 1975). In most of the brown coal spectra especially those with atomic H/C > 0.9 the band associated with the aromatic C-H stretching vibration (3020 cm^{-1}) is extremely weak, indicating a very low concentration of aromatic hydrogen.

Least-square curve-fitting techniques have been attempted in order to resolve the composite bands within the aliphatic carbon-hydrogen stretching region. On the basis of minimum number of bands for the best fit, five bands at approximately 2950 cm^{-1}, 2922 cm^{-1}, 2895 cm^{-1}, 2865 cm^{-1} and 2850 cm^{-1} were used to resolve the spectrum. This approach is consistent with the work of Senftle et al. [1984]. The initial parameters of peak positions, intensities and full widths at half height was left optimised until a convergence of the data was obtained. Although the final result showed a good fit, as assessed by a low discrepancy factor (< 0.025) [Maddams, 1980], between the experimental and calculated data, some difficulties arose. Firstly, the half-widths of the component bands are not constant throughout the samples in this study. Secondly, when more bands were used to fit the experimental profile, the optimized fit was of similar quality to that when five bands were used.
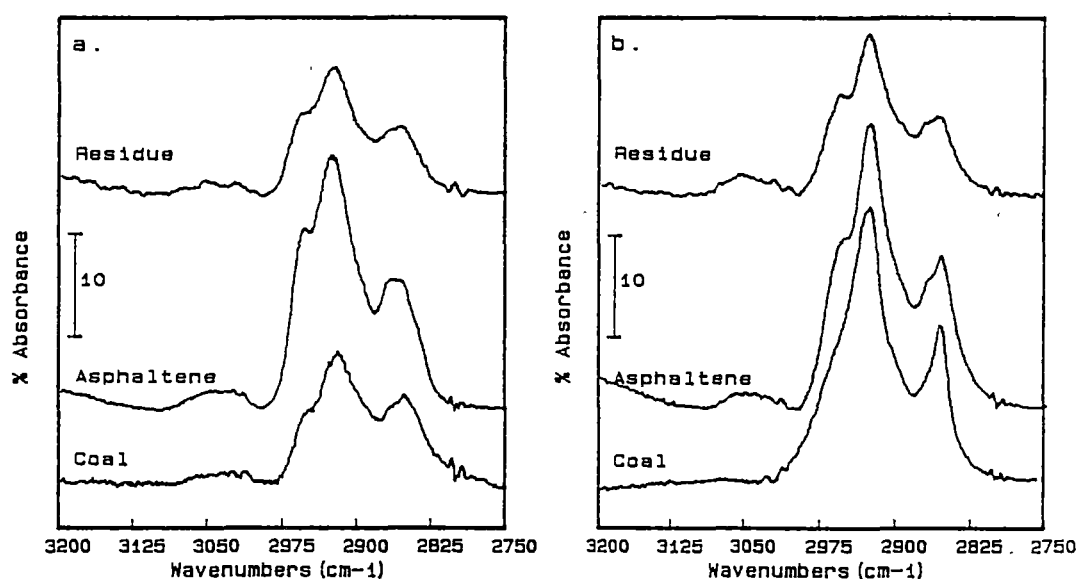
Figure 3.15 Carbon-hydrogen stretching region of the FTIR spectra of **a)** a brown coal, Loy Yang 1279 (ABR12) and its asphaltene and residue and **b)** a high volatile bituminous coal, Pike Gully Vitrinite (ABL10) and its asphaltene and residue.
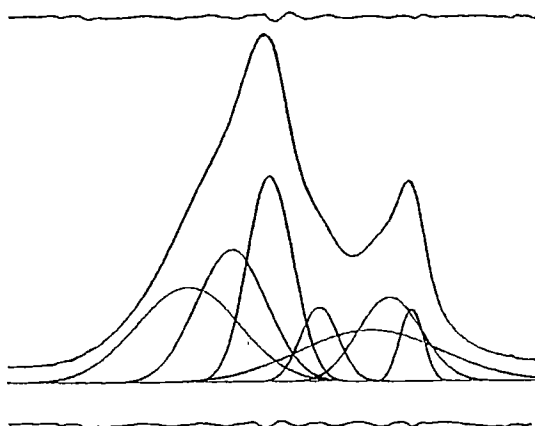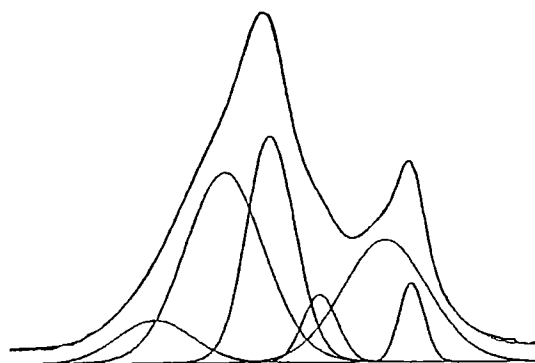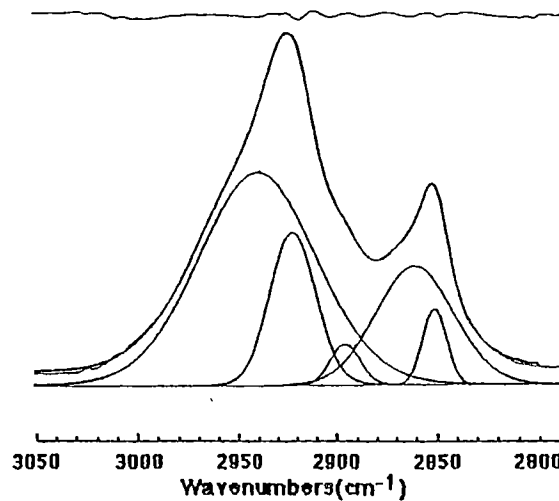
Figure 3.16   Curve-resolved bands in the aliphatic **CH** stretching region of the IR spectrum of a brown coal, Bacchus Marsh Pale, ABR14.

Typical results of curve-resolved fitting with five, six and seven bands are shown in **Figure 3.16**. The five deconvoluted bands in the aliphatic **C-H** stretching region are composite bands, reflecting the heterogeneous nature of coal. We were unable to identify objective criteria to justify further deconvolution. While previous workers have used the deconvolution approach [Senftle et al., 1984; Kuehn et al., 1984; Youtcheff et al., 1986] the sets of coal samples investigated were less diverse. They also reported uncertainties in band assignments. We have found that the results from least-square curve-fitting techniques can give no better scientific insight for the current study than just using the total peak area for the aliphatic region of the spectrum. However, the band areas obtained from the five-band fitting for coals studied are reported in **Table 3.4**.

To measure the areas of aliphatic and aromatic carbon-hydrogen bands, a linear background was first subtracted from the aromatic and aliphatic **C-H** stretching bands in the regions generally from 3200 to 2995 cm^{-1} and from 2995 to 2750 cm^{-1} respectively. The integration limits for the **C-H** areas were chosen within these ranges according to the peak positions. This procedure does not correct for the small overlap of the tails of the aliphatic and aromatic bands; however, previous work [Riesser et al., 1984] and our experience indicated that the correction required was small and was not of significance for the conclusions drawn from the present study.

Table 3.4   Areas[a] of five component bands in the aliphatic **CH** stretch region of the IR spectra of Australian coals.

Coal	Band position (cm^{-1})				
	2950	2922	2895	2865	2850
ABL1	47.31	43.32	14.30	27.76	25.22
ABL2	59.73	172.38	62.38	217.51	104.32
ABL3	168.12	484.10	77.95	326.45	232.83
ABL4	32.32	65.20	96.57	197.62	71.58
ABL5	40.74	184.43	17.38	172.72	57.08
ABL6	148.65	292.44	76.64	454.92	230.33
ABL7	61.11	185.24	100.54	153.02	63.00
ABL8	52.76	97.41	55.99	257.99	40.16
ABL9	179.97	358.02	135.51	592.01	56.08
ABL10	186.34	329.34	181.46	405.09	141.66
ABL11	201.39	455.45	106.33	705.70	89.78
ABL12	77.15	259.28	59.69	312.89	33.19
ABL13	201.32	345.97	120.49	450.22	62.82
ABL14	148.39	325.56	71.42	477.82	68.26
ABL15	194.98	449.45	156.13	517.86	75.20
ABR1	102.14	151.73	33.07	161.88	23.72
ABR2	102.14	161.78	24.14	224.51	32.77
ABR3	219.77	260.53	36.75	272.48	35.55
ABR4	346.71	300.61	78.88	272.74	43.22
ABR5	392.36	354.55	81.81	305.84	57.61
ABR6	553.88	431.50	81.22	351.11	70.86
ABR7	691.30	478.04	123.88	372.54	98.48
ABR8	610.86	513.05	124.93	552.91	68.42
ABR9	857.82	487.59	127.81	427.63	115.40
ABR10	1027.19	642.66	188.93	556.60	80.18
ABR11	1171.32	746.27	241.97	575.30	117.65
ABR12	1190.72	558.89	129.12	496.00	136.40
ABR13	1681.25	662.25	147.87	592.20	199.40
ABR14	2371.25	692.94	174.80	785.47	180.04

[a] In absorbance cm^{-1}.

The aliphatic hydrogen contents of all samples were determined by relating the integrated intensities of the two bands to the elemental analysis value of the hydrogen content, H_{tot}, [Riesser et al., 1984] as follows :

$$H_{al} = (H_{tot} - H_{OH} - H_{COOH}) / (H_{ar}/H_{al} + 1) \qquad (3.1)$$

where H_{al} and H_{ar} are the aliphatic and aromatic hydrogen contents, H_{OH} and H_{COOH} are the hydrogen contents for phenolic and carboxylic H_{tot} is the total hydrogen content of the coal, representing all functional groups. groups. / The value of $H_{OH} + H_{COOH}$ is determined from the results of non-aqueous titration experiments [Redlich et al.,1989a]. All these values are expressed on a wt.% dmif coal basis. For the asphaltene and residue samples the term H_{COOH} is assumed to be negligible. This assumption is supported by the low intensity of the band at approximately 1700 cm^{-1} for the two types of samples. The amount of phenolic hydrogen was estimated from a calibration curve established using the intensity at 3200 cm^{-1} and the phenolic hydrogen content determined from non-aqueous titrations for a number of asphaltene samples (see Table 3.1). The ratio H_{ar}/H_{al} was calculated from the integrated intensities and average extinction coefficients for the two regions. The extinction coefficients used in this study were 853 abs. cm^{-1} mg/cm^2 and 225 abs. cm^{-1} mg/cm^2 for the aliphatic and aromatic regions respectively. They were derived from the FTIR spectra of model compounds as reported by Solomon and Carangelo [1981]. They found the extinction coefficients to be in good agreement with the values determined from the spectra of coals and coal products. The choice of average extinction coefficients is an inherent deficiency of the IR method when applied to complex materials; however, at the present time this procedure is the most acceptable one available.

The aromatic hydrogen content of the sample can be obtained by replacing the term H_{ar}/H_{al} in equation (3.1) with H_{al}/H_{ar}. The hydrogen contents were also expressed on an atomic percent basis, when relevant, using the following expression :

$$H \text{ (at \%)} = [H \text{ (wt. \%)} . 100] / \Sigma_i a_i . A_i^{-1} \qquad (3.2)$$

where a_i is the weight percent of element i determined from elemental analysis and A_i is the atomic weight of element i. We considered that it is preferable to use hydrogen atomic percent values when correlating the data with other atomic properties such as atomic H/C and hydrogen weight percent values when correlating with extensive parameters such as liquefaction yields. However, similar scientific conclusions may be obtained from consideration of correlations based solely on weight percent data.

The aliphatic and aromatic hydrogen data for the coals are given in **Table 3.5**. As a consequence of the extremly small area of the aromatic **CH** band in the brown coal spectra, especially in the spectra of brown coals having a high **H/C** value, their H_{ar} values are subject to the largest uncertainties. The relevant data for the asphaltenes and the liquefaction residue are reported in **Table 3.6** and **Table 3.7** respectively.

The integrated intensity of the aliphatic carbon-hydrogen stretch for each of the coals is plotted against the coal atomic **H/C** ratio in **Figure 3.17**. For the brown coals (▲) there is a strong trend between the two parameters, whereas, a considerable scatter in the data is found for the higher-rank coals (□). The results also show that the data for the higher-rank coals having **H/C** greater than 0.85 are on the trend of the brown coal data,
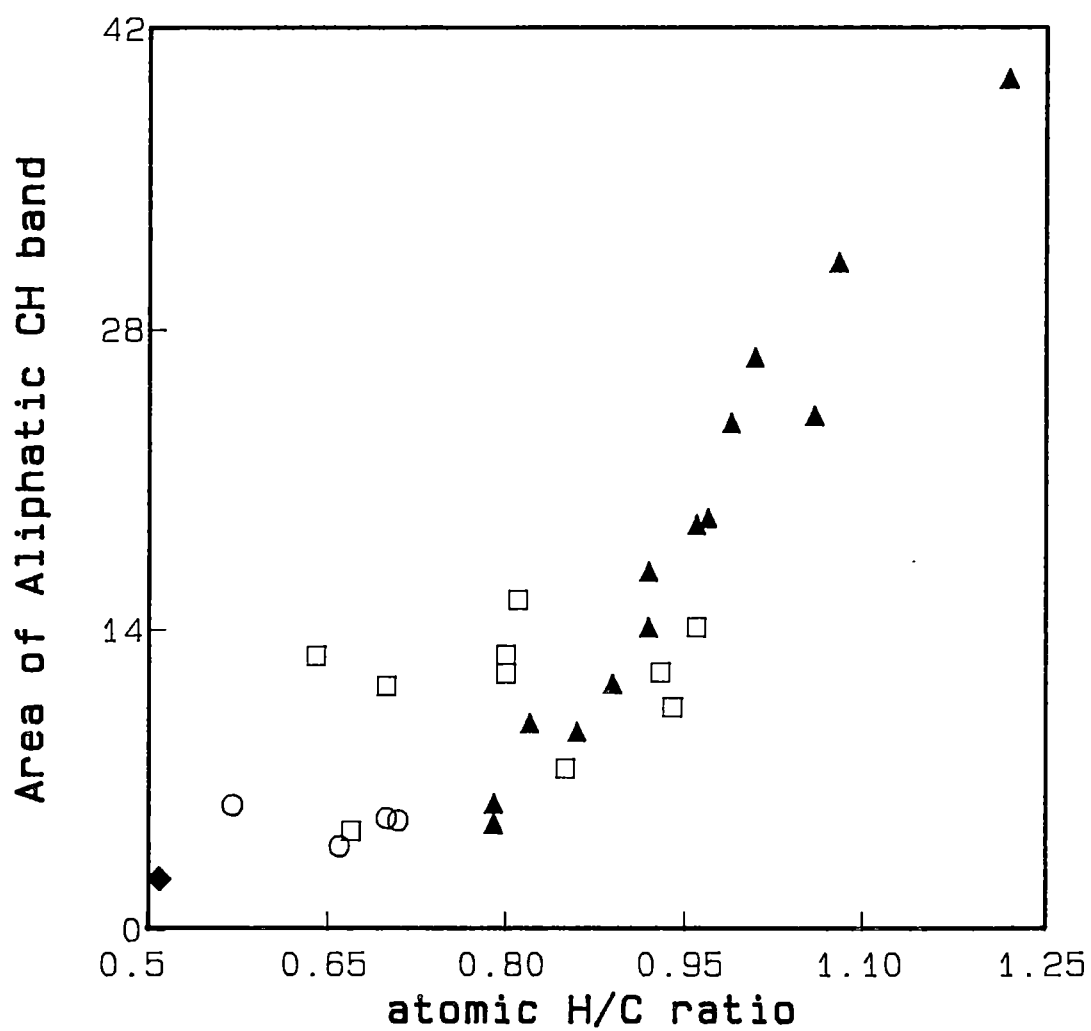
Figure 3.17 Plot of aliphatic **C-H** stretch band area against the atomic **H/C** ratio for Australian coals : ▲ , brown coals ; □ , higher-rank coals ; o , oxygen-rich subbituminous coals ; ◇ , semianthracite.

Table 3.5 Hydrogen distribution in Australian coals.

Coal	$^aH_{OH}$	H_{al}	H_{ar}	H_{al}	H_{ar}
		wt. %		at. %	
ABL1	0.02	1.21	2.62	10.33	22.30
ABL2	0.34	2.58	0.86	22.54	7.51
ABL3	0.06	3.25	1.43	25.92	11.44
ABL4	0.53	2.69	0.97	22.83	8.24
ABL5	0.22	3.23	1.27	26.01	10.20
ABL6	0.21	3.58	1.29	27.92	10.08
ABL7	0.55	3.25	0.52	27.50	4.40
ABL8	0.54	2.67	1.09	22.61	9.23
ABL9	0.28	4.07	1.20	30.85	9.10
ABL10	0.31	4.38	0.76	33.52	5.83
ABL11	0.30	4.70	0.60	35.53	4.52
ABL12	0.30	5.02	0.57	37.21	4.20
ABL13	0.44	5.07	0.48	37.59	3.57
ABL14	0.44	5.10	0.39	38.03	2.94
ABL15	0.33	5.60	0.38	40.57	2.78
ABR1	0.62	3.25	0.63	27.37	5.26
ABR2	0.60	3.35	0.59	28.02	4.98
ABR3	0.60	3.58	0.46	29.83	3.85
ABR4	0.55	3.88	0.34	32.04	2.84
ABR5	0.55	4.22	0.36	33.75	2.91
ABR6	0.48	4.47	0.25	35.71	1.99
ABR7	0.63	4.43	0.23	35.04	1.84
ABR8	0.55	5.06	0.19	38.36	1.42
ABR9	0.56	4.87	0.17	37.70	1.28
ABR10	0.52	5.23	0.15	39.43	1.12
ABR11	0.47	5.37	0.11	40.34	0.86
ABR12	0.57	5.49	0.13	40.61	1.00
ABR13	0.62	5.68	0.10	41.41	0.70
ABR14	0.70	6.43	0.05	44.64	0.32

^{a}Acidic hydrogen as in **-COOH** and **-OH** groups, from non-aqueous titration.

Table 3.5 Hydrogen distribution in asphaltenes (405 °C in tetralin) derived from Australian coals.

Coal	H/C	^{a}H$_{OH}$	H$_{al}$	H$_{ar}$	H$_{al}$	H$_{ar}$
			wt. %		at. %	
ABL2	0.79	0.49	3.28	1.79	25.04	13.70
ABL3	0.77	0.27	3.41	1.93	25.52	14.46
ABL4	0.84	0.53	3.72	1.57	28.19	11.90
ABL5	0.87	0.42	4.64	1.11	33.53	8.02
ABL6	0.85	0.32	4.25	1.60	30.64	11.51
ABL8	0.85	0.54	3.69	1.71	27.48	12.72
ABL10	0.86	0.45	4.56	1.04	33.32	7.57
ABL12	0.94	0.43	5.15	1.02	36.22	7.18
ABL13	0.92	0.49	4.87	0.97	34.99	6.99
ABL14	0.94	0.50	5.25	0.84	36.99	5.91
ABL15	0.96	0.48	5.32	0.87	37.30	6.07
ABR2	0.86	0.59	3.89	1.33	29.01	9.93
ABR3	0.87	0.68	4.07	1.08	30.31	8.06
ABR4	0.87	0.71	4.16	1.00	30.94	7.45
ABR5	0.88	0.59	4.30	0.94	32.07	7.03
ABR6	0.87	0.64	4.16	0.95	31.30	7.13
ABR9	0.89	0.55	4.41	1.08	32.35	7.96
ABR10	0.91	0.53	4.77	0.83	34.82	6.07
ABR11	0.90	0.62	4.70	0.74	34.48	5.41
ABR12	0.89	0.60	4.82	0.67	35.24	4.88
ABR13	0.90	0.55	4.64	0.90	33.96	6.57
ABR14	0.96	0.53	5.14	0.79	36.68	5.63

^{a}Acidic hydrogen mainly as in **-OH** groups , from calibration in **Figure 3.4.**

Table 3.6 Hydrogen distribution in residues(405 °C in tetralin) from Australian coals.

Coal	H/C	^{a}H$_{OH}$	H$_{al}$	H$_{ar}$	H$_{al}$	H$_{ar}$
			wt. %		at. %	
ABL3	0.60	0.35	2.77	1.42	22.29	11.45
ABL5	0.59	0.41	3.02	0.87	24.92	7.20
ABL6	0.66	0.32	3.30	1.37	25.71	10.64
ABL10	0.72	0.44	3.58	0.91	28.38	7.22
ABL11	0.72	0.45	3.32	1.22	26.17	9.61
ABL15	0.85	0.28	4.75	0.94	34.89	6.07
ABR2	0.59	0.40	2.40	1.35	20.16	11.31
ABR3	0.63	0.54	2.81	0.98	23.34	8.13
ABR4	0.64	0.49	2.56	1.32	21.19	10.93
ABR7	0.67	0.52	3.00	1.06	24.58	8.68
ABR8	0.66	0.55	3.07	0.95	25.00	7.75
ABR9	0.67	0.38	3.00	1.17	24.53	9.55
ABR11	0.67	0.55	3.11	0.94	25.33	7.62
ABR13	0.68	0.51	2.99	1.08	24.46	8.79
ABR14	0.75	0.49	3.55	0.85	28.47	6.82

^{a}Acidic hydrogen mainly as in **-OH** groups , from calibration in **Figure 3.4.**

while coals with **H/C** less than 0.85 show a greater aliphatic **CH** peak area than their brown coal counterparts. The strong relationship between the aliphatic peak area and the **H/C** ratio observed for the brown coals indicates that the aliphatic structure in these coals is somewhat uniform across the samples studied compared to that in the higher-rank coals. This interpretation is consistent with a guest-host model for brown coals [Redlich et al., 1985].

The atomic percent aliphatic hydrogen content of the coal as defined by **equation (3.2)** was correlated to the **H/C** ratio in **Figure 3.18**. A good trend of increasing aliphatic hydrogen content with an increase in the coal **H/C** value is evident for the brown coals. A similar analysis was undertaken for the higher-rank coals. A scatter in the data for the higher-rank coals was still found although it is not as pronounced as in **Figure 3.17**. This scatter is probably a reflection of a variability in the aliphatic structure of these coals. All the higher-rank coals studied have a higher aliphatic hydrogen content than do the brown coals with a similar **H/C** value. This observation is due to differences in the nature of the aliphatic groups and to variations in the aromatic and polycyclic structures of brown versus higher-rank coals especially in relation to oxygen containing functional groups.

In the earlier studies [Redlich et al., 1985; Redlich et al., 1989b] on the hydroliquefaction potential of this suite of coals, a guest-host model was proposed as a convenient first order model to describe the liquefaction behaviour of brown coals. It was found that the oil yields showed a strong correlation with the **H/C** values of the coals (see also **Chapter 2**). Therefore, the relationship between the aliphatic content and the liquefaction yield data was examined.
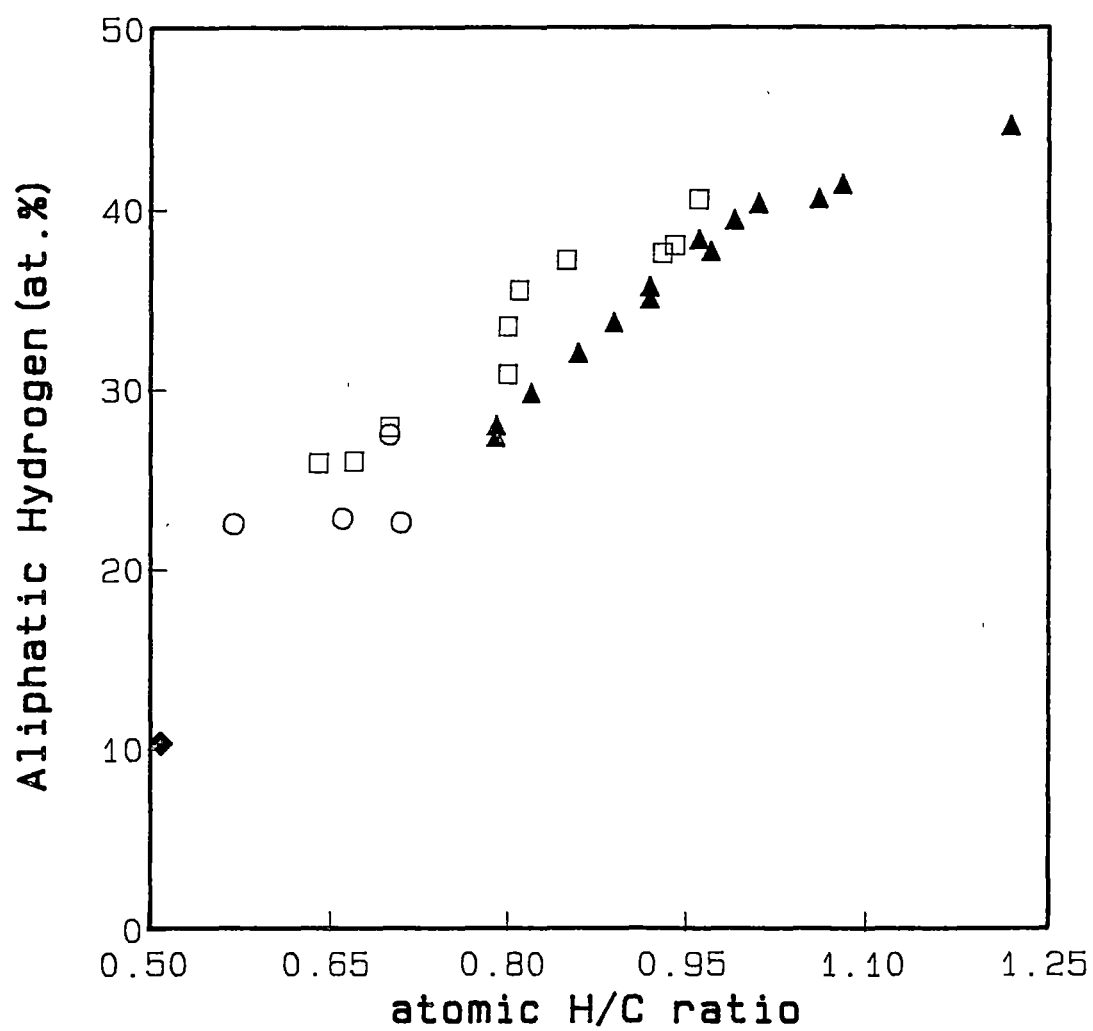
Figure 3.18 Plot of atomic percent aliphatic hydrogen content against atomic **H/C** value for Australian coals (see **Figure 3.17** for symbols)

Figure 3.19 displays plots of oil yield and total yield of hydrocarbon products (oil + asphaltene + hydrocarbon gases) as a function of wt. percent aliphatic hydrogen content.

GC-MS analyses of the oils from the brown coals have confirmed that long chain hydrocarbons are the predominant aliphatic compounds present in the oil [Chaffee et al., 1986]. A good correlation between the oil yield and the aliphatic hydrogen content as observed for the brown coals supports the conclusion that long chain aliphatic species are probably a major proportion of the aliphatic groups in these coals. These groups account for the variation in coal H/C value and the conversion to oil. According to the liquefaction study these long chain alkyl groups are mainly present in the guest component of the coals [Redlich et al., 1985]. It has been shown that a significant concentration of long chain alkyl groups is present even in a bituminous coal [Snape et al., 1985].

GC-MS analyses of the oils obtained from the higher-rank coals also show a distribution of aliphatic structures similar to those found in the oils of brown coals [Chaffee et al., 1986]. The dependence of oil yield on the aliphatic hydrogen content observed for the higher-rank coals is support for a model in which some higher-rank coals contain a substantial amount of long alkyl chains which can be found in the oil fraction of the liquefaction product. These long chain aliphatics are considered to be strongly bound or incorporated into the aromatic structure [Redlich et al., 1989b]. The separate trend of increasing, but lower oil yield, with aliphatic hydrogen content indicates that the higher-rank coals may also contain other types of aliphatic groups in a large proportion. Since these groups, including the long chain aliphatics, are bonded to the aromatic structures, they may be converted to product asphaltene or remain in the residue.

Figure 3.19 Relationships between the yields of liquefaction products and wt. percent aliphatic hydrogen contents for Australian coals.

Oil yield : ▲ , brown coals ; □ , higher-rank coals ; ○ , oxygen-rich subbituminous ; ◇ , semianthracite.

Total hydrocarbon products : △ , brown coals ; ■ , higher-rank coals ; ● , oxygen-rich subbituminous ; ◆ , semianthracite.

Some of these aliphatic groups may function as linkages for the aromatic structures, thus the availability of the groups is also important for the reactivity of these coals. The plot for the total hydrocarbon products (**Figure 3.19**), which shows the data of most coals now lying on a single trend, supports the proposal.

The good correlations between the total hydrocarbon products and aliphatic content, as shown in **Figure 3.19** , may be useful for predicting the conversion reactivity of a coal. One sample in this study, a **Yarrabee** (**ABL1**, **H/C** = 0.51) semianthracite, showed a very low reactivity at least under the liquefaction condition used in this study. This is not unexpected since it contains an extremely low aliphatic hydrogen content and a low concentration of oxygen (3.1 wt %). A sample of low volatile bituminous coal, **Bulli** (**ABL3**, **H/C** = 0.64), also showed a low conversion especially to asphaltene, in spite of having quite a high aliphatic hydrogen content (see **Figure 3.19**). In this bituminous coal the predominant aliphatic structure is probably a very short alkyl chain or a methyl group. Examination of the maceral characteristics of coals given in Appendix A, shows that there is a little correlation between total conversion and inertinite content. It is concluded that the evidence supports the view that the conversion behaviour of a coal is not simply dependent upon the amount of aliphatic groups in the coal, but it is also dependent on the structural details of those aliphatic groups.

The dissimilarity between the structural features of brown coals and higher-rank coals discussed above, is illustrated more clearly in the variation in the structural characteristics of the asphaltenes and residues. The results in **Figure 3.20** demonstrate that for the asphaltenes and residues there is a relatively small variation in atomic percent aliphatic hydrogen content with the **H/C** values of the parent brown coals as

compared to those for the coals. Since the asphaltenes and residues are mainly derived from the macromolecular host component, this finding strongly supports the inference that the main contributor to the change in brown coal **H/C** values and thus to the variation in coal liquefaction reactivity is the amount of guest material (see **Chapter 2**). The small variations of aliphatic hydrogen content in the asphaltenes and residues are probably due to the unremoved guest material which has interacted with the host component. In contrast, the results for higher-rank coals in **Figure 3.21** show that the atomic percent aliphatic hydrogen contents in the asphaltenes and residues depend more strongly on the coal **H/C** values in a similar manner to the data for the parent coals. This observation supports the view that to first order a guest-host model is not appropriate for describing the structural features of the high-rank coals.

The differences between the aliphatic hydrogen content in the coals and in the products are clearly seen in **Figure 3.22** where the ratios of the atomic percent aliphatic hydrogen contents in the asphaltenes and residues to that in the corresponding coal were plotted against atomic **H/C** ratio of the coal. For the brown coals the ratios of aliphatic content for both asphaltene and residue decrease as a function of coal **H/C** values. Liquefaction results in oxygen elimination from the coal as well as removal of the aliphatic-rich component into the oil fraction. Oxygen elimination may lead to an increase in aliphatic hydrogen while removal of guest material is expected to decrease the aliphatic hydrogen in the residual asphaltene or residue. Most brown coals have high oxygen contents and are rich in guest material. The evidence in **Figure 3.22** supports the conclusion that in general the guest-removal effect is more dominant.
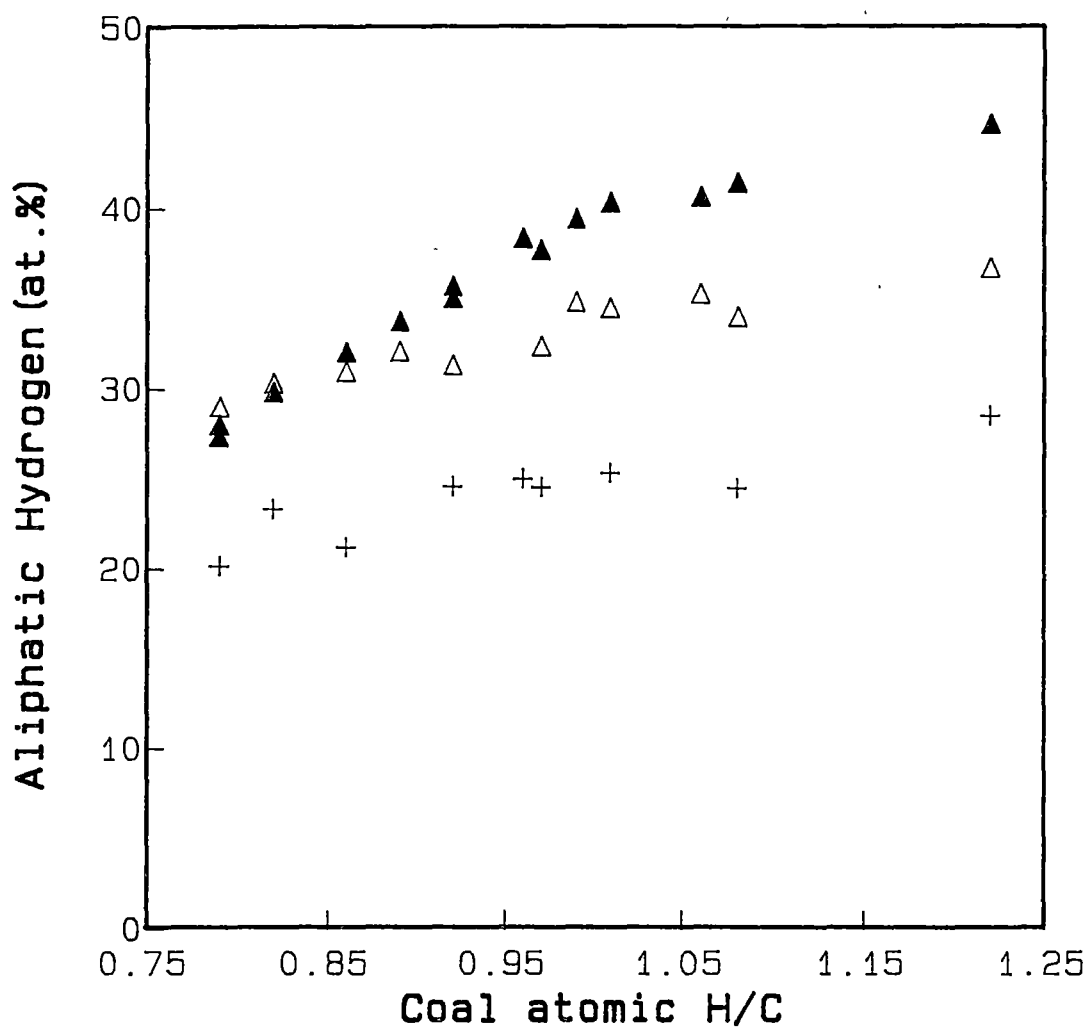
Figure 3.20   Plot of atomic percent aliphatic hydrogen contents in Australian brown coal (▲), asphaltene (△) and residue (+) versus atomic H/C ratio of the parent coal..
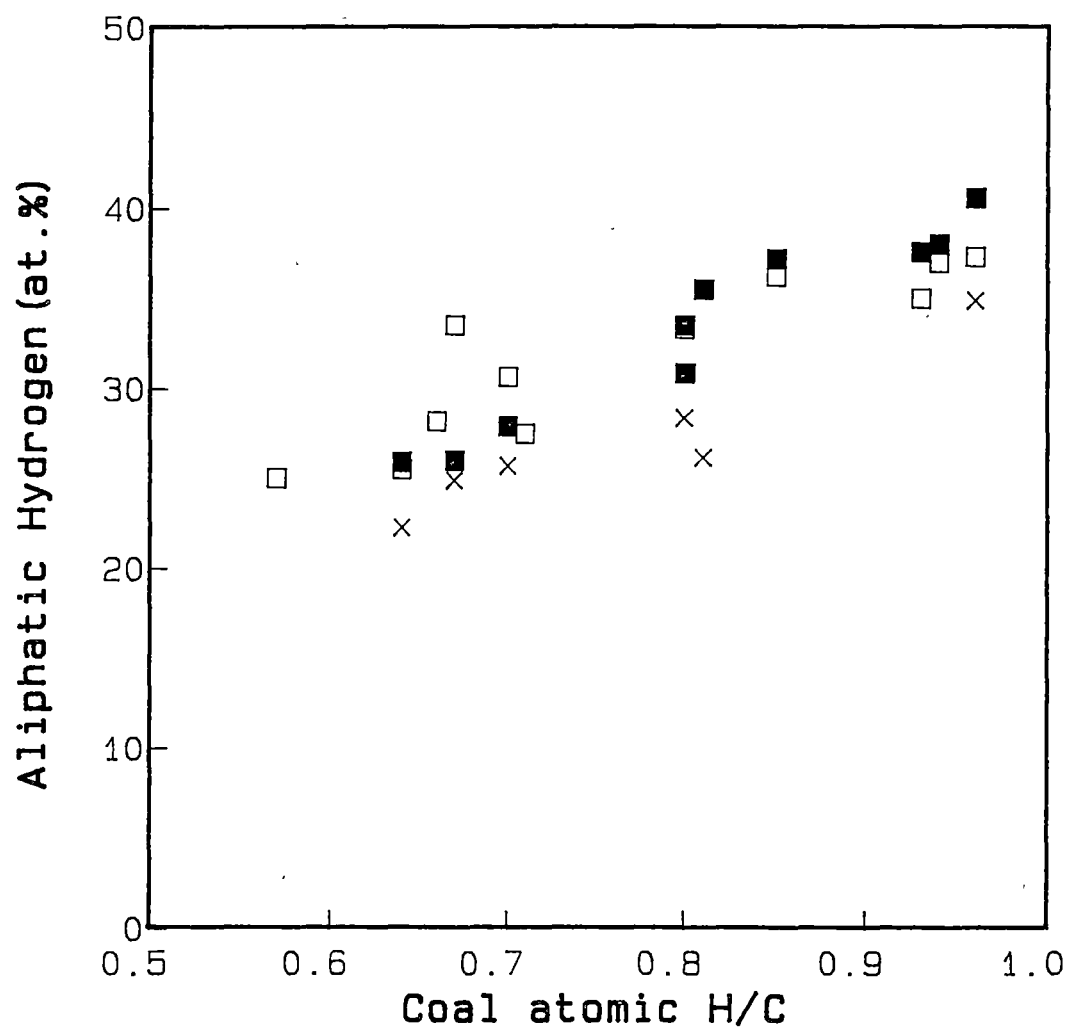
Figure 3.21 Plot of atomic percent aliphatic hydrogen content in Australian higher-rank coal (■), asphaltene (□) and residue (x) versus atomic H/C ratio.of the parent coal.
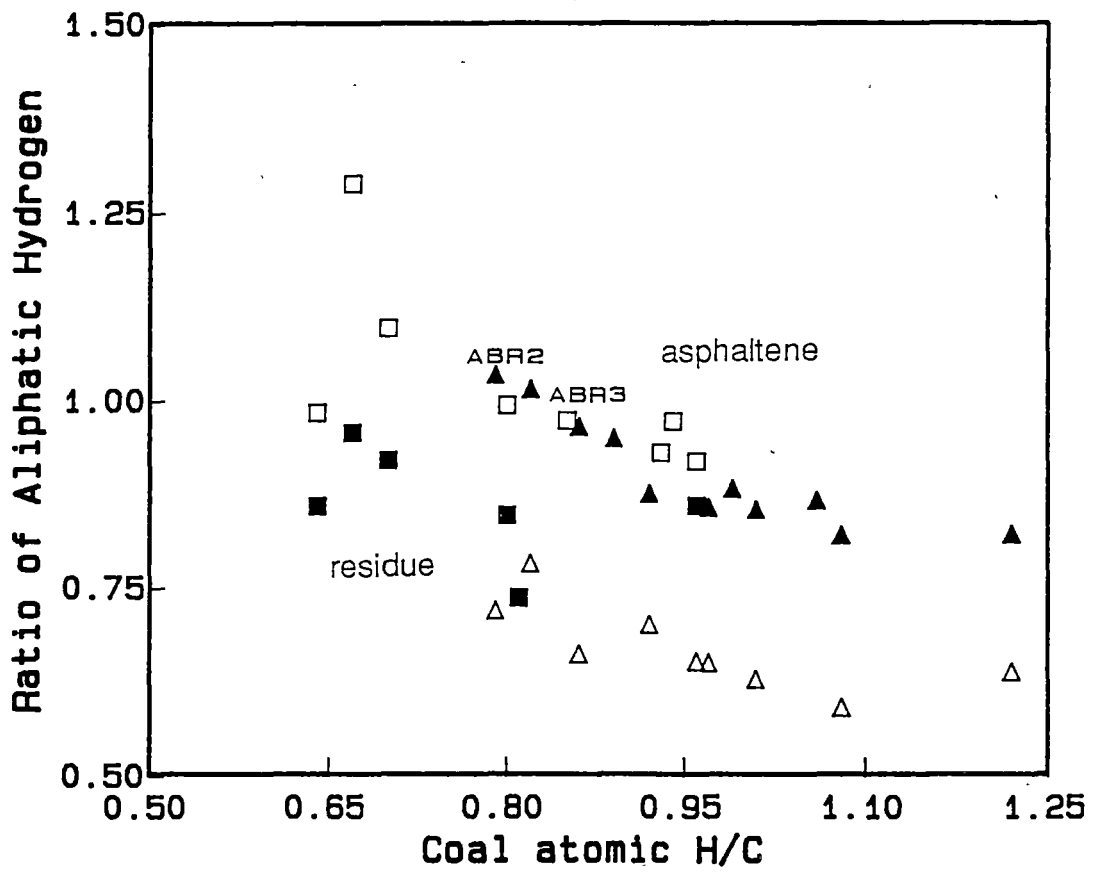
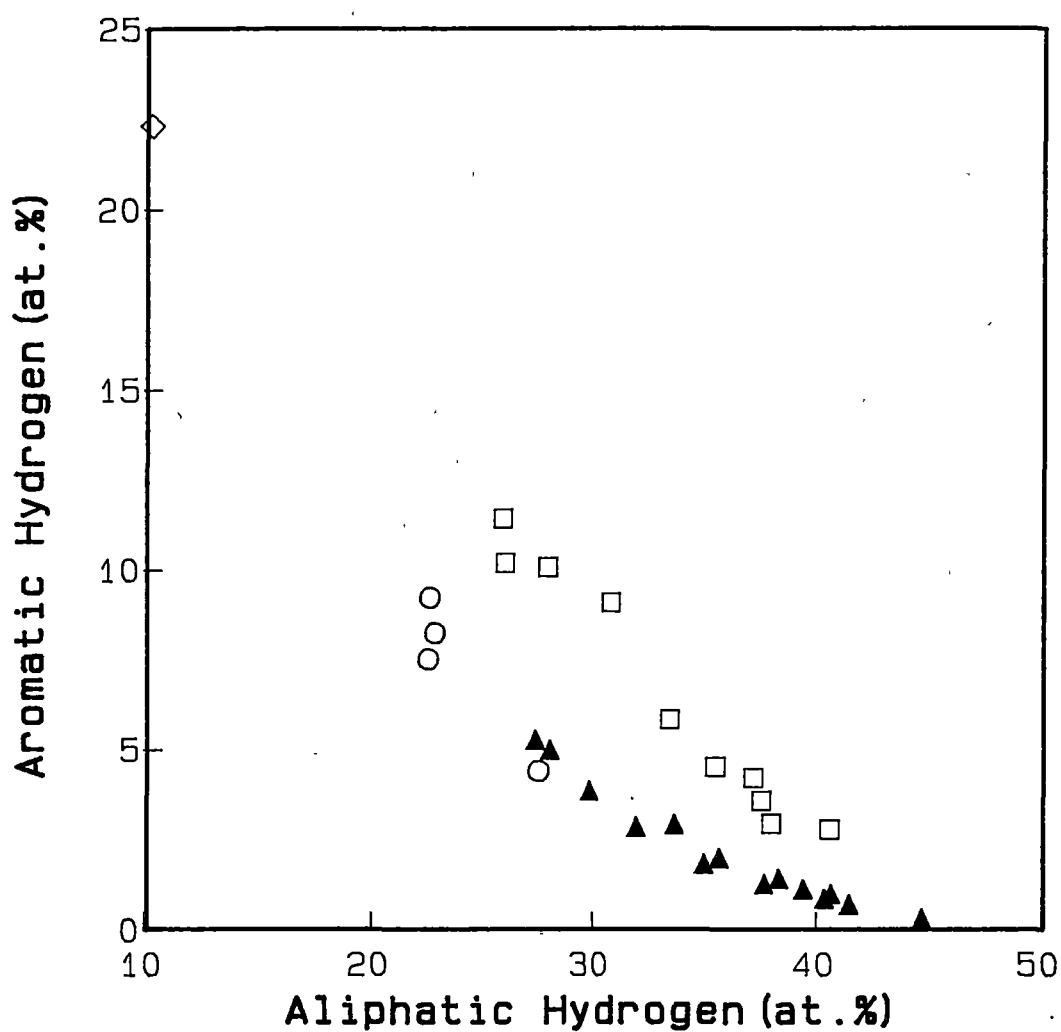**Figure 3.22** Plot of ratio of atomic percent aliphatic hydrogen content of asphaltene to that of coal (▲, brown coals ; □ , higher-rank coals) and ratio of atomic percent aliphatic hydrogen content of residue to that of coal (△ , brown coals ; ■ , higher-rank coals).

However, for two brown coals with a low guest material content (**Rosedale 29, ABR2** and **Rosedale 7, ABR3**) the asphaltenes are richer in aliphatic hydrogen than the parent coals. In these cases the oxygen-removal effect is dominant. For the higher-rank coals, there is no such a clear trend in the asphaltene data, especially for **H/C** values less than 0.7.

The residue samples which are assumed to be unreacted material from the coals or repolymerized products [Hooper and Evans, 1978] have a lower concentration of aliphatic hydrogen than do their parent coals for both brown and higher-rank coals.

The relationship between the aromatic and aliphatic hydrogen contents for coals on an atomic percent basis is shown in Figure 3.23. The trend is for decreasing aromatic hydrogen content as the aliphatic hydrogen content increases. Since the latter increases with atomic **H/C** ratio (**Figure 3.18**) the aromatic hydrogen content decreases as the atomic **H/C** ratio increases. The higher-rank coals contain a higher aromatic hydrogen content than do the brown coals with a similar aliphatic hydrogen content and similar atomic **H/C** value. It was noted earlier that higher-rank coals also contain a higher aliphatic content than brown coals of similar atomic **H/C** (**Figure 3.18**). This apparent contradiction arises because of the higher oxygen contents in the brown coals. When coals with similar non-oxygenated hydrogen contents are compared ,i.e., when they have a similar $H_{tot} - H_{OH} - H_{COOH}$ value, then the higher-rank coal has a higher aromatic hydrogen content and the brown coal has a higher aliphatic content. This finding is consistent with a representation for coal in which the higher-rank coals have a greater concentration of aromatic ring structures as part of the basic macromolecular network.

Figure 3.23 Relationship between atomic percent aromatic hydrogen content and atomic percent aliphatic hydrogen content for Australian coals: ▲ , brown coals ; □ , higher-rank coals ; o , oxygen-rich subbituminous coals; ◇ , semianthracite.

Because of the interrelationship between H_{ar} and H_{al} no new scientific conclusions can be drawn from a comparison of H_{ar} with the liquefaction yield data. Comparison of the data in **Table 3.5** with that presented in **Tables 3.6** and **3.7** reveals that asphaltenes and residues generally contain higher aromatic hydrogen contents than the parent coal.

Data concerning aromatic hydrogen contents, especially for brown coals with atomic **H/C** values greater than 0.9, must be treated with caution because of the low absolute values resulting in difficulties in area measurements and because of uncertainties with extinction coefficient values.

3.4   CONCLUSIONS

The FTIR data in the aromatic and aliphatic **C-H** stretching, **O-H** bending and **C=O** stretching regions for a suite of Australian coals and their liquefaction products have been investigated.

The relationship of the absorbance at 3200 cm^{-1}, associated with hydroxyl groups, to **O/C** values and to acidic-oxygen contents determined by non-aqueous titration has been determined for the coal and asphaltene samples. The good relationship between the absorbance at 3200 cm^{-1} and the acidic-oxygen contents suggest that the calibration may be used to estimate acidic oxygen contents in higher-rank coals or coal related samples. For the brown coals there is no clear trend.

The results of least-square curve fitting techniques applied to the carbonyl stretching region for the coals revealed the presence of esters, carboxylic

acid and ketonic groups in the coals studied. For the higher-rank coals, the contents of the carbonyl functional groups, as measured from the band areas, are related to the oxygen contents in the coals, whereas the results for the brown coals showed no simple relationship of the data. The brown coals having oxygen contents mainly > 24 wt% contain less guest material and have a lower concentration of carbonyl groups both as acids and esters than brown coals with a lower oxygen content. The brown coals with a high oxygen content contain a significant amount of non-acidic oxygen principally as ethers. The carbonyl groups in the coals were removed as carbon oxide gases by the liquefaction reaction. However, for the brown coals the results supported the view that there could be other sources of carbon oxide gases in coal structures such as the methoxyl groups and that ester groups do not significantly decarboxylate or decarbonylate under the reaction conditions.

The FTIR data in the **C-H** stretching region have been used to estimate the aliphatic and aromatic hydrogen contents in the Australian coals and their asphaltenes and residues, resulting from liquefaction reactions. The aliphatic hydrogen contents in the coals are strongly correlated with coal **H/C** values and with the yields of liquefaction products. Different trends were observed for the higher-rank coals and for the brown coals. The aliphatic structure of the two categories of coals are dissimilar.

The variation in aliphatic and aromatic hydrogen contents in the asphaltenes and in residues from the brown coals is remarkably small. This finding is consistent with a model for brown coal in which variations in coal **H/C** values and liquefaction reactivities are directly related to the amount of guest material. The host component of the brown coals is considered to be rather homogeneous. By way of contrast,

the aliphatic and aromatic hydrogen contents in the asphaltenes and residues from the higher-rank coals are more strongly correlated with coal **H/C** values. For the higher-rank coals, this finding is more consistent, to first order, with a structural representation that the aliphatic material is incorporated as an integral part of the macromolecular matrix.

CHAPTER FOUR

SOLID-STATE ^{13}C NMR STUDIES

of

AUSTRALIAN COALS

4.1 INTRODUCTION

Detailed solid-state ^{13}C nmr studies of the 29 Australian coals are reported in this Chapter. The experiments have been carried out at a magnetic-field-strength of 7.05 T by using the combined technique of CP/MAS/HPPD in conjunction with a TOSS pulse sequence. Modifications of the standard TOSS sequence have been made for the dipolar-dephasing (DD) experiment. With the high-field spectrometer and the techniques used, various carbon types have been identified. Cross-polarization dynamics in the coals have been investigated by means of variable contact time experiments. The methods provided more accurate measurements of carbon fractions in the samples. Carbon distributions in the coals have been determined from the TOSS and TOSS/DD spectral data. Additional structural parameters related to aromatic structures, namely, the degree of substitution of aromatic rings and the average aromatic cluster size have been estimated. The values of relaxation time constants related to the cross-polarization and dipolar dephasing are reported.

The relationships between the estimated structural parameters and elemental compositions of the coals are examined in the light of the general structural features of the coals studied.

4.2 EXPERIMENTAL DETAILS

All solid-state ^{13}C nmr experiments were carried out on a **Bruker AM300** spectrometer equipped with 7.05 T superconducting magnet and a **Spectrospin** single-coil double-tuned solid-state probe. A double-air-bearing system was used to control a magic-angle spinning. **Figure 4.1** illustrates diagrammatically the general configuration of the system.

An alumina rotor (99.5%) capped with **Kel-F** spinner was used as a sample holder. In all experiments, a MAS speed of 3.000 ± 0.005 kHz was employed. The magic angle was set by monitoring ^{79}Br FID from a mixture of **KBr** and **adamantane**. The **Hartmann-Hahn** matching condition for the ^{1}H-^{13}C cross-polarization was obtained by adjusting the power of the ^{1}H channel for a maximum ^{13}C FID signal of **adamantane**.

In general the acquisition parameters were as follows:

- quadrature detection for 1K and zero-filled to 16K
- 29.4 kHz spectral width and 36.8 kHz filter width
- 3000-5000 signal averages
- 5-6 μs 90° ^{1}H pulse width and 2 s repetition time
- 1 ms contact time.

All FID spectra were Fourier Transformed (FT) with a line broadening of 50 Hz. Chemical shifts were calibrated with respect to tetramethylsilane by using hexamethylbenzene as a secondary standard.
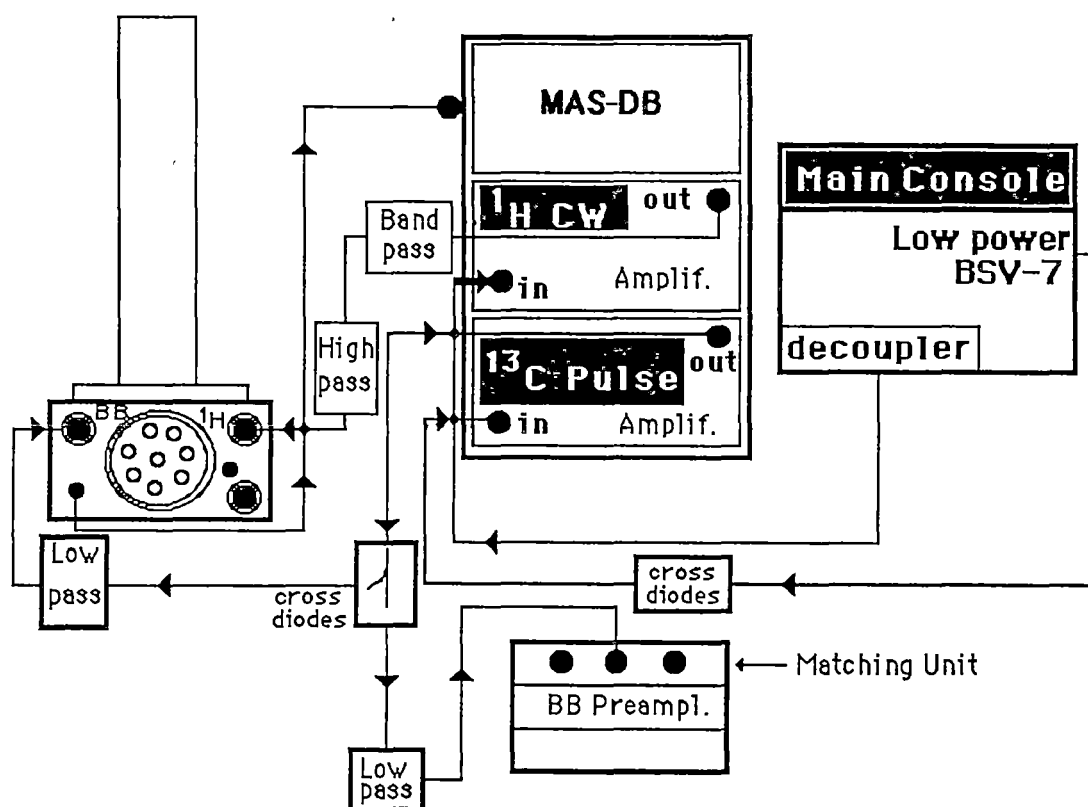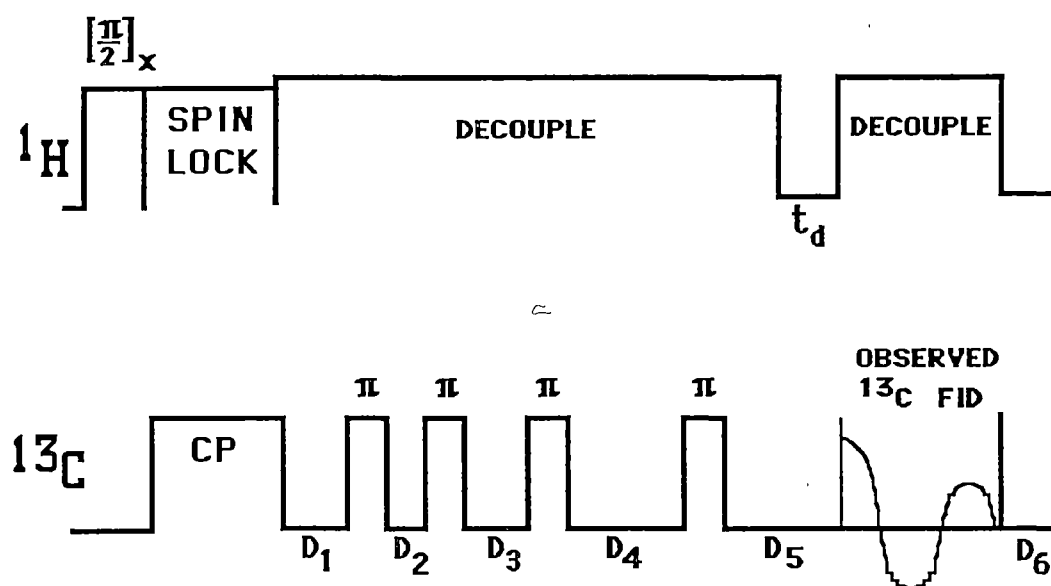
Figure 4.1 A general configuration of the system for solid-state ^{13}C nmr experiments.

Since the TOSS result is very sensitive to pulse errors and delays, in this study the 180° ^{13}C pulse width and the delay between the last pulse and acquisition time were adjusted by monitoring the sidebands of aromatic carbons in hexamethylbenzene sample for minimal intensities. This procedure was conducted during every experimental session prior to sample measurements. The 180° ^{13}C pulse width was normally in the range 10.5 - 12 μs.

The dipolar-dephasing (DD) technique was implemented in the TOSS sequence by introducing a decoupler-off period in the last TOSS delay before the ^{13}C acquisition time (**D$_5$** in **Figure 4.2**). The decoupler was turned on again during the ^{13}C FID acquisition. As can be seen in the pulse diagram shown in **Figure 4.2**, among the five delays around the four 180° ^{13}C pulses the other two delays designated **D$_3$** and **D$_4$** are also long enough for a typical DD observation (> 40 μs). It has been reported that the DD results are independent on the placement of the DD time in the TOSS delay [Raleigh et al., 1987]. However, in this study we found that when the decoupler was gated off during the **D$_3$** or **D$_4$** period for longer than 60 μs, phasing artifacts were observed in the resulting FT spectra. The problem was not detected if the DD delay (**t$_d$**) was inserted during the **D$_5$** period. Moreover, the final delay, **D$_5$**, allows the dephasing delay to vary from 0 μs to approximately 250 μs. The delay length is sufficiently long for monitoring the dephasing of most aromatic and aliphatic ^{13}C signals in coals studied. In all DD experiments, a single contact time of 1 ms was used.

Analyses of the dipolar-dephasing and variable contact time data were performed by using a numerical method of non-linear least-squares to evaluate the relevant parameters. A general outline of the procedure has

been given by Mayne et al. [1975]. A similar method of error analyses of the estimates was used in this study. The numerical calculation was performed on a personal computer using a program written in Pascal language. The iteration procedure was based on an algorithm proposed by Marquardt [1963].

$$[\tfrac{\pi}{2}]_x$$

^{1}H SPIN LOCK DECOUPLE t_d DECOUPLE

^{13}C CP π π π π OBSERVED ^{13}C FID

D_1 D_2 D_3 D_4 D_5 D_6

$D_1 = 35.7$ μs, $D_2 = 15.7$ μs, $D_3 = 64.5$ μs, $D_4 = 337.7$ μs, $D_5 = 252.8$ μs, $D_6 = 2$ s.

**Figure 4.2** The pulse diagram for a TOSS/DD experiment.

4.3   RESULTS AND DISCUSSION

4.3.1   Coal spectra

In order to demonstrate the result of the TOSS technique, a comparison of TOSS and solution-state spectra of a model compound, **rutin**, has been made as shown in **Figure 4.3**. The solution-state spectrum (in **DMSO-D$_6$**) was acquired using an inverse-gated decoupling technique. The assignments were taken from Wenkert and Gottlieb [1977]. Although the resolution of the solid-state TOSS spectrum is not as good as the spectrum in the solution, it can be seen that substantial spectral details are still present in the solid-state spectum.

The normal TOSS and TOSS/DD spectra of representative brown coals and higher-rank coals are shown in **Figure 4.4** and **Figure 4.5** respectively. The TOSS/DD spectra were acquired with 45 μs dephasing delay.

The DD technique relies on a fundamental principle that in the absence of proton decoupling field, ^{13}C magnetizations will dephase or decay as a result of ^1H-^{13}C dipolar interaction. The rate of the dephasing of the ^{13}C signal is related to the magnitude of the dipolar interaction which, in turn, depends on geometrical factors, namely, the ^1H-^{13}C internuclear distance, r_{CH}, as r_{CH}^{-3} and to the angle θ, between the internuclear vector and the static magnetic field (see **Figure 4.6**) [Yannoni, 1982]. Therefore, in the DD spectrum with a long dephasing delay (> 40 μs), the resonances observed are mainly of non-protonated and weakly coupled carbons that have long decaying rates. The weakly coupled carbons also include carbons in the groups such as -**CH$_3$** that may have free molecular motion which can partially average the ^1H-^{13}C dipolar-interaction experienced by the carbon nuclei.
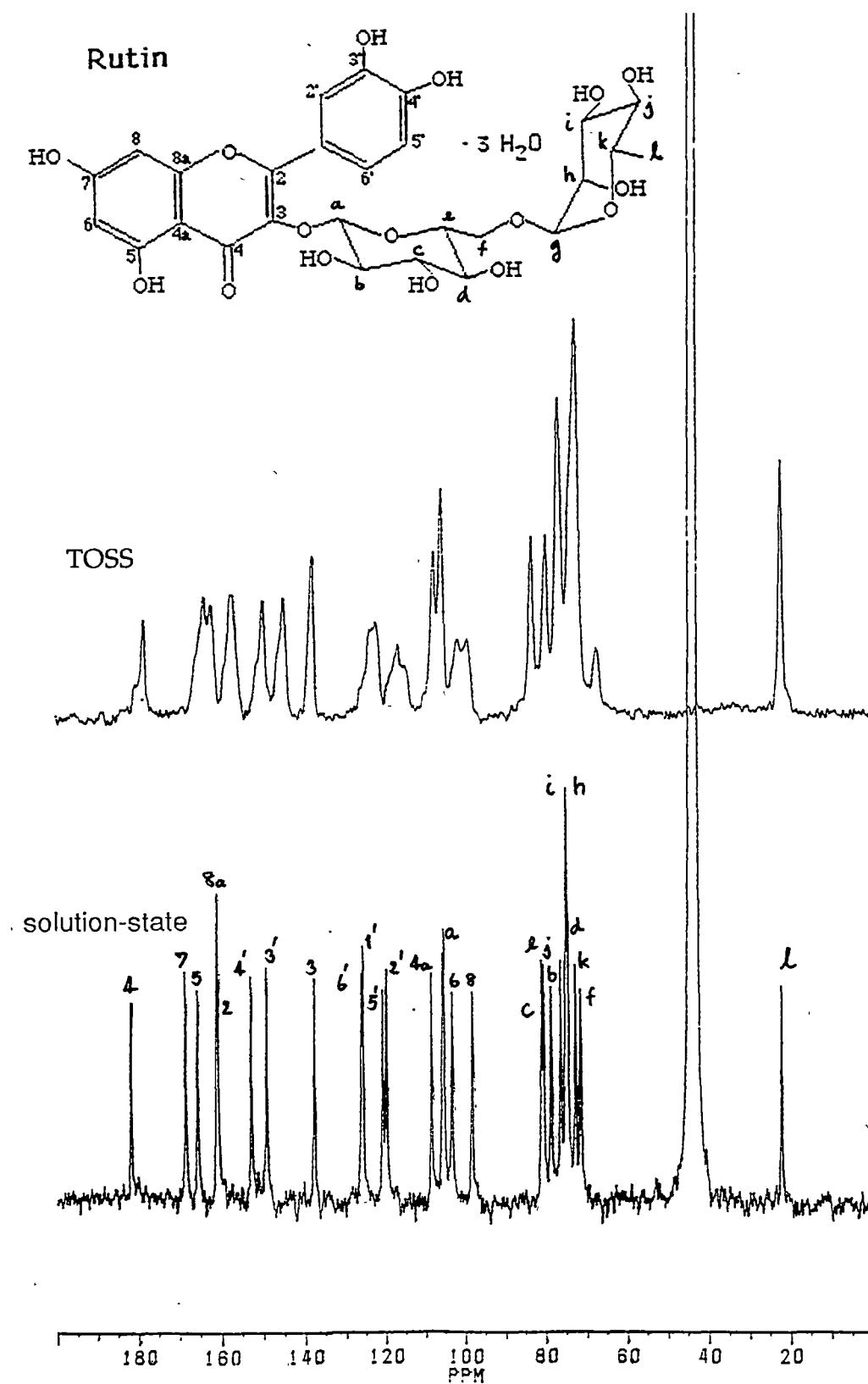
Figure 4.3 A comparison of TOSS and solution-state ^{13}C nmr spectra for a model compound, **rutin.**
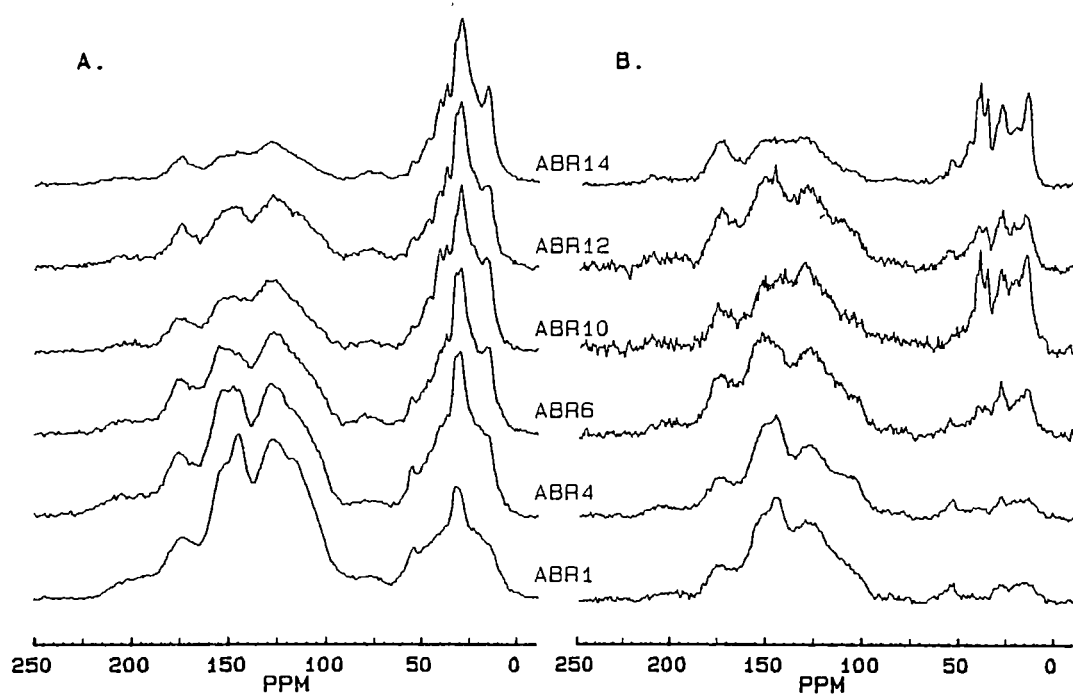
Figure 4.4 Selected TOSS (A) and TOSS/DD (B) spectra of brown coals: ABR1, H/C=0.79; ABR4, H/C=0.86; ABR6, H/C=0.92; ABR10, H/C=0.99; ABR12, H/C=1.06; ABR14, H/C=1.22.
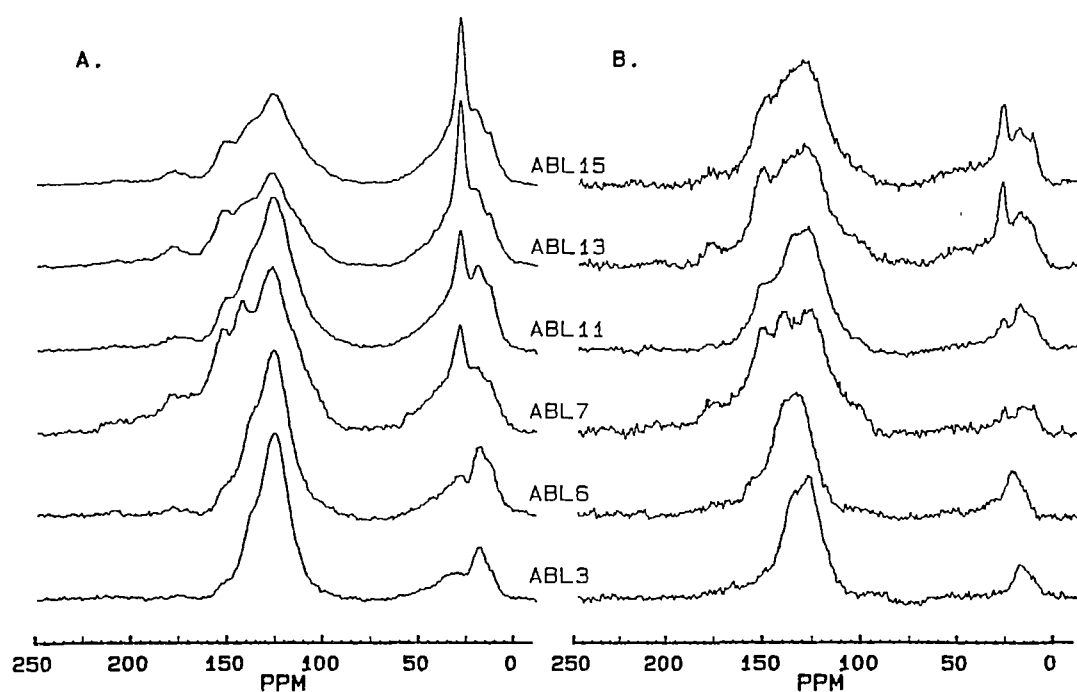
Figure 4.5 Selected TOSS (A) and TOSS/DD (B) spectra of higher-rank coals: ABL3, **H/C**=0.64; ABL6, **H/C**=0.70; ABL7, **H/C**=0.70; ABL11, **H/C**=0.81; AB13, **H/C**=0.93; ABL15, **H/C**=0.96.
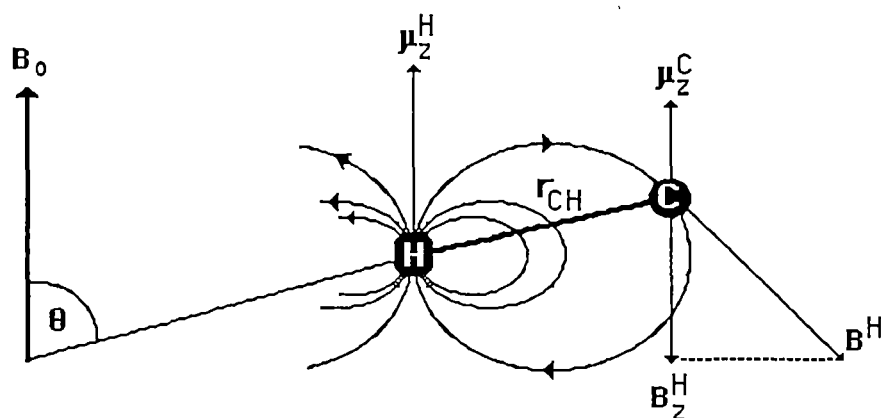
Magnitude of a dipolar interaction :

$$\Delta\omega_{CH} = \{\ \gamma_C \cdot \gamma_H / 2\pi . r_{CH}{}^3 \}\ .\ \hbar^2 .(1\text{-}3\cos^2\theta\ )$$

where γ_C and γ_H are ^{13}C and ^1H gyro—magnetic ratios respectively, r_{CH} is a carbon-hydrogen internuclear vector and θ is the angle between the internuclear vector and external field B_O.
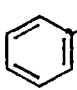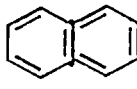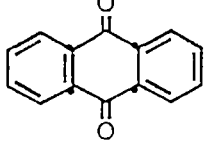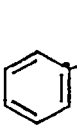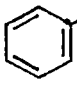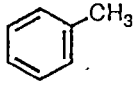
μ_Z^H and μ_Z^H are magnetic moments of ^1H and ^{13}C nuclei. ^{13}C nucleus experiences a field B^H generated by ^1H, with the z-component, B_Z^H, being antiparallel to external field B_O.

Figure 4.6   A diagram describing ^1H-^{13}C dipolar interaction (adapted from Yannoni, 1982).

Based on the dipolar-dephasing interpretation and on chemical-shift data reported by others [Pretch et al.,1983; Breitmaier and Voelter, 1974; Snape et al., 1979], various carbon functionalities in coals studied can be identified from the TOSS and TOSS/DD spectra. They are summarized in **Table 4.1**. In general the spectra of brown coals showed more spectral details than those of the higher-rank coals, suggesting the presence of a wider range of carbon functional groups in the brown coals. The weak signals between 210 ppm and 190 ppm, corresponding to carbonyl carbons in ketonic or aldehyde-type structure, can be distinguished from comparatively strong resonances of carboxyl carbons which appear between 190 ppm and 169 ppm. The observation is consistent with the FTIR studies which provided evidence for the presence of various carbonyl functional groups in the coals (see **section 3.3.2**). A prominent band at approximately 155 ppm, on the low-field end of the aromatic region (165 ppm - 95 ppm), can be observed in most coal spectra. The signals are associated with oxygenated-aromatic carbons. The resonances of alkyl-substituted aromatic carbons observed in the region of 145 ppm-135 ppm are also distinguishable from other aromatic resonances. The signals appear as a shoulder on the aromatic carbon band in most spectra except in the spectra of low **H/C** brown coals where the resonances appear as a pronounced peak (see **Figure 4.4**). A distinctive shoulder at the high-field end of the aromatic envelope was observed in all TOSS/DD spectra of the brown coal and some higher-rank coals that have a substantial carbonyl content. The resonances in this 115 ppm-100 ppm range can be attributed to aromatic carbons attached to carbonyl structures.

The fine structures in the aliphatic region (95 ppm - 0 ppm) are also of interest. The weak signals between 95 ppm and 65 ppm was found only in brown coal spectra. The resonances in this region have been assigned to

Table 4.1 Various carbon types observed in Australian coals.

Carbon type	Chemical shift (ppm)
$R-\overset{O}{\underset{\parallel}{C}}-R(H)$	220-195
$R-\overset{O}{\underset{\parallel}{C}}-O-R(H)$	195-169
(phenyl)$-O-R(H)$	169-145
(phenyl)$-R$	145-135
(naphthalene)	135-115
(anthraquinone) / (phenyl)$\overset{O}{\underset{\parallel}{C}}-O-R(H)$	115-100
(phenyl)$-H$	120-95
$R-CH_n-O-R$	95-75 [a]
$Ar-O-CH_3$	60-50 [a]
$R-\overset{R}{\underset{R}{C}}-H$	50-35
$R-\overset{R}{\underset{R}{C}}-R$	45-35 [a]
$R-CH_2-R$	35-25
$R-CH_3$ / (toluene) CH_3	25-0

[a] observed in brown coals only

aliphatic carbons attached to oxygens as in alcohols, ethers [Yoshida et al., 1982] and cellulose-like structures [Newman and Davenport,1986]. For our brown coals, a contribution to the peak from the alkyl carbons of ester groups is also probable, according to the observation of these functional groups from the FTIR studies (see section 3.3.2). A relatively strong peak at a higher field near 56 ppm was also observed only in the spectra of brown coal. The peak can be assigned to methoxyl carbon. This characteristic peak is a good evidence for the presence of lignin-like structures in brown coals. The intensity of this peak is more pronounced in the spectra of brown coals having a high oxygen content (low H/C values), indicating a high proportion of methoxyl groups in these coals (see Figure 4.4). The finding agrees with previous work which suggested that the brown coals with a high oxygen content contain a high concentration of non-acidic oxygens [Redlich et al., 1989a]. The resonances occurring at a higher field of aliphatic area are attributed to various aliphatic structures. The peaks in the 16 ppm-0 ppm region are resonances of terminal methyl groups of straight chain aliphatic groups while the signals on a lower field (27 ppm - 16 ppm) arise from methyl carbons attached to aromatic and alicyclic structures [Pretch et al., 1983]. Evidently the latter peaks are more prominent in the higher-rank coals, indicating the significance of methyl-substituted aromatic structures for the higher-rank coals (see Figure 4.5). However, it is also probable that some methylenic carbons in alicyclic structures can have resonances in the region [Breitmaier and Voelter, 1974]. The strongest signals generally observed in the aliphatic area are in the range between 36 ppm - 28 ppm. The distinctively sharp peak was found in the spectra of coals having high H/C values. The most probable aliphatic structures related to the peak are methylenic groups both as in straight chain aliphatics and in alicyclic compounds. The contribution from other -CH_n- groups in this region is

considered to be small based upon previous studies [Soderquist et al., 1987; Sfihi et al., 1986; Theriault and Axelson, 1988].

The DD spectra of the coals revealed that the signals in the 36 ppm - 28 ppm region are composed of two components of different decaying rates (see **Figure 4.7**). They were still observable in the spectra with dephasing delay longer than 100 μs. The fast decay can be related to **-CH$_2$-** groups, having a strong ^{1}H-^{13}C dipolar interaction while the slow component is associated with the relaxations of **-CH$_2$-** groups in the aliphatic structures having a free motion of the structures resulting in the reduction of the dipolar interaction in the groups. This interpretation is consistent with the dipolar-dephasing studies reported elsewhere for other coal samples [Soderquist et al., 1987; Sfihi et al., 1986; Theriault and Axelson, 1988].

Two sharp peaks in 45 ppm-35 ppm range were detected in some brown coal spectra (see **Figure 4.4**). Although many aliphatic carbons such as **-CH$_2$-** and **-CH-** can have resonances in the region, the results from dipolar dephasing studies suggested that the signals may arise from quaternary aliphatic carbons according to the variable dephasing-delay experiments which showed that the signals were observed in all DD spectra (see **Figure 4.7**). This type of carbon is common in terpenoids which were known to be present in the brown coals, according to GC-MS analyses of the oils from hydroliquefaction of these coals [Chaffee et al., 1986]. The two peaks are more prominent for brown coals having **H/C** greater than 0.97. However, the GC-MS study showed that no clear relationship existed between the concentration of terpenoid materials and the **H/C** ratio of the original coal.
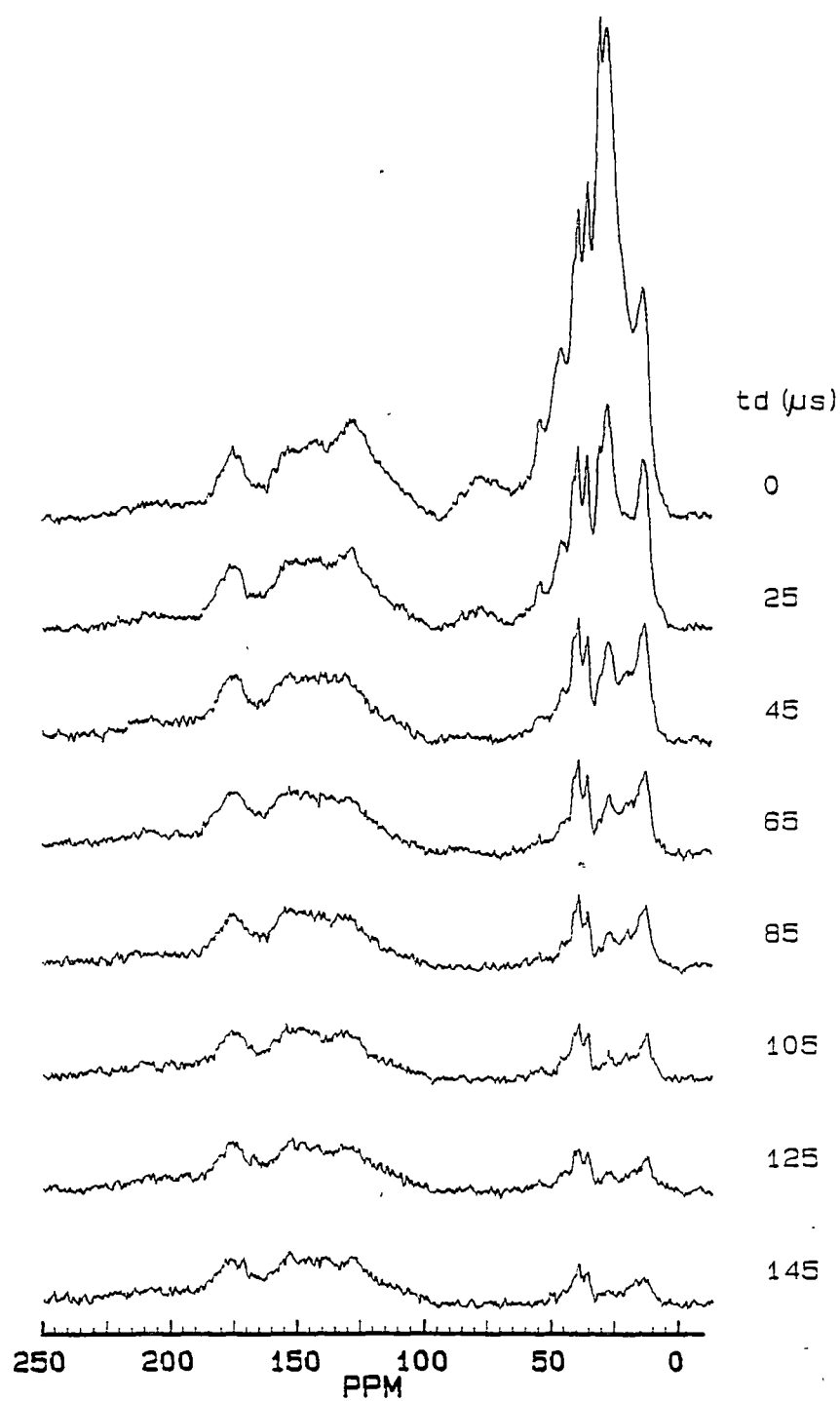
Figure 4.7 TOSS/DD spectra at various dephasing time for a brown coal, ABR14.

The interpretations of the solid-state ^{13}C spectra of the coals as outlined above were also supported by the solution-state ^{13}C nmr studies of the asphaltenes derived from the coals. A typical result for an asphaltene obtained from the liquefaction reaction at 320 °C for a brown coal, ABR10 (see **section 3.2.1**) is shown in **Figure 4.8** in comparison with the corresponding TOSS and TOSS/DD spectra. The solution-state spectra were edited from the combined DEPT/QUAT/inversed-gated decoupling spectra using the method described by Netzel [1987]. The sample for analysis was prepared in **CDCl$_3$** solution, containing **chromium(III) acetylacetonate** (~3 wt.%) as a relaxation reagent.

The general acquisition conditions for the solution-state spectra are as follows:

- 10.7 μs 90° ^1H pulse width and 4.1 μs 90° ^{13}C pulse width

- 5 s recycle time

- 25 kHz spectral width and 31.3 kHz filter width

- 1200 real scans with 8 dummy scans and 16K datasize

- 3.5 μs delay, corresponding to a spin- coupling constant, J, of 143 Hz, was used in DEPT and QUAT experiments.
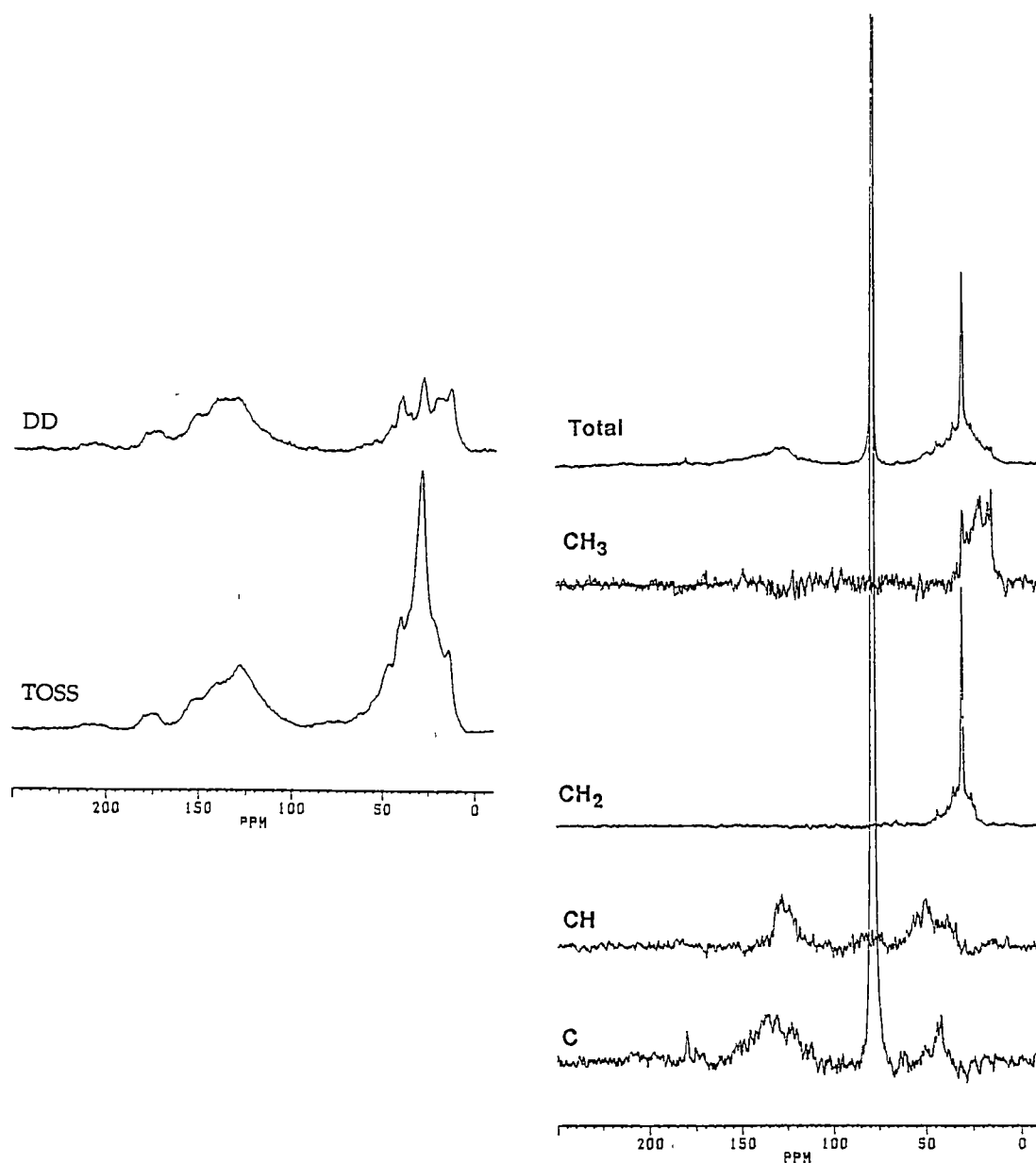
Figure 4.8 Comparison of TOSS, TOSS/DD and the spectra edited from solution-state ^{13}C nmr DEPT, QUAT and Inverse-gated decoupling techniques.

4.3.2 Cross-polarization dynamics in the coals.

The variable contact time experiments have been carried out for all brown coals and nine higher-rank coals. The aim was to study the cross-polarization dynamics in these coals. For some coals studied the variable contact time methods are necessary for quantitative measurements of the carbon fractions. **Figure 4.9** shows a typical observation of the change in ^{13}C signals as a function of contact times for a brown coal. The increase in signal intensities of all carbons in the spectra with the contact times between 0.1 ms and 2 ms demonstrated the effect of cross-polarization process while the decaying of the signals with a contact time longer than 2 ms resulted from a competitive process of the ^1H spin-lattice relaxation in the rotating frame [Sullivan and Maciel, 1982b]. According to the spin-temperature model [Mehring, 1983; Gerstein and Dybowski, 1985] the ^{13}C magnetization, $M(t_{cp})$, at any contact time, t_{cp} , is related to the cross-polarization time, T_{CH} , and the ^1H spin-lattice relaxation time in the rotating frame, $T_{1\rho}{}^H$, by the equation :

$$M(t_{cp}) = M°. \lambda^{-1}. [1\text{-exp}(-\lambda\ t_{cp}\ /T_{CH}\ )] . \text{exp}(-t_{cp}\ /T_{1\rho}{}^H)\qquad (4.1)$$

where $\lambda = (T_{1\rho}{}^H - T_{CH}\ )/T_{1\rho}{}^H$ and $M°$ is the maximum ^{13}C magnetization under the condition that $T_{CH} \ll t_{cp} \ll T_{1\rho}{}^H$. The relative integrated intensities of the carbonyl (220 ppm - 169 ppm), aromatic (169 ppm - 95 ppm) and aliphatic (95 ppm - 0 ppm) regions, measured from the spectra with contact time in the range 0.1 ms to 8.0 ms, were fitted to **equation (4.1)** to estimate T_{CH} , $T_{1\rho}{}^H$ and $M°$ for the three regions. A typical result from the non-linear least-squares fit of the data for a brown coal is shown in **Figure 4.10.**

tcp (ms)

8.1

5.1

3.1

1.1

0.4

0.1

250	200	150	100	50	0

PPM
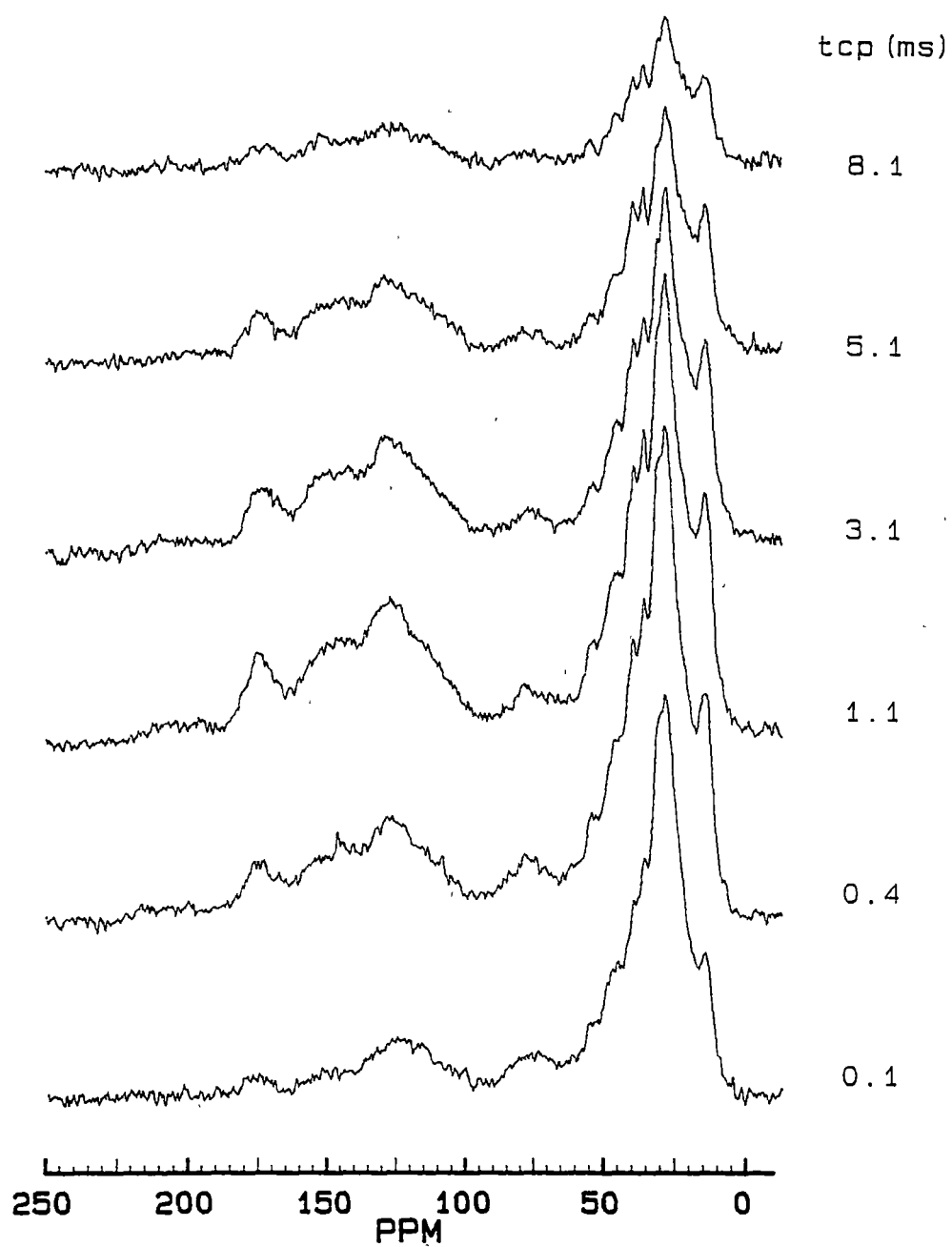
Figure 4.9   TOSS spectra at various contact times for a brown coal, ABR14.
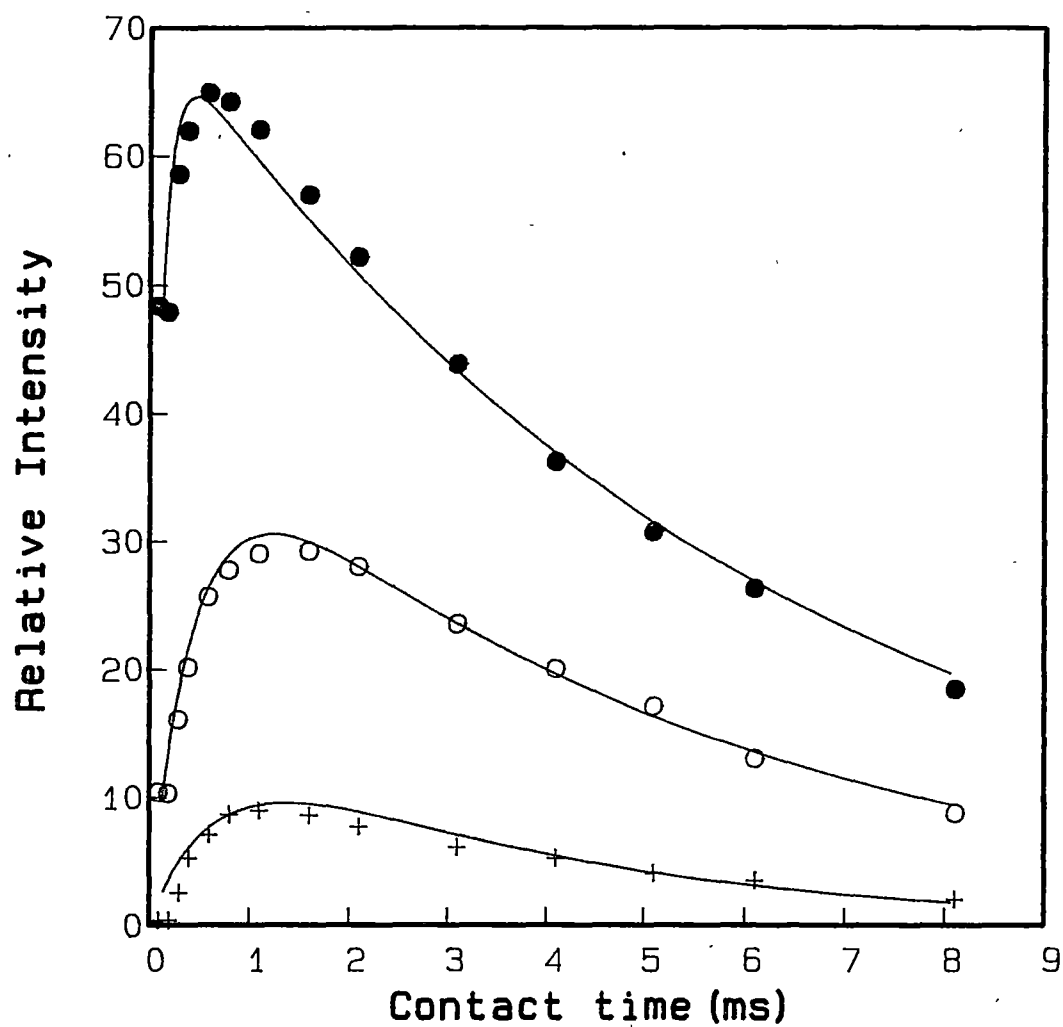
Figure 4.10 Variation in ^{13}C signals with contact time for a brown coal, ABR14. The solid line represents the least-squares fits of the data (● , Aliphatic; ○ , Aromatic; + , Carbonyl).

The values of T_{CH} and $T_{1\rho}{}^H$ for the coals studied are given in **Table 4.2** and **Table 4.3** respectively. From **equation (4.1)** the expression for a contact time with maximum ^{13}C magnetization, t_{cpmax}, is given by [Jelinski and Melchior, 1987] :

$$t_{cpmax} = \lambda^{-1}\, T_{CH}\; \ln\,(T_{1\rho}{}^H / T_{CH}) \qquad (4.2)$$

The values of t_{cpmax} estimated from **equation (4.2)** for the three regions are given in **Table 4.4**.

The cross-polarization rates $(T_{CH}{}^{-1})$ for both brown coals and higher-rank coals are in the order, aliphatic > aromatic > carbonyl. Theoretically, the value of $T_{CH}{}^{-1}$ is related to the magnitude of ^1H-^{13}C dipolar interaction [Pines et al., 1973; Demco et al., 1975]. The results thus suggested that, on average, the degree of protonation of the three main carbon-types are also in the same order as $T_{CH}{}^{-1}$. There is no clear trend of the variation in T_{CH} values with any rank parameter. The range of the aromatic or aliphatic T_{CH} values in this study, however, is comparable to those reported previously for other coals [Dudley and Fyfe, 1982; Botto et al., 1987; Solum et al., 1989].

Within estimated errors, the values of $T_{1\rho}{}^H$ for the three main spectral regions are in a similar range. The common $T_{1\rho}{}^H$ for all carbon types suggested that the spin-diffusion process is the effective path for the ^1H spin relaxation in these coals. Solum et al.[1989] also reported a marginal difference between the aromatic and aliphatic $T_{1\rho}{}^H$ values for Argonne Premium coals.

Table 4.2 Cross-polarization time, T_{CH} , for Australian coals.

Coal	T_{CH} (ms)[a]		
	aromatic	aliphatic	carbonyl
ABL2	0.27	0.06	0.44
ABL3	0.27	0.10	-
ABL6	0.37	0.16	-
ABL7	0.30	0.05	0.75
ABL8	0.30	0.06	0.63
ABL10	0.39	0.12	0.68
ABL11	0.42	0.16	0.75
ABL13	0.44	0.11	0.65
ABL15	0.54	0.12	1.06
ABR1	0.51	0.14	0.63
ABR2	0.62	0.16	0.88
ABR3	0.55	0.09	0.76
ABR4	0.48	0.10	0.76
ABR5	0.50	0.09	0.67
ABR6	0.51	0.08	0.71
ABR7	0.55	0.10	0.81
ABR8	0.35	0.10	0.45
ABR9	0.48	0.09	0.65
ABR10	0.46	0.13	0.65
ABR11	0.50	0.12	1.07
ABR12	0.40	0.08	0.79
ABR13	0.49	0.11	0.67
ABR14	0.50	0.12	0.81

[a] For all data, a standard error is less than ±0.01 ms.

Table 4.3 ^{1}H Spin-lattice relaxation time in the rotating frame, $T_{1\rho}H$, for Australian coals.

Coal	$T_{1\rho}H$ (ms)[a]		
	aromatic	aliphatic	carbonyl
ABL2	4.68 (0.05)	3.90 (0.06)	3.56 (0.27)
ABL3	4.47 (0.22)	3.56 (0.13)	-
ABL6	4.00 (0.02)	3.37 (0.03)	-
ABL7	4.95 (0.03)	3.74 (0.01)	3.97 (0.14)
ABL8	5.56 (0.09)	4.54 (0.05)	4.37 (0.32)
ABL10	4.22 (0.11)	4.00 (0.11)	3.64 (0.60)
ABL11	4.55 (0.01)	4.08 (0.01)	4.53 (1.98)
ABL13	4.88 (0.10)	4.96 (0.12)	4.07 (0.43)
ABL15	4.47 (0.15)	4.38 (0.15)	3.63 (2.00)
ABR1	6.20 (0.31)	5.46 (0.30)	5.24 (0.44)
ABR2	6.63 (0.14)	6.06 (0.28)	4.86 (1.50)
ABR3	6.86 (0.25)	5.45 (0.15)	5.49 (0.52)
ABR4	5.62 (0.08)	5.06 (0.03)	4.92 (0.10)
ABR5	7.17 (0.33)	7.16 (0.30)	5.39 (0.35)
ABR6	5.47 (0.11)	5.28 (0.05)	4.15 (0.22)
ABR7	6.30 (0.21)	6.05 (0.21)	5.13 (0.60)
ABR8	7.27 (0.17)	7.13 (0.08)	7.72 (0.55)
ABR9	6.65 (0.25)	6.32 (0.22)	5.50 (0.31)
ABR10	7.70 (0.46)	8.36 (0.62)	6.63 (0.59)
ABL11	6.84 (0.26)	7.32 (0.38)	4.19 (0.28)
ABL12	6.53 (0.16)	5.68 (0.02)	4.32 (0.07)
ABL13	6.97 (0.30)	6.94 (0.32)	5.54 (0.41)
ABL14	5.39 (0.23)	6.27 (0.38)	3.56 (1.17)

[a] The number in parenthesis is an estimated error of ± standard error.

By contrast, in an earlier study, Botto et al. [1987] observed that the $T_{1\rho}{}^H$ values for aromatic carbons were significantly larger than those for aliphatic carbons. It was suggested that molecular motion may play an important role in the ^1H relaxation process in such a way that the aromatic parts of the coal structure, having a sufficient size, may have an average molecular mobility less than the aliphatic subunits.

In this study, generally the brown coals have higher values of both aromatic and aliphatic $T_{1\rho}{}^H$ than the higher-rank coals. The observation is also consistent with the above suggestion that the spin diffusion is the predominant relaxation mechanism in the coals studied. Since the higher-rank coals contain higher mineral matter and have a higher aromatic content than the brown coals, the spin diffusion in the higher-rank coals can be expected to be relatively more effective as being due to the effect of electron-^1H spin interaction.

The effects of T_{CH} and $T_{1\rho}{}^H$ are manifested in the optimum contact time, t_{cpmax}. The significant differences in t_{cpmax} estimated for the three regions suggested that the variable contact time experiment may be necessary in the quantitative estimation of the carbon fractions in these coals. However, if a single contact time experiment is desirable, the optimum contact time of 1.5 ms would be appropriate for coals studied. In addition, with the average values of $T_{1\rho}{}^H$ and T_{CH}, one can also estimate a corrected signal intensity at any contact time by using equation (4.1).

The fractions of total carbon as being aromatic (f_{ar}), aliphatic (f_{al}) and carbonyl (f_{car}) carbons for the coals can be determined from the values of

M_i° , the maximum ^{13}C magnetization, estimated for the three regions as follows:

$$f_i \;=\; M_i^\circ \,/\, \Sigma_i \, M_i^\circ \qquad\qquad (4.3)$$

where i denotes the carbon type. The values of f_{ar} , f_{al} and f_{car} will be used later to estimate other structural parameters.

Table 4.4 Optimum contact time, t_{cpmax}, for Australian coals.

Coal	t_{cpmax} (ms)		
	aromatic	aliphatic	carbonyl
ABL2	0.81	0.27	1.04
ABL3	0.81	0.36	-
ABL6	0.97	0.51	-
ABL7	0.90	0.21	1.54
ABL8	0.93	0.27	1.42
ABL10	1.02	0.43	1.41
ABL11	1.11	0.53	1.62
ABL13	1.16	0.44	1.42
ABL15	1.29	0.45	1.84
ABR1	1.38	0.52	1.52
ABR2	1.62	0.55	1.84
ABR3	1.51	0.37	1.74
ABR4	1.30	0.40	1.68
ABR5	1.43	0.41	1.60
ABR6	1.34	0.34	1.51
ABR7	1.47	0.43	1.78
ABR8	1.11	0.42	1.36
ABR9	1.35	0.40	1.58
ABR10	1.38	0.55	1.65
ABR11	1.42	0.50	1.96
ABR12	1.19	0.35	1.64
ABR13	1.41	0.48	1.61
ABR14	1.31	0.48	1.55

4.3.3 Dipolar-dephasing analysis and carbon distribution.

A sub group of coals, consisting of nine brown coals and four higher-rank coals, was chosen as representative samples for DD studies. In general, the decays of both aromatic and aliphatic signals, as a function of dephasing delays, are composed of fast and slow components characterized by time constants T'_{2f} and T'_{2s} respectively. The relative integrated intensity, $I(t_d)$, of either aromatic or aliphatic signal was found to be best fitted to the equation:

$$I(t_d) = (I_0)_f \cdot exp[-0.5(t_d /T'_{2f})^2] + (I_0)_s \cdot exp(-t_d /T'_{2s}) \quad (4.4)$$

where t_d is a dephasing delay and $(I_0)_f$ and $(I_0)_s$ are the relative intensities at $t_d = 0$ for the fast and slow components respectively. A typical result of the two-component fitting is presented in **Figure 4.11**. The values of aromatic and aliphatic T'_{2f} and T'_{2s} for coals studied are given in **Table 4.5**. Although it has been reported by Theriault and Axelson [1988] that there was a relationship between aromatic T'_{2s} and wt. % **C**, the results observed here showed no trend either for aromatic or aliphatic T'_{2s} values. However, the ranges of T'_2 values are comparable with those reported previously for other coals [Wilson, et al.,1984; Theriault and Axelson 1988; Solum et al., 1989].

Although the full DD analysis is useful for the estimation of protonated and non-protonated carbons from $(I_0)_f$ and $(I_0)_s$ values, the experiment is time consuming. Wilson et al. [1984] used a different approach to estimate the two parameters. Only two spectra obtained at $t_d = 0$ and 40 μs were used, with the factors derived from the full DD analyses of five samples, to estimate the protonated aromatic carbon fractions of the coals.
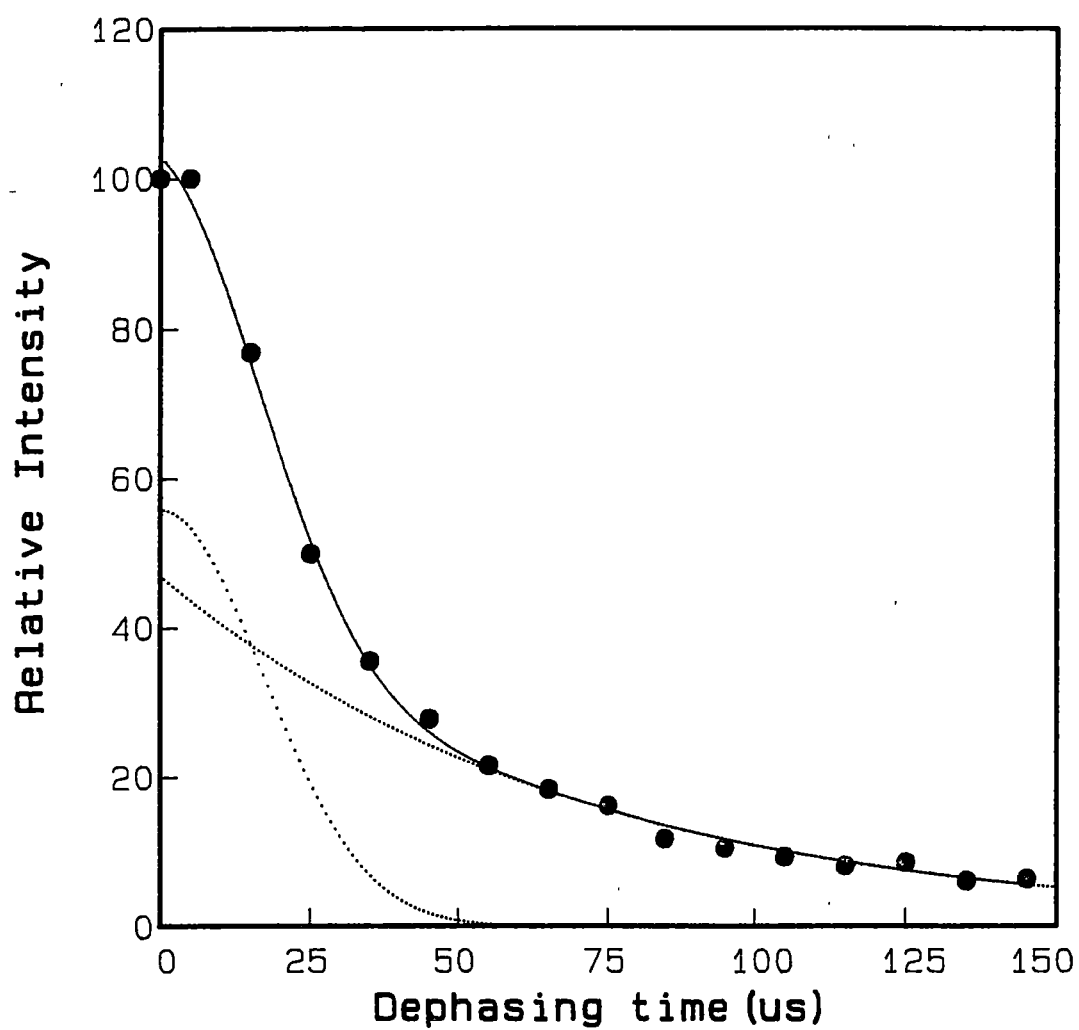
Figure 4.11 Variation in aliphatic ^{13}C signals with dephasing delays for a brown coal, ABR14. The solid line represents the least-squares fits of the data. The dotted lines represent the fast and slow components.

Table 4.5 Dipolar-dephasing time constants[a] and compensation factor, **k**, derived from dipolar-dephasing analyses of Australian coals.

Coal	aromatic			aliphatic		
	T'_{2f}	T'_{2s}	k	T'_{2f}	T'_{2s}	k
ABL8	29.90	367.92	1.02	13.41	95.53	1.49
ABL11	27.07	315.65	1.10	14.42	66.44	1.91
ABL13	26.17	288.68	1.05	15.54	76.34	1.58
ABL14	27.67	296.42	1.14	17.46	72.53	2.19
ABR1	23.77	334.03	1.06	13.46	87.53	1.60
ABR2	23.06	295.49	1.07	12.86	61.68	2.17
ABR3	21.29	352.25	1.06	14.35	87.49	1.63
ABR4	30.35	375.03	1.15	14.78	108.63	1.44
ABR6	21.95	372.00	1.03	14.09	75.26	1.89
ABR7	31.46	366.63	1.02	17.47	77.75	2.03
ABR10	29.15	366.63	1.02	17.47	77.75	2.03
ABR13	20.98	258.49	0.82	14.68	67.88	1.86
ABR14	27.60	473.63	0.85	17.13	67.96	1.68

[a]The unit of dephasing time constant is in μs.

In this study a similar method was used. The calculations involved an estimation of a compensation factor, $k(i)$, for any carbon-type i by the equation:

$$k(i) = [(I_0)_s / (I_{45})_s] \cdot [(I_{45})_s / (I_{45})_m] \qquad (4.5)$$

where $(I_{45})_m$ is the integrated intensity of aromatic or aliphatic region, measured from 45 μs TOSS/DD spectrum, relative to that of the corresponding region from normal TOSS spectrum and

$$(I_{45})_s = (I_0)_s \cdot exp[-45 / T'_{2s}] \qquad (4.6)$$

All parameters used in **equation (4.5)** were derived from the full DD analyses of the representative samples. The values of $k(i)$ for the aromatic and aliphatic carbons are included in **Table 4.5**. The parameters $(I_0)_s$ was then estimated from the equation

$$(I_0)_s = k(i) \cdot (I_{45})_m \qquad (4.7)$$

by using the average values of $k(i)$ from **Table 4.5** for the higher-rank coals and the brown coals separately.

In the aromatic region, $(I_0)_s$ is proportional to the relative amount of non-protonated carbons while in the aliphatic region, it represents the fractions from quaternary carbons, methyl groups and mobile $-CH_2-$ and $-CH-$.

By using the integrated areas obtained from TOSS and 45 µs TOSS/DD spectra and using the values of $(I_0)_s$ for the aromatic and aliphatic regions, the distribution of carbon-types in coals studied can be estimated.

For the aliphatic carbons, the value of $(I_0)_s$ was used to estimate the methyl, methoxyl and quaternary carbon fractions by assuming that the three carbon-types have a similar dipolar-dephasing behaviour with a common T'_{2s} time constant. The operational definitions of various carbon fractions are given in **Table 4.6**. The values of the carbon fractions identified in coals studied are reported in **Table 4.7, Table 4.8** and **Table 4.9** for the aromatic, aliphatic and carbonyl regions respectively. The three main parameters f_{ar}, f_{al} and f_{car} were obtained from the variable contact time measurements (**equation (4.3)**) for all brown coals and nine higher-rank coals reported earlier. For other coals the values from the single contact time experiments were used.

Table 4.6 Operational definitions of various carbon fractions.

Carbon fraction	Definition[a]
Total aromatic (aromaticity)	$f_{ar} = (I_{169-95} / I_{total})_0$
Protonated aromatic	$f_{ar}{}^H = f_{ar} \cdot [1- (I_0)_s{}^{ar}]$
Oxygenated aromatic	$f_{ar}{}^O = f_{ar} \cdot (I_{169-145} / I_{ar})_0$
Alkyl-substituted aromatic	$f_{ar}{}^C = f_{ar} \cdot (I_{145-135} / I_{ar})_0$
Carbonyl-substituted aromatic	$f_{ar}{}^{C=O} = f_{ar} \cdot (I_{145-135} / I_{ar})_{45} \cdot (I_0)_s{}^{ar}$
Bridgehead aromatic	$f_{ar}{}^{ar} = f_{ar} - $ (other aromatic fractions)
Total aliphatic	$f_{al} = (I_{95-0} / I_{total})_0$
Methyl	$f_{al}{}^{CH_3} = f_{al} \cdot (I_{26-0} / I_{al})_{45} \cdot (I_0)_s{}^{al}$
Methylenic	$f_{al}{}^{CH_2} = f_{al} \cdot (I_{36-26} / I_{al})_0$
Quaternary aliphatic	$f_{al}{}^C = f_{al} \cdot (I_{45-36} / I_{al})_{45} \cdot (I_0)_s{}^{al}$
Methoxyl	$f_{al}{}^{OCH_3} = f_{al} \cdot (I_{60-50} / I_{al})_{45} \cdot (I_0)_s{}^{al}$
Oxygenated aliphatic	$f_{al}{}^O = (I_{95-60} / I_{total})_0$
Methine	$f_{al}{}^{CH} = f_{al} - $ (other aliphatic fractions)
Total carbonyl	$f_{car} = 1 - f_{ar} - f_{al}$
Ketonic-type	$f_{car}{}^{CO} = f_{car} \cdot (I_{225-195} / I_{225-169})_0$
Carboxyl	$f_{car}{}^{COO} = f_{car} - f_{car}{}^{CO}$
Aromatic carbonyl	$f_{car}{}^{ar} = f_{ar}{}^{C=O}$
Aliphatic carbonyl	$f_{car}{}^{al} = f_{car} - f_{car}{}^{ar}$

[a]Subscripts **0** and **45** denote the data obtained from TOSS and 45 μs TOSS/DD spectra respectively. The subscript of I denotes the chemical-shift range. **al, ar** and **car** stand for aliphatic (95-0), aromatic (169-95) and carbonyl (225-169) regions respectively. **"total"** stands for the full ppm range (225-0).

Table 4.7 Structural data related to aromatic structure of Australian coals.

Coal	f_{ar}	f_{ar}^H	f_{ar}^O	f_{ar}^C	f_{ar}^{CO}	f_{ar}^{ar}	σ	R_n
ABL1	0.95	0.33	0.01	0.24	-	0.37	0.43	6
ABL2	0.71	0.19	0.09	0.17	0.04	0.22	0.61	3
ABL3	0.81	0.27	0.02	0.20	-	0.32	0.45	7
ABL4	0.64	0.18	0.08	0.20	0.04	0.14	0.64	2
ABL5	0.72	0.21	0.09	0.19	0.01	0.22	0.59	3
ABL6	0.70	0.22	0.04	0.18	0.02	0.23	0.52	4
ABL7	0.63	0.14	0.11	0.19	0.04	0.15	0.71	2
ABL8	0.66	0.17	0.09	0.19	0.06	0.16	0.67	2
ABL9	0.69	0.21	0.08	0.21	0.02	0.18	0.59	3
ABL10	0.66	0.18	0.09	0.20	0.03	0.16	0.63	2
ABL11	0.58	0.14	0.05	0.16	0.02	0.19	0.59	4
ABL12	0.58	0.17	0.06	0.14	0.02	0.19	0.56	4
ABL13	0.53	0.13	0.10	0.15	0.04	0.12	0.69	2
ABL14	0.52	0.15	0.09	0.13	0.03	0.12	0.63	2
ABL15	0.52	0.14	0.08	0.13	0.03	0.14	0.63	3
ABR1	0.64	0.18	0.11	0.18	0.06	0.11	0.66	2
ABR2	0.65	0.18	0.11	0.21	0.07	0.08	0.68	2
ABR3	0.57	0.15	0.10	0.20	0.05	0.07	0.71	2
ABR4	0.58	0.13	0.13	0.15	0.06	0.10	0.72	2
ABR5	0.56	0.12	0.13	0.14	0.06	0.10	0.73	2
ABR6	0.50	0.12	0.09	0.14	0.06	0.09	0.71	2
ABR7	0.49	0.12	0.12	0.11	0.05	0.09	0.70	2
ABR8	0.48	0.14	0.10	0.13	0.04	0.07	0.66	2
ABR9	0.48	0.12	0.11	0.11	0.05	0.10	0.70	2
ABR10	0.40	0.09	0.07	0.12	0.05	0.07	0.72	2
ABR11	0.41	0.08	0.08	0.12	0.04	0.09	0.74	2
ABR12	0.39	0.09	0.08	0.10	0.04	0.08	0.70	2
ABR13	0.36	0.09	0.06	0.12	0.04	0.05	0.71	2
ABR14	0.32	0.07	0.06	0.09	0.02	0.08	0.72	2

Table 4.8 Structural data related to aliphatic structure of Australian coals.

Coal	f_{al}	$f_{al}^{CH_3}$	$f_{al}^{CH_2}$	f_{al}^{CH}	f_{al}^{C}	$f_{al}^{OCH_3}$	f_{al}^{O}
ABL1	0.05	0.02	(0.03)[a]		-	-	-
ABL2	0.21	0.05	0.07	0.09	-	-	-
ABL3	0.19	0.06	0.02	0.11	-	-	-
ABL4	0.25	0.04	0.09	0.12	-	-	-
ABL5	0.27	0.06	0.09	0.12	-	-	-
ABL6	0.28	0.08	0.05	0.15	-	-	-
ABL7	0.23	0.04	0.09	0.10	-	-	-
ABL8	0.20	0.03	0.08	0.09	-	-	-
ABL9	0.29	0.07	0.06	0.16	-	-	-
ABL10	0.29	0.07	0.07	0.15	-	-	-
ABL11	0.37	0.08	0.14	0.15	-	-	-
ABL12	0.39	0.08	0.19	0.12	-	-	-
ABL13	0.39	0.06	0.19	0.14	-	-	-
ABL14	0.42	0.06	0.23	0.13	-	-	-
ABL15	0.42	0.07	0.22	0.13	-	-	-
ABR1	0.22	0.05	0.08	0.06	-	0.02	0.01
ABR2	0.23	0.04	0.06	0.09	0.01	0.01	0.02
ABR3	0.28	0.05	0.09	0.08	0.02	0.02	0.02
ABR4	0.27	0.06	0.08	0.06	0.01	0.03	0.03
ABR5	0.29	0.05	0.11	0.07	0.02	0.02	0.02
ABR6	0.37	0.05	0.14	0.10	0.03	0.02	0.03
ABR7	0.35	0.07	0.13	0.07	0.03	0.02	0.03
ABR8	0.40	0.06	0.13	0.12	0.05	0.01	0.03
ABR9	0.40	0.04	0.16	0.13	0.03	0.01	0.03
ABR10	0.48	0.10	0.18	0.08	0.06	0.02	0.04
ABR11	0.43	0.06	0.17	0.11	0.05	0.01	0.03
ABR12	0.48	0.06	0.21	0.10	0.05	0.02	0.04
ABR13	0.49	0.08	0.21	0.09	0.05	0.02	0.04
ABR14	0.57	0.09	0.25	0.10	0.08	0.01	0.04

[a] $f_{al}^{CH_2} + f_{al}^{CH}$

**Table 4.9** Structural data related to carbonyl structure of Australian coals.

| Coal	f_{car}	f_{car}^{CO}	f_{car}^{COO}	f_{car}^{al}	f_{car}^{ar}
ABL2	0.08	0.02	0.06	0.04	0.04
ABL4	0.11	0.03	0.08	0.07	0.04
ABL5	0.01	(0.01)[a]		-	0.01
ABL6	0.02	0.01	0.01	-	0.02
ABL7	0.14	0.05	0.09	0.10	0.04
ABL8	0.14	0.04	0.10	0.08	0.06
ABL9	0.02	0.01	0.01	-	0.02
ABL10	0.05	0.02	0.03	0.02	0.03
ABL11	0.05	0.01	0.04	0.03	0.02
ABL12	0.03	0.01	0.02	0.01	0.02
ABL13	0.08	0.03	0.05	0.04	0.04
ABL14	0.06	0.02	0.04	0.03	0.03
ABL15	0.06	0.02	0.04	0.03	0.03
ABR1	0.14	0.04	0.10	0.09	0.05
ABR2	0.12	0.04	0.08	0.05	0.07
ABR3	0.15	0.05	0.10	0.09	0.06
ABR4	0.15	0.05	0.10	0.09	0.06
ABR5	0.15	0.05	0.10	0.09	0.06
ABR6	0.13	0.03	0.10	0.07	0.06
ABR7	0.16	0.04	0.12	0.11	0.05
ABR8	0.12	0.05	0.07	0.08	0.04
ABR9	0.12	0.03	0.09	0.07	0.05
ABR10	0.12	0.03	0.09	0.07	0.05
ABR11	0.16	0.05	0.11	0.12	0.04
ABR12	0.13	0.04	0.09	0.09	0.04
ABR13	0.15	0.05	0.10	0.11	0.04
ABR14	0.11	0.03	0.08	0.09	0.02

[a] $f_{car}^{CO} + f_{car}^{COO}$

a)   Aromatic structures.

Recently, problems concerning the accuracy of TOSS measurements have been addressed by Axelson [1987b]. He has demonstrated that for a more limited range of coal samples the measurements from the TOSS technique were comparable to those obtain from normal ^{13}C nmr spectra. For coals in this suite we have also compared the f_{ar} values from TOSS spectra(single contact time data) with those derived from normal spectra acquired on a different instrument (**Bruker CXP 200**) operated at a lower magnetic-field of 50 MHz ^{13}C frequency.   Details regarding the instrumentation and f_{ar} calculations for the normal spectra of the coals have been reported elsewhere [Redlich 1989a].   The comparisons of the f_{ar} values from the two experiments are shown in **Figure 4.12**. With the estimated experimental errors for both measurements of ± 0.03, a correlation coefficient for the best fit of the two sets of values is 0.98. As indicated by the 1:1 relationship line, the results are encouraging for the application of the TOSS technique to coal studies.

For the whole suite of coals studied, there is no single trend between the carbon aromaticities and coal carbon contents. However, the f_{ar} values do correlate with atomic **H/C** ratios in an inverse manner as shown in **Figure 4.13**.   The trend and range of f_{ar} values are similar to those reported previously for Australian [Russell et al., 1983] and Canadian coals [Furimsky and Ripmeester, 1983; Axelson 1987a]. The f_{ar} values for the higher-rank coals are slightly higher than those of the brown coals with similar **H/C** values. As can be seen in **Table 4.8** and **Table 4.9**, the brown coals have a higher carbonyl-carbon fraction but a lower aliphatic-carbon fraction than the higher-rank coals with similar **H/C** values.
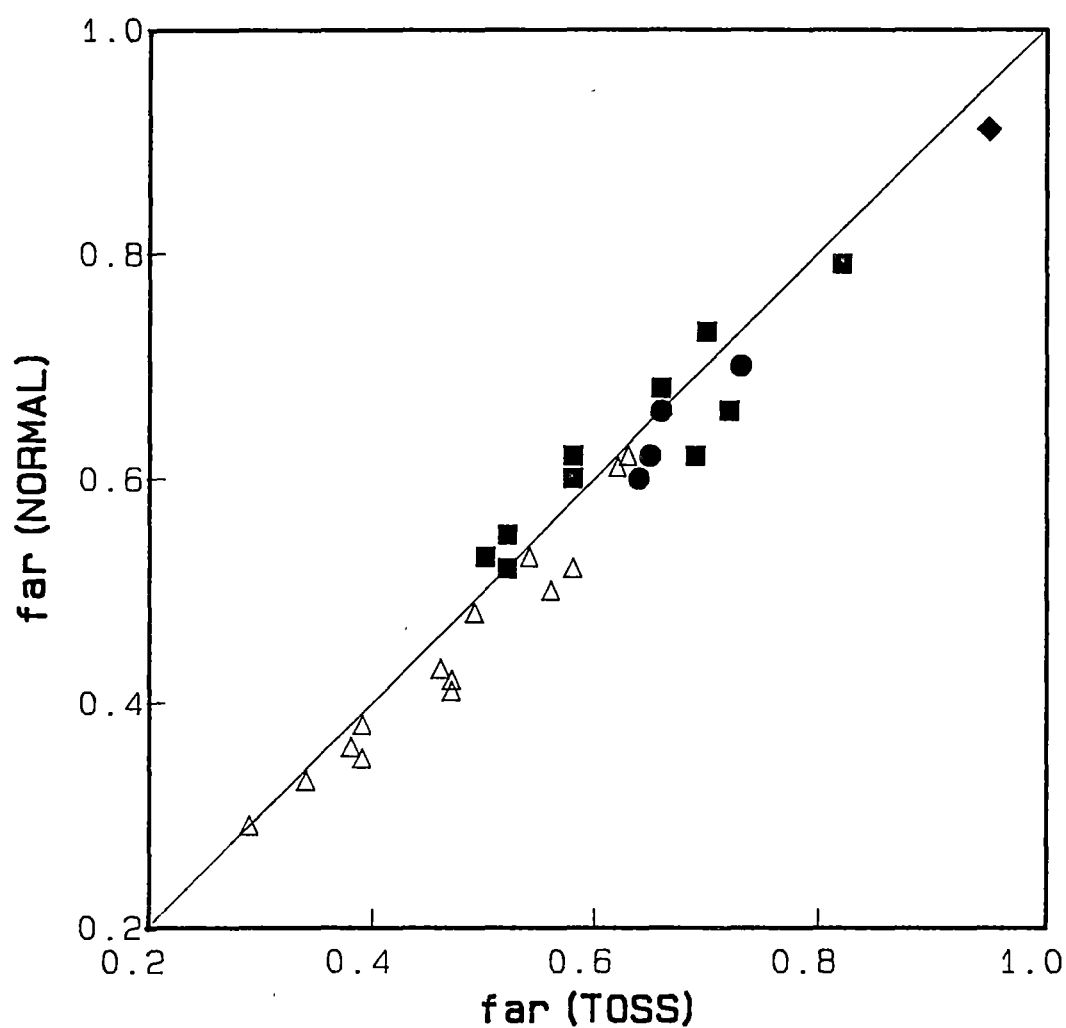
Figure 4.12 Comparison of carbon aromaticity obtained from TOSS spectra, f$_{ar}$ (TOSS), with that derived from normal spectrum, f$_{ar}$(NORMAL): △ , brown coals; ■ , higher-rank coals; ● , oxygen-rich subbituminous; ◆ , semianthracite.
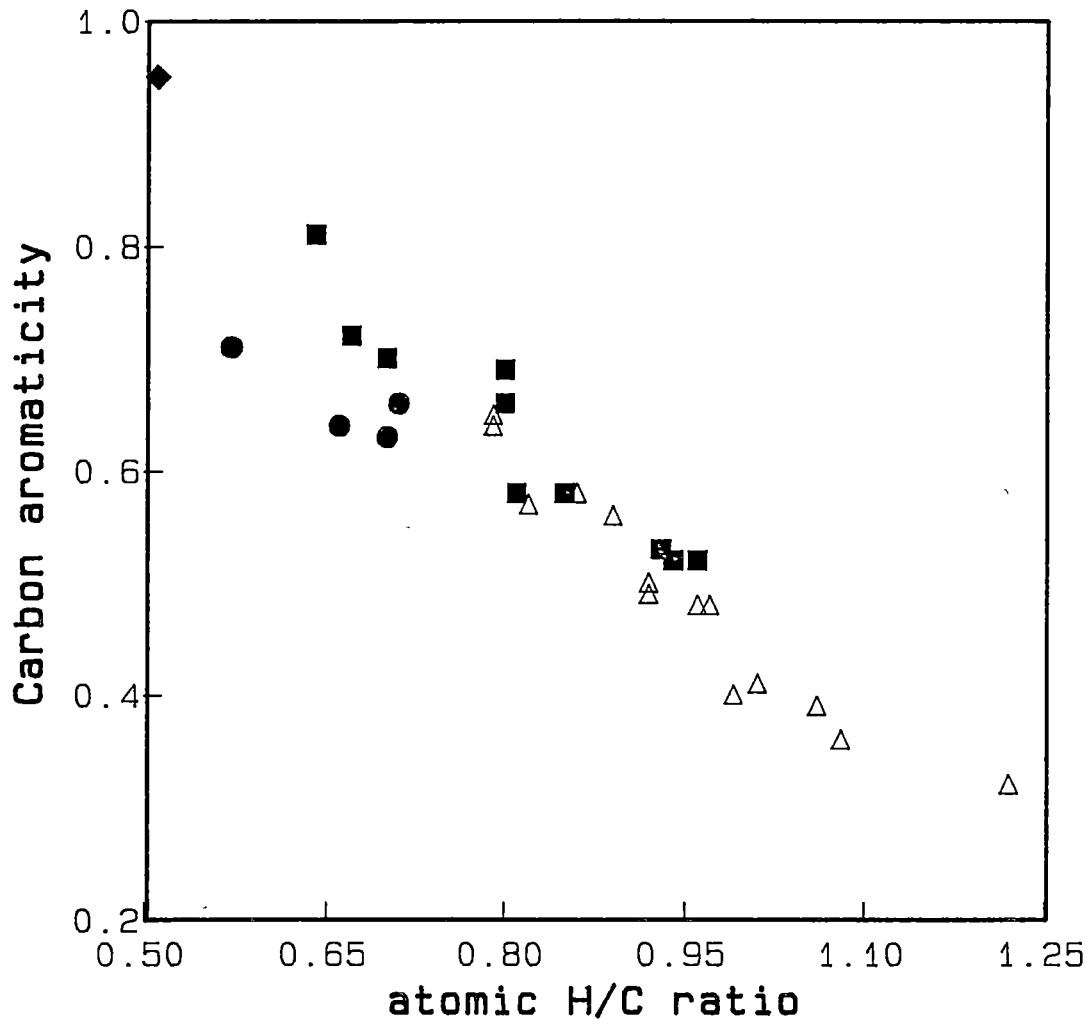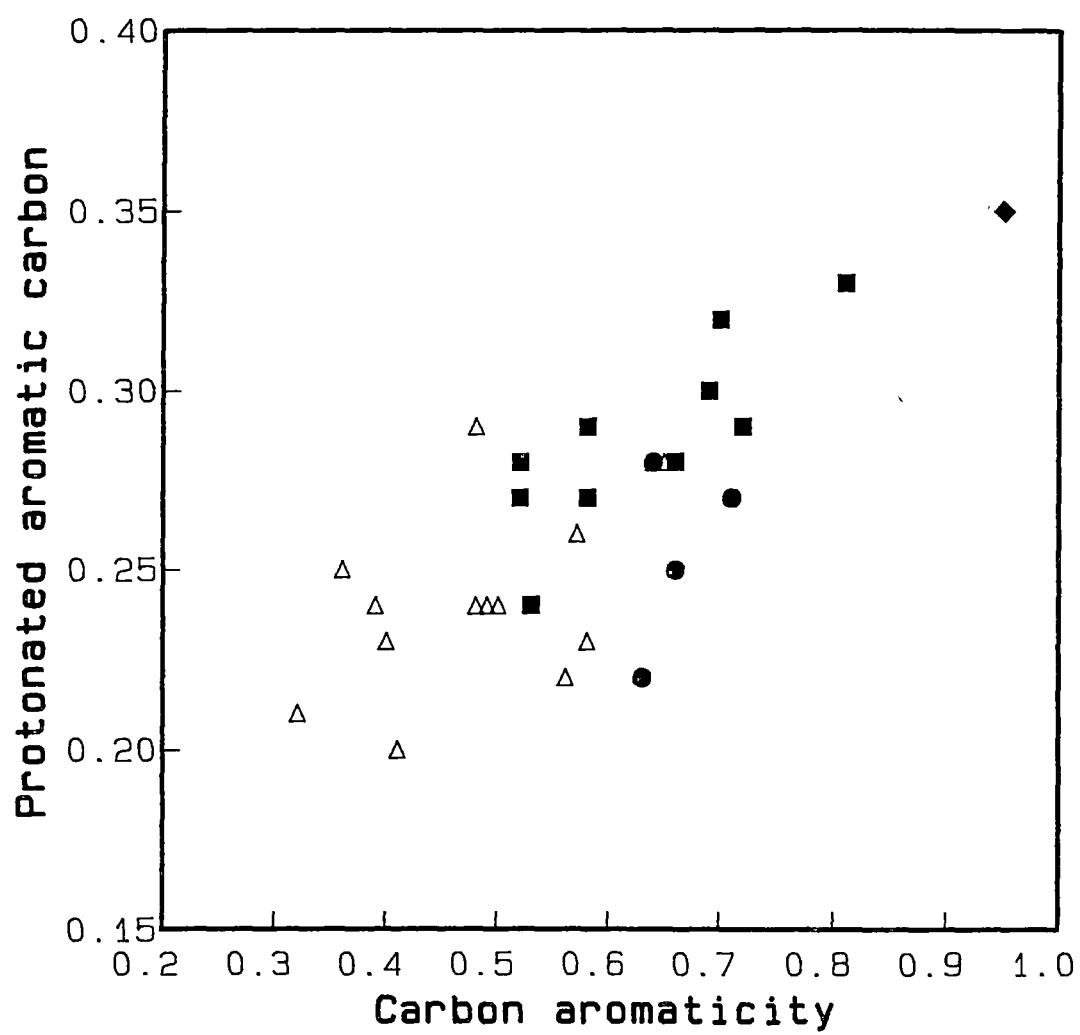
Figure 4.13   Plot of carbon aromaticity, f_{ar} , versus coal **H/C** ratio (see **Figure 4.12** for symbols).

A similar observation was found when comparing the data of oxygen-rich subbituminous coals (black circles in **Figure 4.13**) with those of other high-rank coals having a similar **H/C** ratio. The results are consistent with the distributions of hydrogens in the coals as found from FTIR studies (see **section 3.3.3**).

From the parameters, f_{ar}^H , f_{ar}^O , f_{ar}^C , f_{ar}^{ar} and $f_{ar}^{C=O}$ the fractions of aromatic carbons associated with the five parameters, designated C_{ar}^H/C_{ar} , C_{ar}^O/C_{ar}, C_{ar}^C/C_{ar}, C_{ar}^{ar}/C_{ar} and $C_{ar}^{C=O}/C_{ar}$ can be readily estimated. One can then determine the degree of aromatic substitution, σ , from the equation:

$$\sigma = \frac{(C_{ar}^O/C_{ar} + C_{ar}^C/C_{ar} + C_{ar}^{C=O}/C_{ar})}{(C_{ar}^O/C_{ar} + C_{ar}^C/C_{ar} + C_{ar}^{C=O}/C_{ar} + C_{ar}^H/C_{ar})} \qquad (4.8)$$

The values of σ for the coals are also given in **Table 4.7**. Among the five aromatic carbon fractions only C_{ar}^H/C_{ar} shows a significant trend of increasing in its value with carbon aromaticity (see **Figure 4.14**). However, with the increase in the f_{ar} values, a trend of decreasing in C_{ar}^O/C_{ar} values was observed. The values of C_{ar}^O/C_{ar} also decrease with the increase in carbon content of coals as shown in **Figure 4.15**. **Figure 4.16** demonstrates the relationship between the degree of aromatic substitition, σ, and protonated-aromatic-carbon fraction, C_{ar}^H/C_{ar} . The results are consistent with the above finding that the loss of aromatic substitution, mainly of oxygenated substituents, is found with the increase in protonated-aromatic carbons. Moreover, as seen in **Figure 4.16**, the diminishing of aromatic substituents is more pronounced for the higher-rank coals.

Figure 4.14 Plot of protonated-aromatic-carbon fraction, C_{ar}^H/C_{ar}, versus carbon aromaticity, f_{ar} (see **Figure 4.12** for symbols).
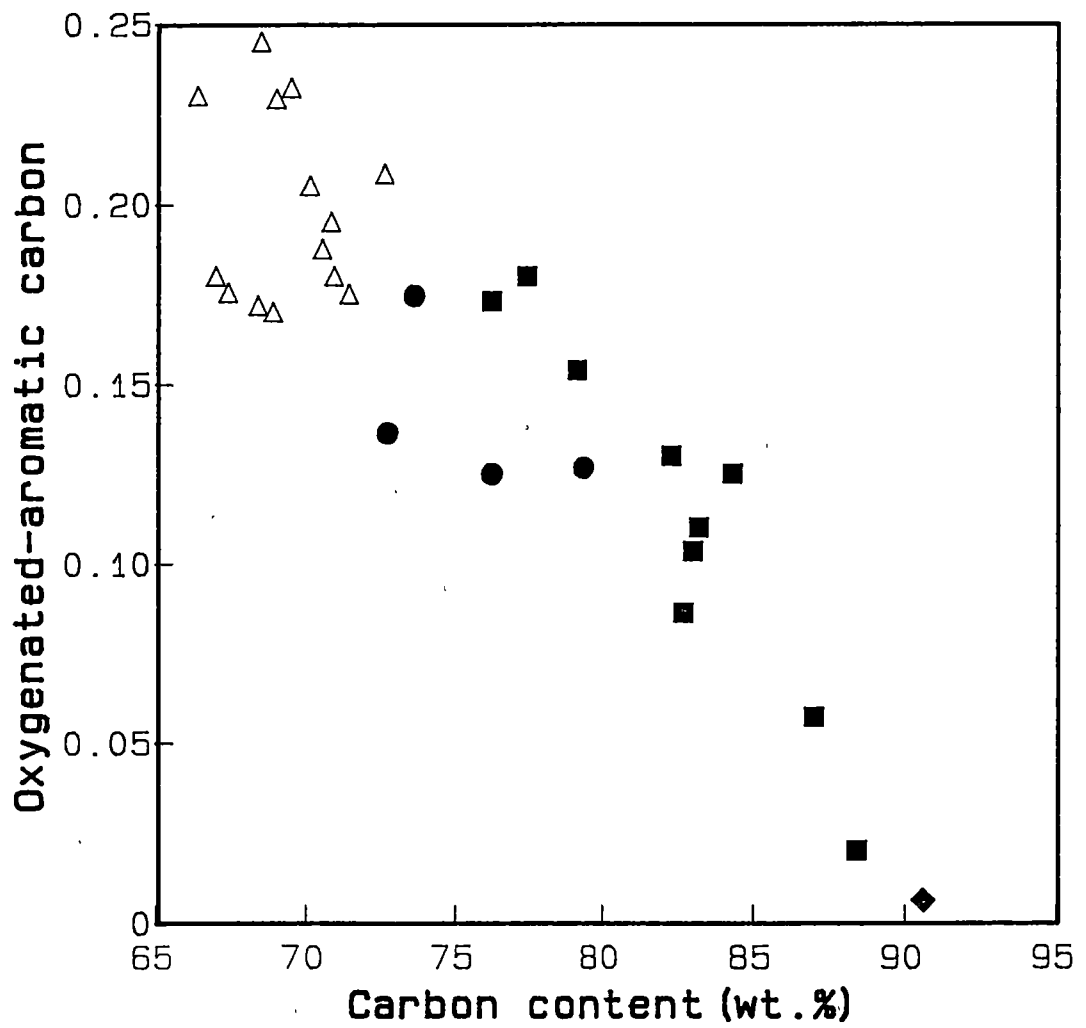
Figure 4.15 The relationship between oxygenated-aromatic-carbon fraction, C_{ar}^O/C_{ar} , and coal carbon content (see **Figure 4.12** for symbols).
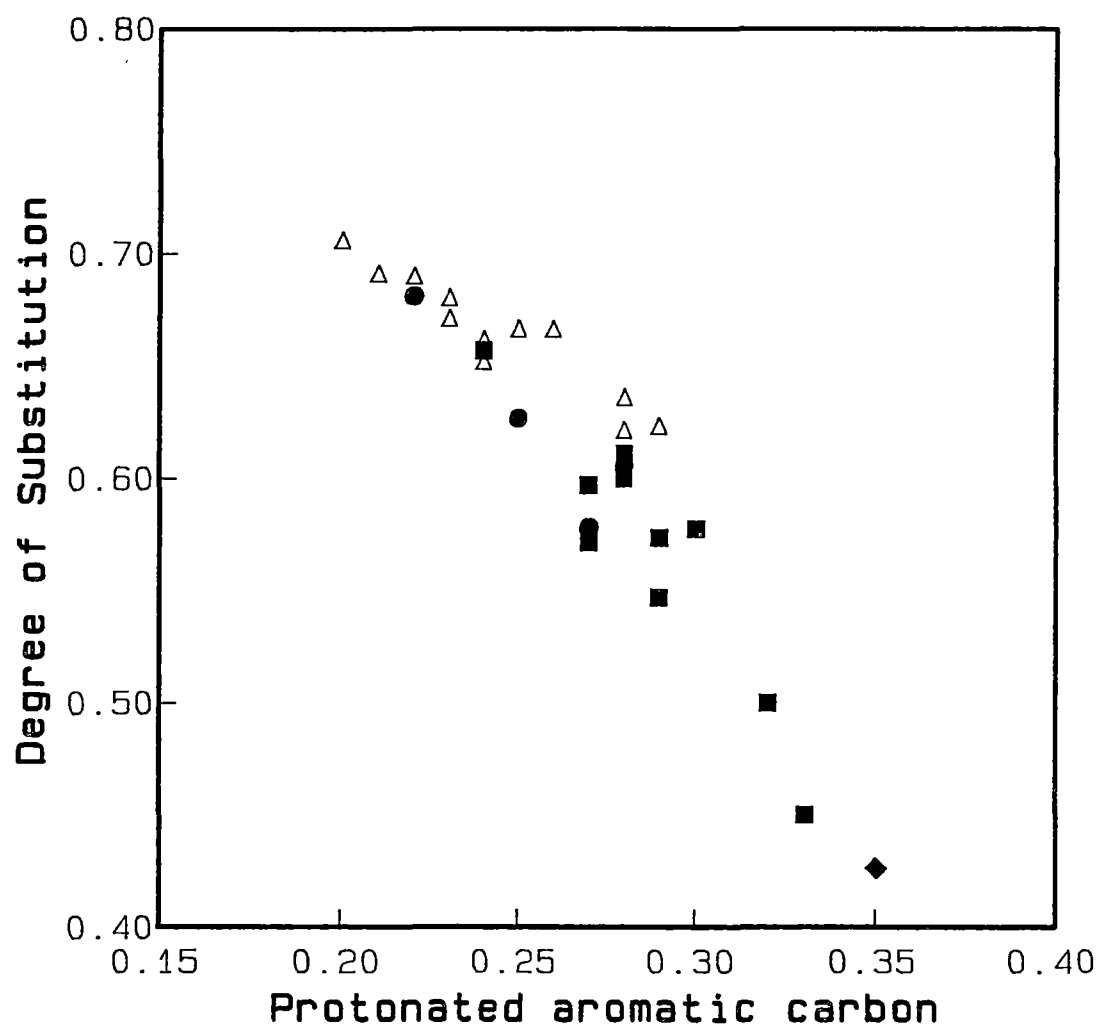
Figure 4.16 Plot of degree of aromatic substitution, σ, versus protonated-aromatic-carbon fraction, C_{ar}^H/ C_{ar} (see **Figure 4.12** for symbols).

These observations thus suggest that the removal of oxygenated substituents via the hydrogenation reaction is an important mechanism in the coalification process. The conclusion is consistent with the studies on other coals [Wilson et al., 1984; Theriault and Axelson, 1988].

Another useful parameter, related to the aromatic structures, is the number of aromatic rings per cluster, R_n. The R_n parameter can be estimated from the fraction for bridgehead-aromatic carbon, C_{ar}^{ar}/C_{ar}, by using the equation describing a model for pericondenced, two-dimentional aromatic cluster [Murphy et. al., 1982].

$$R_n = (1 + C_{ar}^{ar}/C_{ar}) / (1 - 2 \cdot C_{ar}^{ar}/C_{ar}) \qquad (4.9)$$

The equation (4.9) is for the case that C_{ar}^{ar}/C_{ar} value is less than 0.5. A more general expression can be obtained from a previous study [Burgar et al., 1985]. The estimated R_n values for coals studies are included in Table 4.7.

The data indicated that the average cluster size of the aromatic structure for brown coals is 2 to 3 units while those for the higher-rank coal are in the range of 2 to 7 units. The average size of the aromatic cluster in a semianthracite ABL1 is 6 rings while a low volatile bituminous coal, ABL3 has a cluster size of 7 aromatic rings. For the bituminous coals, the R_n value is in the range of 2 to 4 aromatic rings whereas the average aromatic-cluster size in subbituminous coals is of 2 or 3 rings.

It should be noted that the value of R_n estimated from equation (4.9) is very sensitive to the variance in C_{ar}^{ar}/C_{ar} value. However, the average aromatic-cluster size estimated seems to represent a reasonable model for

the aromatic structure of coals studied. The increase in aromatic cluster size with rank as observed is consistent with the general view of coal structures [Davidson, 1980].

b)   Aliphatic structures.

The relationship between the aliphatic-carbon fractions and coal **H/C** ratios is shown in **Figure 4.17**. Since the higher-rank coals contain less oxygen-functional groups, they have a higher aliphatic carbon fraction than do the brown coals of a similar **H/C** ratio. The results in **Figure 4.17** also show a less scatter in the data points of the brown coals than in those of the higher-rank coals. The observation suggested that the variation in the higher-rank coal **H/C** ratios is more dependent upon the aromatic structures of the coals. The findings observed here are consistent with the FTIR data for the aliphatic hydrogen content in the coals (see **Figure 3.18** in **Chapter 3**).

The relationships between the aliphatic carbon fractions and the liquefaction yields of the coals are shown in **Figure 4.18**. With a similar aliphatic content, the brown coals have a relatively higher oil yield than the higher-rank coals. The plot for the total hydrocarbon products, however, shows a single trend with a slightly higher product yield for the higher-rank coals. Similar relationships were observed for the aliphatic hydrogen content data derived from the FTIR studies (**Figure 3.19** in **Chapter 3**). Therefore the results observed here confirm the conclusion outlined earlier in **section 3.3.3 (p. 81 - p.85)**, in relation to the relationship between the liquefaction behaviour of the coals and their aliphatic structures.
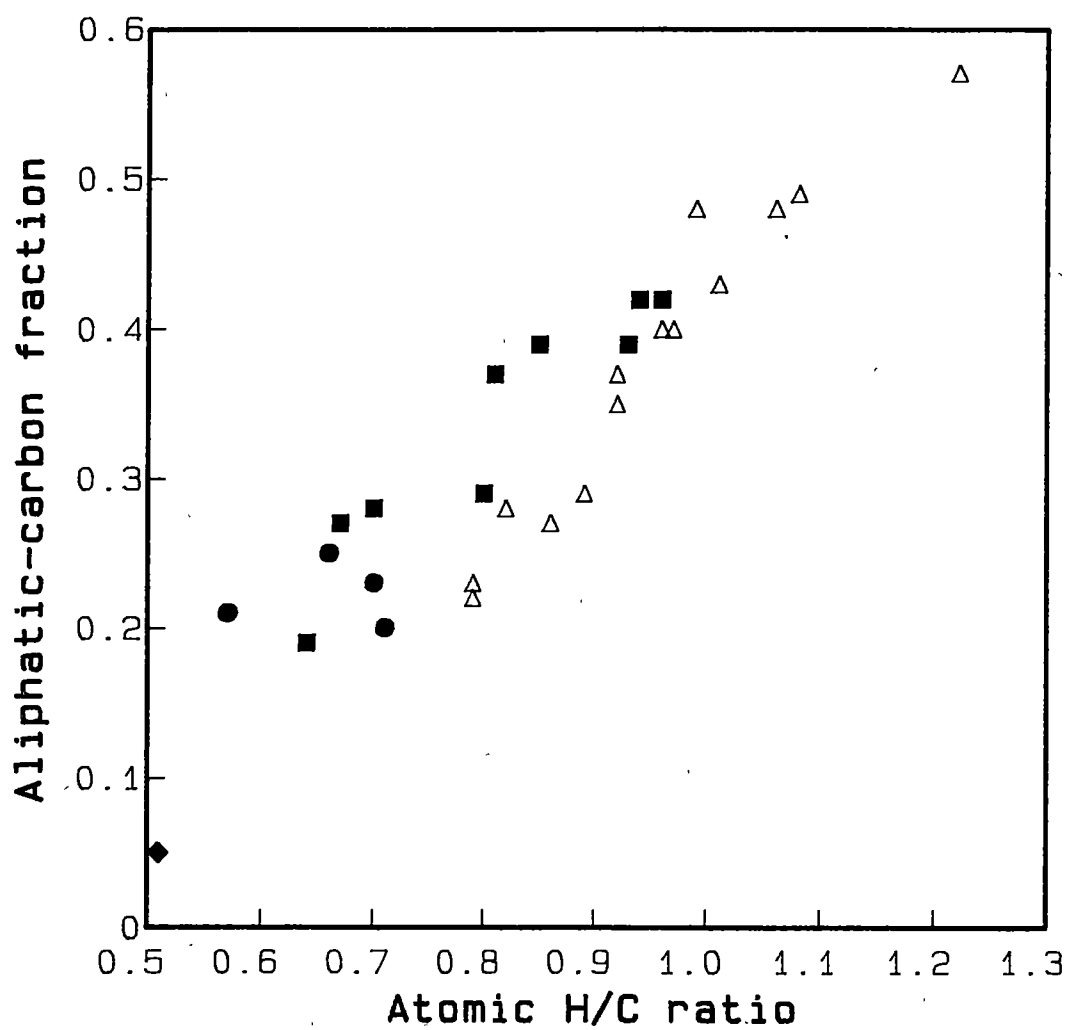
Figure 4.17 Plot of aliphatic-carbon fraction, f_{al} , vursus coal **H/C** ratio (see **Figure 4.12** for symbols).
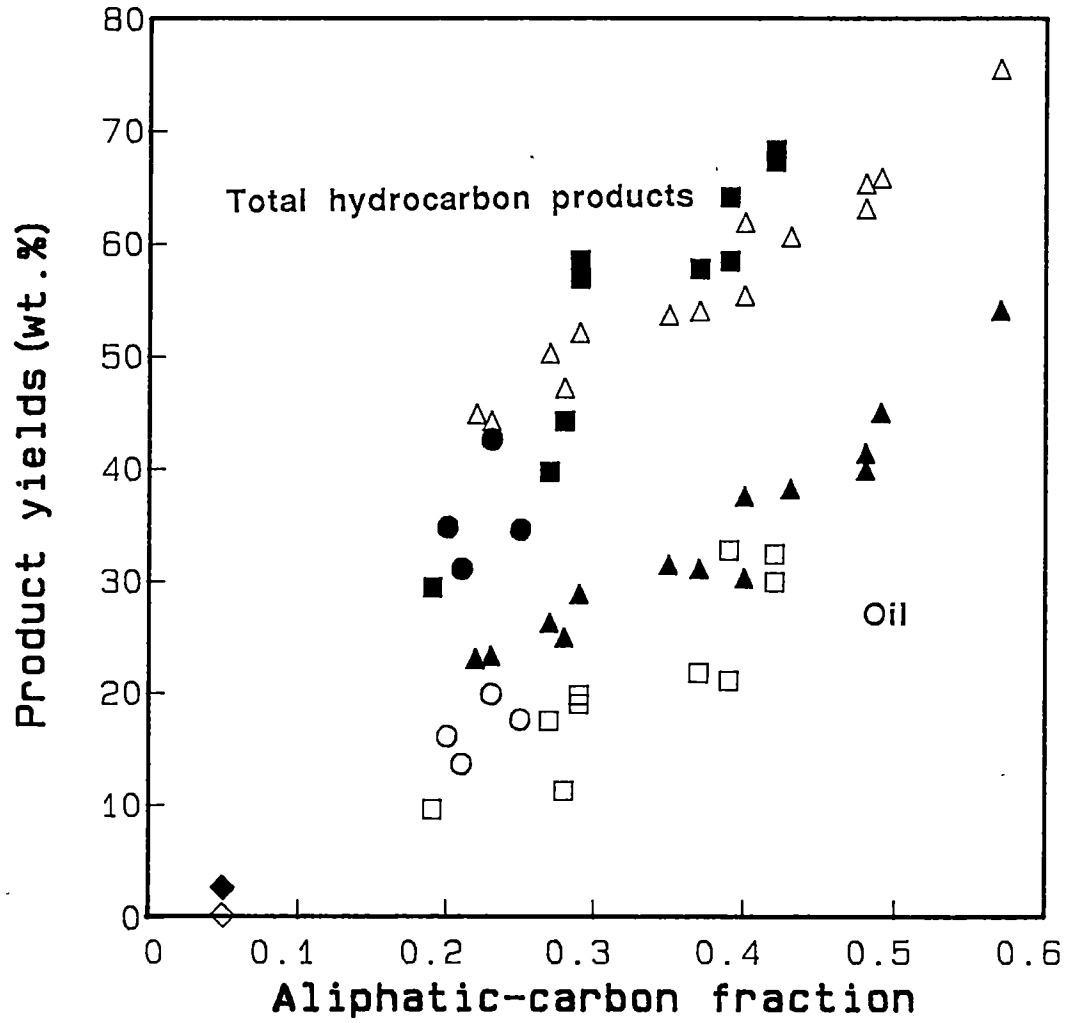
Figure 4.18 Plot of aliphatic-carbon fraction, f_{al} , versus the yields of liquefaction products.

Oil: ▲ , brown coals ; □ , higher-rank coals; O , oxygen-rich subbituminous; ◇ , semianthracite.

Total hydrocarbon products: △ , brown coals ; ■ , higher-rank coals; ● , oxygen-rich subbituminous; ◆ , semianthracite.

The proportions of methyl, methylene, methine and quaternary carbons in the aliphatic structures of the coals can be estimated as a fraction of aliphatic carbons excluding those related to oxygen-functional groups. Only the methylenic carbon fraction, C_{CH_2}/C_{al}, increases with the **H/C** values for both brown coals and higher-rank coals (see **Figure 4.19**). Other aliphatic fractions tend to decrease with the increase in **H/C** ratios of the coals as shown in **Figure 4.20** for the methyl-carbon fraction, C_{CH_3}/C_{al}. The results thus suggested that the methylenic groups are responsible for the increases in the aliphatic contents and the **H/C** values of coals studied. As can be seen in **Figure 4.19**, the increase in the proportion of methylenic carbons is more pronounced among the higher-rank coal than that among the brown coals, indicating that the variation in the aliphatic carbon distribution among the samples is higher for the higher-rank coals than for the brown coals. The data in **Figure 4.19** and **Figure 4.20** also revealed that coals in an inertinite-rich group, ABL2, ABL4, ABL5, ABL7 and ABL8 contain a higher proportion of **-CH$_2$-** but a lower **-CH$_3$** concentration than would be expected from their **H/C** values. The results suggested that the aliphatic structures of the brown coals are comparatively more uniform across the samples studied.
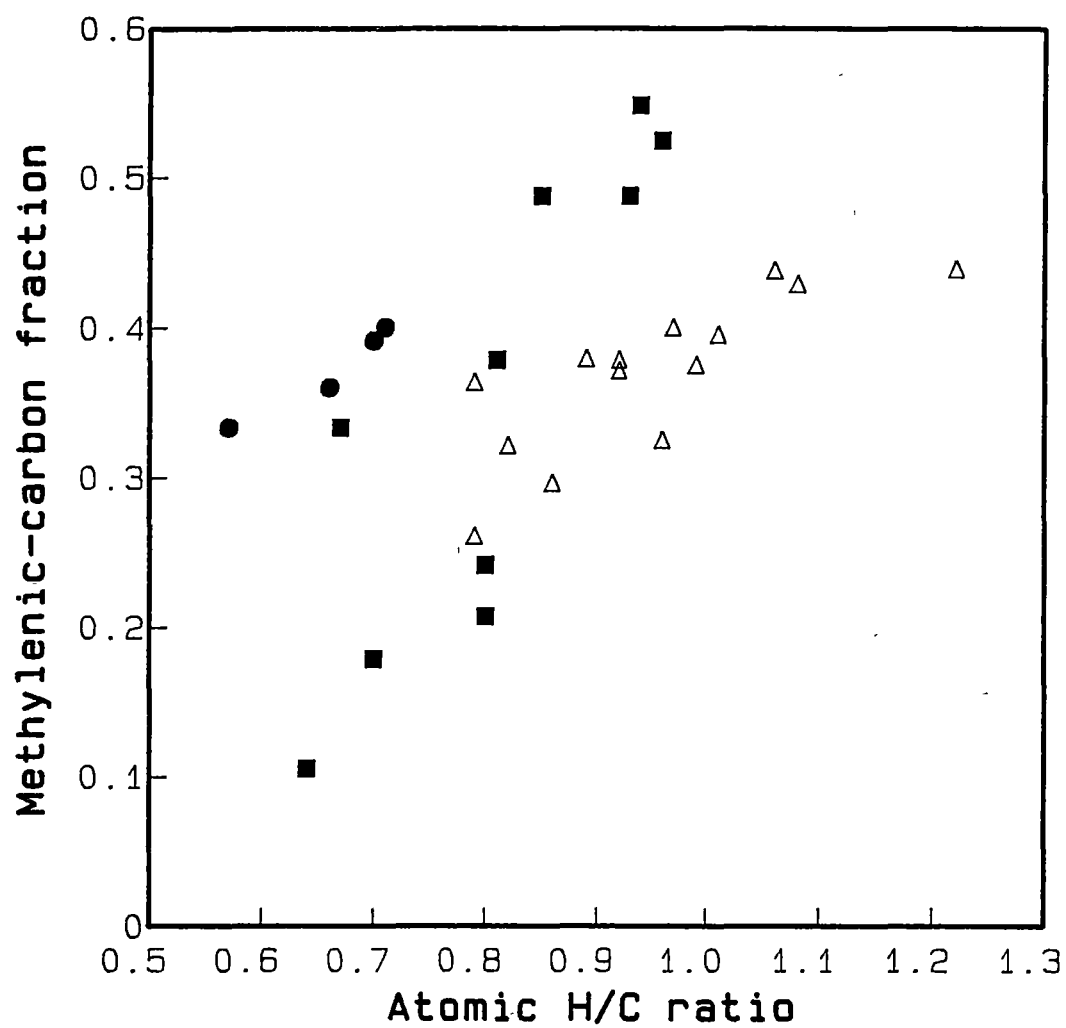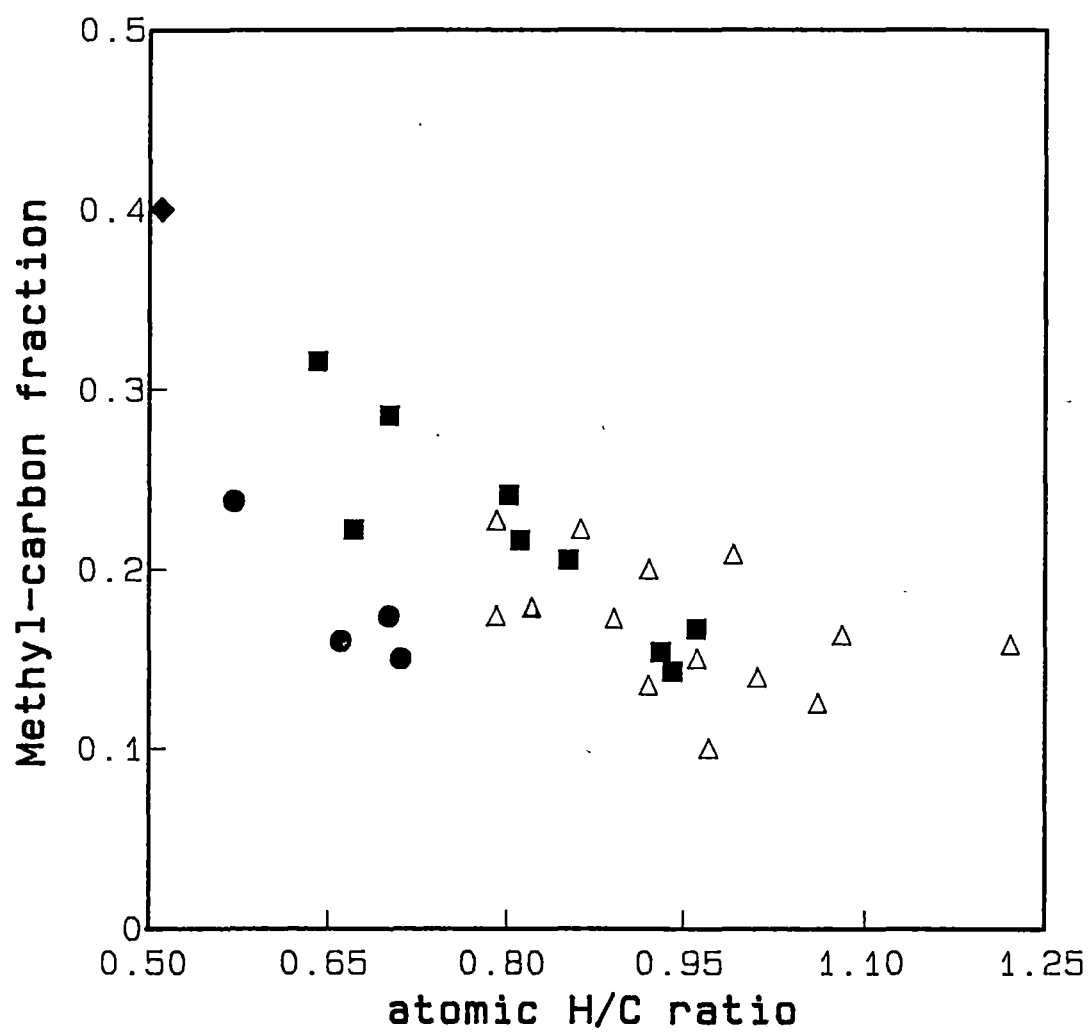
Figure 4.19 Plot of methylenic-carbon fraction, $C_{al}^{CH_2}/C_{al}$, versus coal H/C ratio (see **Figure 4.12** for symbols).

Figure 4.20 Plot of methyl-carbon fraction, $C_{al}CH_3/C_{al}$, versus coal H/C ratio (see **Figure 4.12** for symbols).

c) Oxygen-functional groups.

Four major types of oxygen-functional groups, namely, carbonyl, phenolic, oxygenated aliphatic and methoxyl groups, were identified in coals studied. The total oxygenated-carbon fractions determined as a summation of f_{car}, $f_{ar}{}^{O}$ and $f_{al}{}^{O}$ display a strong correlation with coal O/C ratios as shown in **Figure 4.21**. The good relationship observed suggests that most of the major oxygenated carbons in the coals were detected by the techniques used. The major contributors to the variations in the oxygen contents of the coals are the carbonyl and phenolic groups. The $f_{ar}{}^{O}$ values markedly increase in the O/C range 0.04 to 0.09 corresponding to the data of bituminous coals in which the main oxygen-functional groups are of the phenolic structures (see **Figure 4.22**). The total carbonyl fraction, f_{car}, steadily increase from 0.01 for a bituminous coal to the range of 0.11 to 0.16 for the brown coals (see **Table 4.9**). The carbonyl fractions can be divided further into ketonic-type, $f_{car}{}^{CO}$, and carboxyl, $f_{car}{}^{COO}$, fractions. The values of both parameters increase with coal O/C ratios.   Although the general correlations between the oxygenated-carbon fractions and oxygen contents were observed for the entire suite of coals studied, there is no clear trend of the distribution of oxygenated-carbons in the brown coals. From the values of oxygenated-carbon fractions the distribution of oxygen in the coal can be estimated. The content of an oxygen-functional group i, designated O_i was determined as follows :

$$O_i = f_i{}^k \, / \, [f_{car}{}^{CO} + 2 \cdot f_{car}{}^{COO} + f_{ar}{}^{O} + 0.5 \cdot f_{al}{}^{O}] \qquad (4.10)$$

where i and k specify the type of functional group.
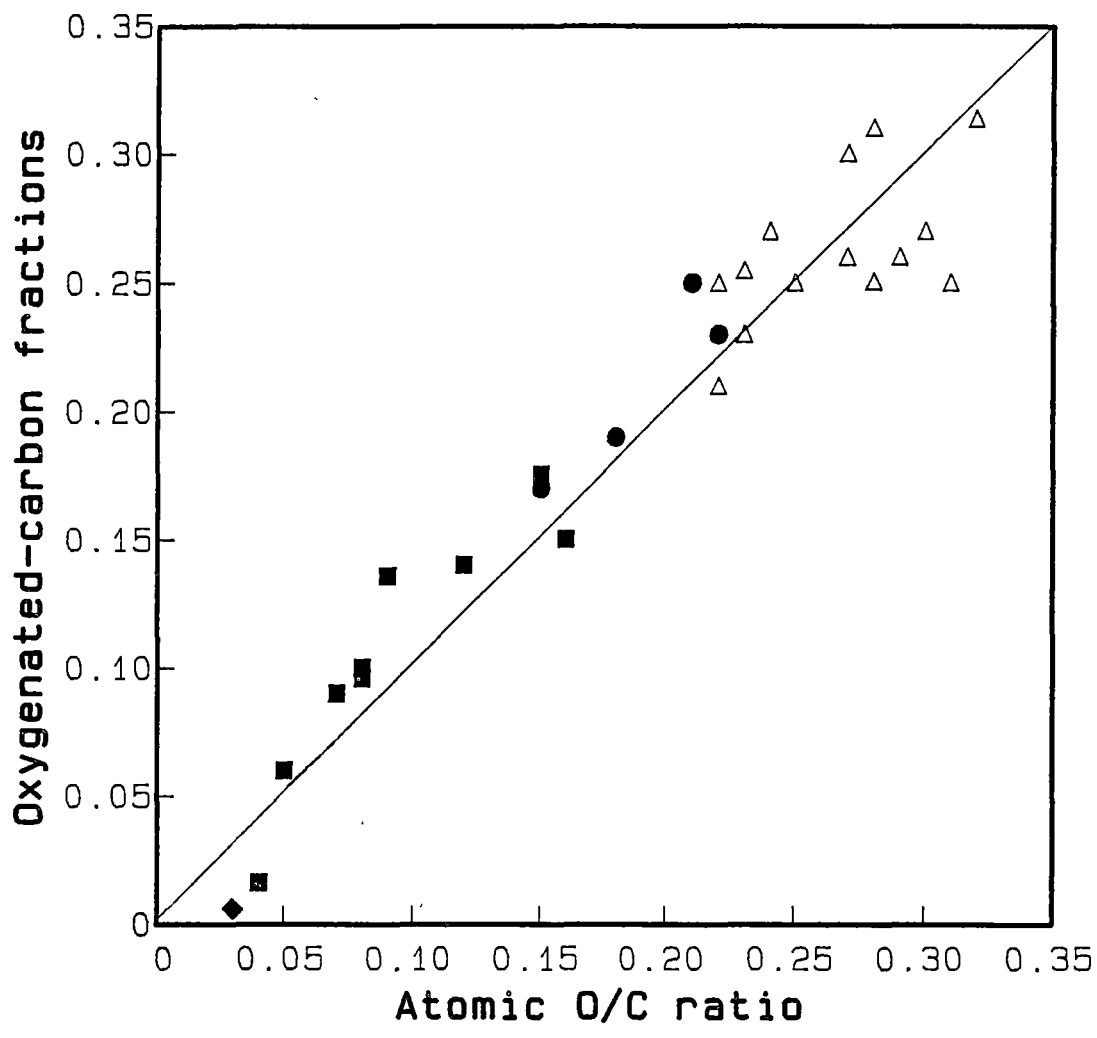
Figure 4.21 Plot of total oxygenated-carbon fractions, $f_{ar}{}^O + f_{al}{}^O + f_{car}$, versus coal O/C ratio (see **Figure 4.12** for symbols).
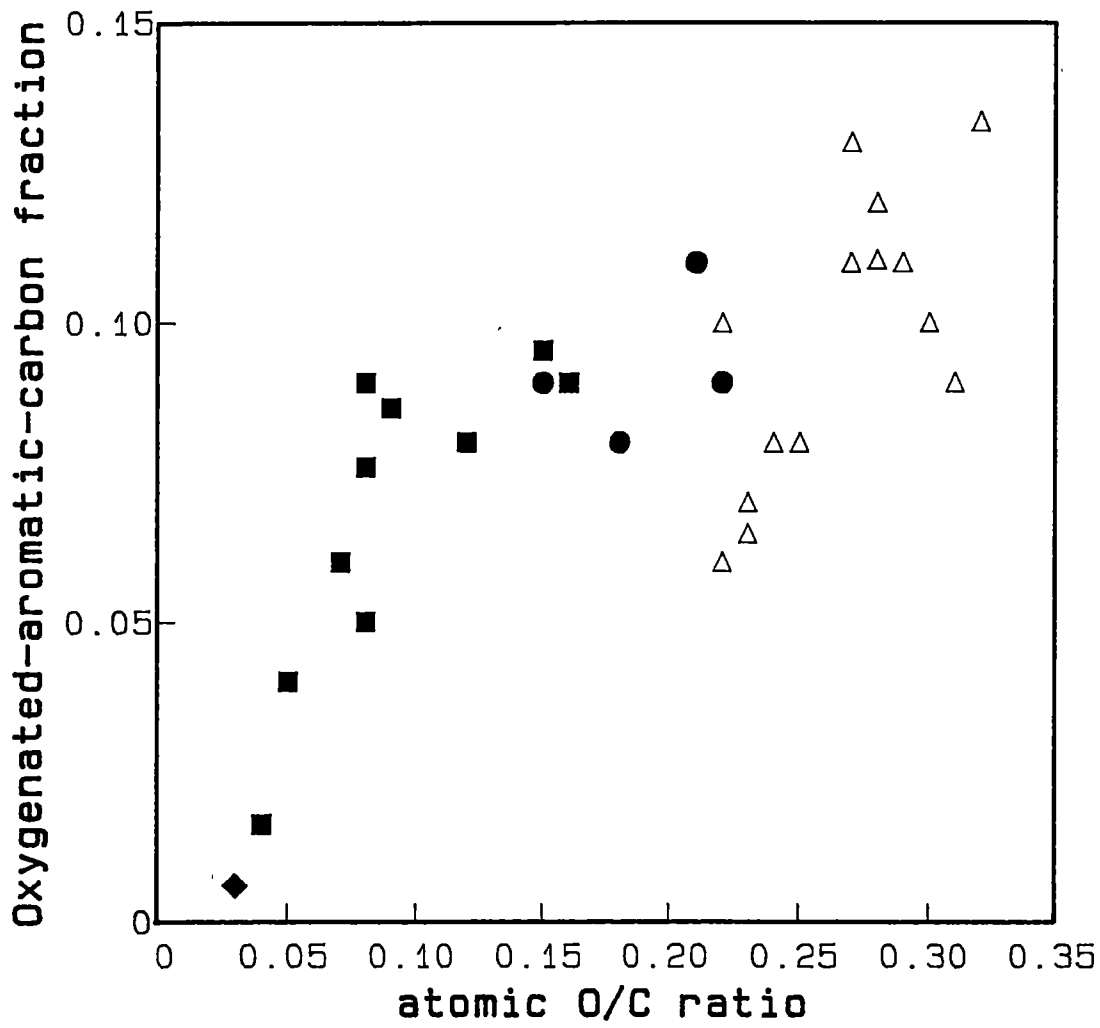
Figure 4.22 Plot of oxygenated-aromatic-carbon fractions, f_{ar}^O, versus coal O/C ratio (see **Figure 4.12** for symbols).

Since the carboxyl group contains two oxygen atoms, in order to calculate the oxygen content related to the group, the carboxyl-carbon fraction was multiplied by 2. The proportion of oxygen related to oxygenated aliphatics was estimated from the corresponding carbon fraction with the value of $0.5 \cdot f_{al}^O$ by assuming that in each oxygenated-aliphatic group, two carbon atoms are attached to one oxygen atom. The data of oxygen distributions estimated are given in **Table 4.10**.

In the brown coals, the carboxyl-oxygen atoms account for 48 to 60 % of the total oxygen observed while the amount of oxygen associated with phenols or phenolic ethers varies from 14 to 32 %. The remaining oxygen atoms distribute among the ketonic, methoxyl and aliphatic-ether groups. The large proportions of the oxygen detected in the higher-rank coals are of phenol or phenolic ether groups. The carboxyl groups were also found in a substantial amount in the coals of subbituminous rank. The oxygen distributions in the coals observed here indicated that the methoxyl groups and aliphatic ethers were the first oxygen-functional groups that were removed from the coal structure in an early stage of coalification process. The loss of carboxyl and carbonyl groups occurred in a later stage during the transition from subbituminous to bituminous rank.

Table 4.10 Oxygen distribution in Australian coals[a].

Coal	[b]$O_{OH(R)}$	O_{CO}	O_{COO}	O_{OCH_3}	$O_{O(CH_n)_2}$
ABL1	100.00	-	-	-	-
ABL2	39.63	10.07	50.30	-	-
ABL3	100.00	-	-	-	-
ABL4	29.70	11.36	58.94	-	-
ABL5	85.40	4.38	10.23	-	-
ABL6	54.15	8.29	37.56	-	-
ABL7	32.00	13.44	54.57	-	-
ABL8	27.18	11.76	61.06	-	-
ABL9	68.73	4.96	26.31	-	-
ABL10	51.80	12.16	36.04	-	-
ABL11	36.81	10.43	52.76	-	-
ABL12	54.71	9.43	35.86	-	-
ABL13	41.62	11.43	46.95	-	-
ABL14	46.35	8.16	45.48	-	-
ABL15	43.70	9.25	47.04	-	-
ABR1	25.41	11.53	56.00	5.65	1.41
ABR2	31.48	12.90	49.35	3.13	3.13
ABR3	21.95	12.51	57.31	5.49	2.74
ABR4	25.82	11.95	50.99	7.49	3.75
ABR5	28.48	13.91	49.85	5.18	2.59
ABR6	21.15	10.26	58.02	6.04	4.53
ABR7	24.33	10.70	56.45	4.87	3.65
ABR8	29.21	15.21	47.47	3.25	4.87
ABR9	30.20	10.24	52.00	3.02	4.53
ABR10	16.62	9.68	60.40	6.65	6.65
ABR11	19.13	13.43	60.61	2.73	4.10
ABR12	18.86	13.16	55.41	6.29	6.29
ABR13	13.57	16.59	57.71	6.06	6.06
ABR14	18.49	10.96	59.45	3.70	7.40

[a] As percentage of apparent oxygen. [b] Phenols and phenolic ethers other than methoxyl groups.

4.4 CONCLUSIONS

The high-resolution TOSS and TOSS/DD ^{13}C nmr spectra provided considerable details of the structural characteristics of the coals studied. The observations of various carbon functionalities are consistent with the FTIR studies. The evidence for the presence of quaternary aliphatic carbons in the coals studied has been observed from the DD spectra. The DD experiments also revealed the presence of mobile components in the aliphatic structures of the coals. The observation is in accordance with those reported on other coals.

The cross-polarization studies revealed the differences in the cross-polarization time among the three main carbon types for each coal. The T_{CH} values for coals studied, however, showed no rank dependence whereas the $T_{1\rho}^{H}$ values for both aromatic and aliphatic carbons in the higher-rank coals are higher than those in the brown coals. The similar values of $T_{1\rho}^{H}$ for the three main carbon types indicated the importance of the spin-diffusion process in the coals. The differences in the cross-polarization time observed suggested that the variable contact time method may be necessary for quantitative analyses of the coals, especially the brown coals. However, an optimum contact time of 1.5 ms has been proposed for using in a single contact time experiment on the coals studied.

The procedures used to determine the estimates of various carbon fractions have been presented. A good correspondence between the values of carbon aromaticity determined from TOSS and normal ^{13}C nmr spectra demonstrated the applicability of the TOSS technique to Australian coals.

The loss in aromatic substitution accompanied by an increase in protonated aromatics was found in the coals studied. The major aromatic substituents, that were found to be decreasing with an increase in coal rank, are phenolic groups. The increase in the aromatic cluster size with coal rank was also observed. In view of the aliphatic structure, the methylenic groups are the main contributor to the increase in the aliphatic content and to the variation in atomic H/C ratios of the coals.

Finally, the distribution of oxygenated carbons has been reported. The total oxygenated-carbon fractions are shown to correlate with atomic O/C ratios of the coals, indicating that the major oxygen-functional groups were detected by the method used in this study.

CHAPTER FIVE

COMPARISON of FTIR
and
SOLID-STATE ^{13}C nmr DATA

5.1 INTRODUCTION

From the results presented in **Chapter 3** and **Chapter 4**, it is demonstrated that FTIR and ^{13}C nmr studies can provide complementary information on the structural features of coals. As regards the oxygen-functional groups, while the FTIR studies indicate a presence of several types of carbonyl groups in the coals, namely, esters, carboxylic acids and ketonic-type structures, the ^{13}C nmr technique can only distinguish the carboxyl from the ketonic-type carbons. On the other hand, more details of the aromatic and aliphatic structures in the coals can be observed by the ^{13}C nmr technique.

In terms of quantitative measurement, there is a general correspondence between the FTIR and solid-state ^{13}C nmr data, as observed from their relationships with elemental-analysis parameters. As the rank of coal increases, the decreases in oxygen-functional groups were consistently observed from both studies. The aliphatic and aromatic contents derived from the FTIR and ^{13}C nmr measurements were found to correlate with

coal atomic. **H/C** ratios and with the liquefaction yields.

In this chapter, a direct comparison of the FTIR and solid-state ^{13}C nmr data is examined in order to evaluate their accuracies. The discrepancies between the values of the parameters derived from the two methods provide additional information on the structural features of the coals.

5.2 RESULTS AND DISCUSSION

5.2.1 Comparisons of parameters related to aromatic and aliphatic contents.

a) Aromatic and aliphatic hydrogen contents.

From the solid-state ^{13}C data, the aromatic hydrogen content in a coal is readily estimated as a fraction of total carbon, H_{ar}/C , from the protonated aromatic carbon fractions. The aliphatic hydrogen to carbon ratio, H_{al}/C, can be estimated from the equation:

$$H_{al}/C = [3 . f_{al}^{CH_3}] + [2 . f_{al}^{CH_2}] + f_{al}^{CH} \qquad (5.1)$$

where $f_{al}^{CH_3}$, $f_{al}^{CH_2}$ and f_{al}^{CH} are the methyl, methylene and methine carbon fractions defined in **Table 4.6** respectively. For the brown coals, additional terms related to methoxyl carbons, $[3.f_{al}^{OCH_3}]$, and oxygenated aliphatics, $[1.5.f_{al}^{O}]$ are included in the calculation of H_{al}/C value in addition to the terms in **equation (5.1)**. The factor 1.5 for the oxygenated-aliphatic term is taken as an average stoichiometry of the $-CH_n-O-$ group (n = 1 or 2).

The values of H_{ar}/C and H_{al}/C can be also determined from the combined data of atomic % H_{ar} and H_{al} , as derived from the FTIR method (see **Table 3.5**), and the atomic % **C** , determined from elemental-analysis data. The values of H_{ar}/C and H_{al}/C calculated from the FTIR and solid-state ^{13}C nmr data are given in **Table 5.1**.

Figure 5.1 compares the the FTIR and ^{13}C nmr values of the aromatic hydrogen to total carbon ratio, H_{ar}/C. Although the results show a correlation between the two sets of data (correlation coeff. = 0.89), a substantial difference between them is also obvious. The ^{13}C nmr data are much greater than those of the FTIR for most coals except for the semianthracite, ABL1 and the oxygen-rich subbituminous, ABL8. The discrepancies are extremely large, as a factor > 4, for a group of brown coals having **H/C** > 0.95 (ABR8-ABR14). A similar range of differences between the aromatic hydrogen contents determined by FTIR and ^{13}C nmr has been reported by Havens et al. [1983] for a set of U.S. vitrinite concentrates. As noted earlier in **Chapter 3** , **section 3.3.3** , the accuracy error in the FTIR aromatic hydrogen content can be identified with the uncertainty in the extinction coefficient used for the aromatic **C-H** stretching band and in the band area measurements, particularly, for the brown coals with a high **H/C** value. Solomon and Carangelo [1988] have also reported the difficulty in the measurement of the aromatic **C-H** stretching band (~3100 cm^{-1}), especially in the spectra of low-rank coals.

In this work, for the high **H/C** brown coals, the aromatic **C-H** stretching band is extremely weak (see **Figure 3.1** and **3.15**), probably being due to the low concentration of these species in these brown coals.

Table 5.1 Comparison of FTIR and ^{13}C nmr data for Australian coals.

Coal	^{13}C nmr			FTIR			
	H_{ar}/C	H_{al}/C	H_{al}/C_{al}	H_{ar}/C	H_{al}/C	f_{ar}[a]	H_{al}/C_{al}[b]
ABL1	0.33	0.11	2.10	0.35	0.16	0.92	3.21
ABL2	0.19	0.38	1.81	0.13	0.39	0.73	1.86
ABL3	0.27	0.33	1.74	0.19	0.44	0.78	2.32
ABL4	0.18	0.42	1.68	0.15	0.42	0.68	1.69
ABL5	0.21	0.48	1.78	0.18	0.46	0.76	1.70
ABL6	0.22	0.49	1.75	0.18	0.49	0.74	1.76
ABL7	0.14	0.40	1.74	0.08	0.53	0.60	2.30
ABL8	0.17	0.34	1.70	0.18	0.44	0.64	2.20
ABL9	0.21	0.49	1.69	0.17	0.59	0.65	2.02
ABL10	0.18	0.50	1.72	0.11	0.64	0.63	2.20
ABL11	0.14	0.67	1.81	0.09	0.68	0.61	1.84
ABL12	0.17	0.74	1.90	0.08	0.73	0.61	1.86
ABL13	0.13	0.70	1.79	0.07	0.79	0.53	2.01
ABL14	0.15	0.77	1.83	0.06	0.80	0.54	1.91
ABL15	0.14	0.78	1.86	0.06	0.85	0.51	2.02
ABR1	0.18	0.44	2.02	0.11	0.57	0.58	2.59
ABR2	0.18	0.39	1.70	0.10	0.58	0.59	2.53
ABR3	0.15	0.50	1.79	0.08	0.64	0.53	2.28
ABR4	0.13	0.54	1.98	0.06	0.70	0.50	2.59
ABR5	0.12	0.53	1.83	0.06	0.73	0.48	2.51
ABR6	0.12	0.63	1.72	0.04	0.80	0.47	2.16
ABR7	0.12	0.65	1.84	0.04	0.78	0.46	2.22
ABR8	0.14	0.63	1.59	0.03	0.84	0.46	2.09
ABR9	0.12	0.64	1.61	0.03	0.85	0.46	2.12
ABR10	0.09	0.86	1.79	0.02	0.88	0.44	1.83
ABR11	0.08	0.70	1.64	0.02	0.91	0.39	2.12
ABR12	0.09	0.82	1.71	0.02	0.94	0.40	1.96
ABR13	0.09	0.87	1.78	0.02	0.96	0.37	1.96
ABR14	0.07	0.96	1.68	0.01	1.09	0.34	1.92

[a] Corrected for carbonyl-carbon fraction. [b] From FTIR (H_{al}/C) and ^{13}C nmr (C_{al}/C).
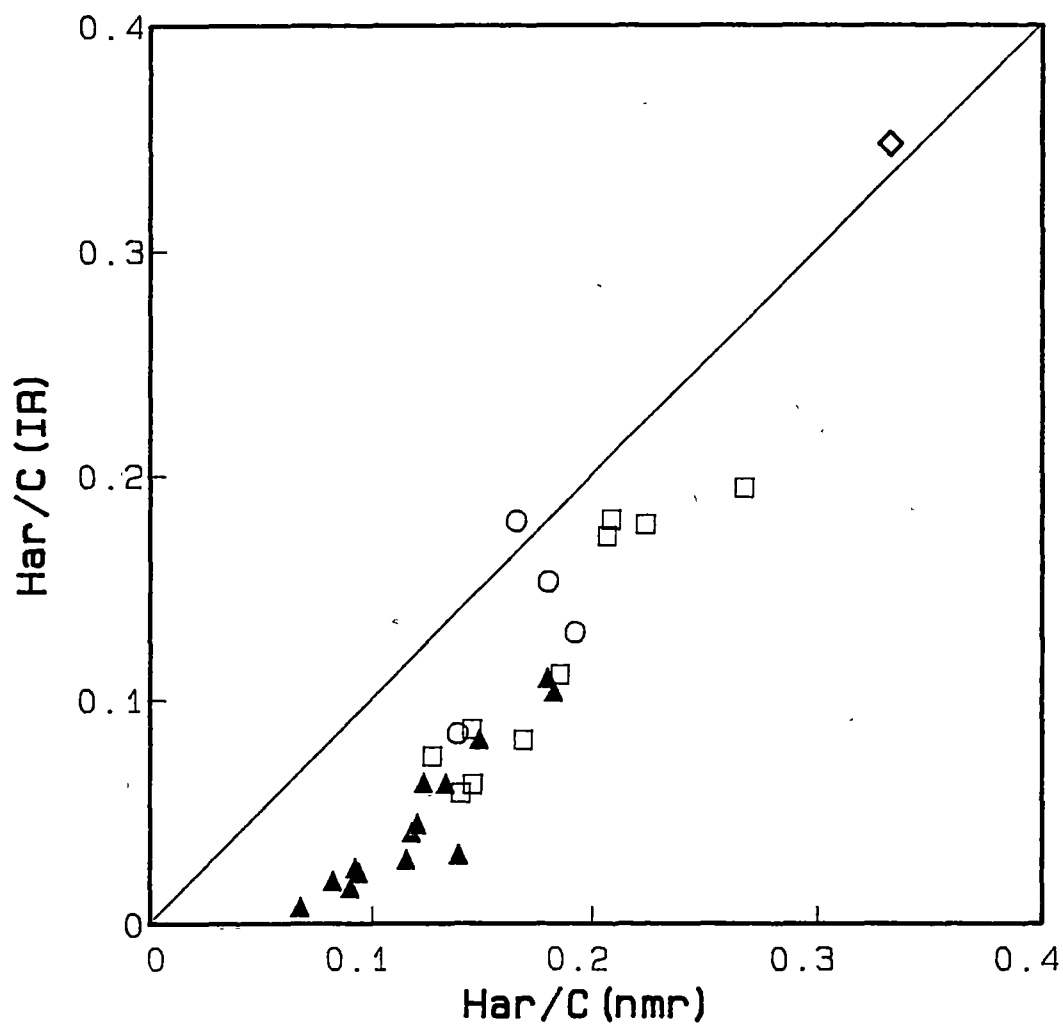
Figure 5.1 Correlation between aromatic hydrogen to carbon ratios derived from ^{13}C nmr and FTIR data: ▲ , brown coals; □ , higher-rank coals; ○ , oxygen-rich subbituminous coal; ◇ , semianthracite.

Furthermore, these brown coals contain a relatively high concentration of **COOH** groups, as indicated by the intensity of 1700 cm^{-1} band (see **Table 3.3**), the weak aromatic **CH** band may be hidden by the strong IR absorption of the hydrogen-bonded **O-H** vibration. The uncertainty in the measurement of aromatic **CH** band area, however, may be equally applied to other coals. Therefore, it is believed that in absolute terms, the H_{ar}/C value obtained from the ^{13}C nmr method is probably more reliable than the IR value.

The values of aliphatic hydrogen to total carbon ratio, H_{al}/C, derived from the FTIR and ^{13}C nmr data, are compared in **Figure 5.2** (correlation coeff. = 0.88). As indicated by the 1:1 relationship line, the H_{al}/C values from the two methods are in a better agreement than those of the aromatic counterparts. The FTIR data for some coals, however, are larger than the ^{13}C nmr values. The error in the FTIR data is probably also related to the extinction coefficient of the aliphatic **CH** stretching band, used in the calculation of aliphatic hydrogen content. The uncertainty in the ^{13}C nmr data is associated with the errors in the aliphatic-carbon fractions. Unlike the H_{ar}/C value, which is readily obtained from the protonated-aromatic-carbon fraction, the estimation of aliphatic hydrogen content from the ^{13}C nmr data is based on the distribution of aliphatic carbons. According to **equation (5.1)**, the error in each aliphatic-carbon fraction is further enlarged by the stoichiometric factor n of the -**CH$_n$**-group, resulting in a great uncertainty in the H_{al}/C value. The major uncertainty in the ^{13}C nmr H_{al}/C value probably arises from the errors in methine and methylenic carbon fractions, since the estimations of the two fractions are based on the chemical-shift data for the two carbon types. Both types of aliphatic carbons can have the resonances in the same chemical-shift ranges [Snape et al.,1979].
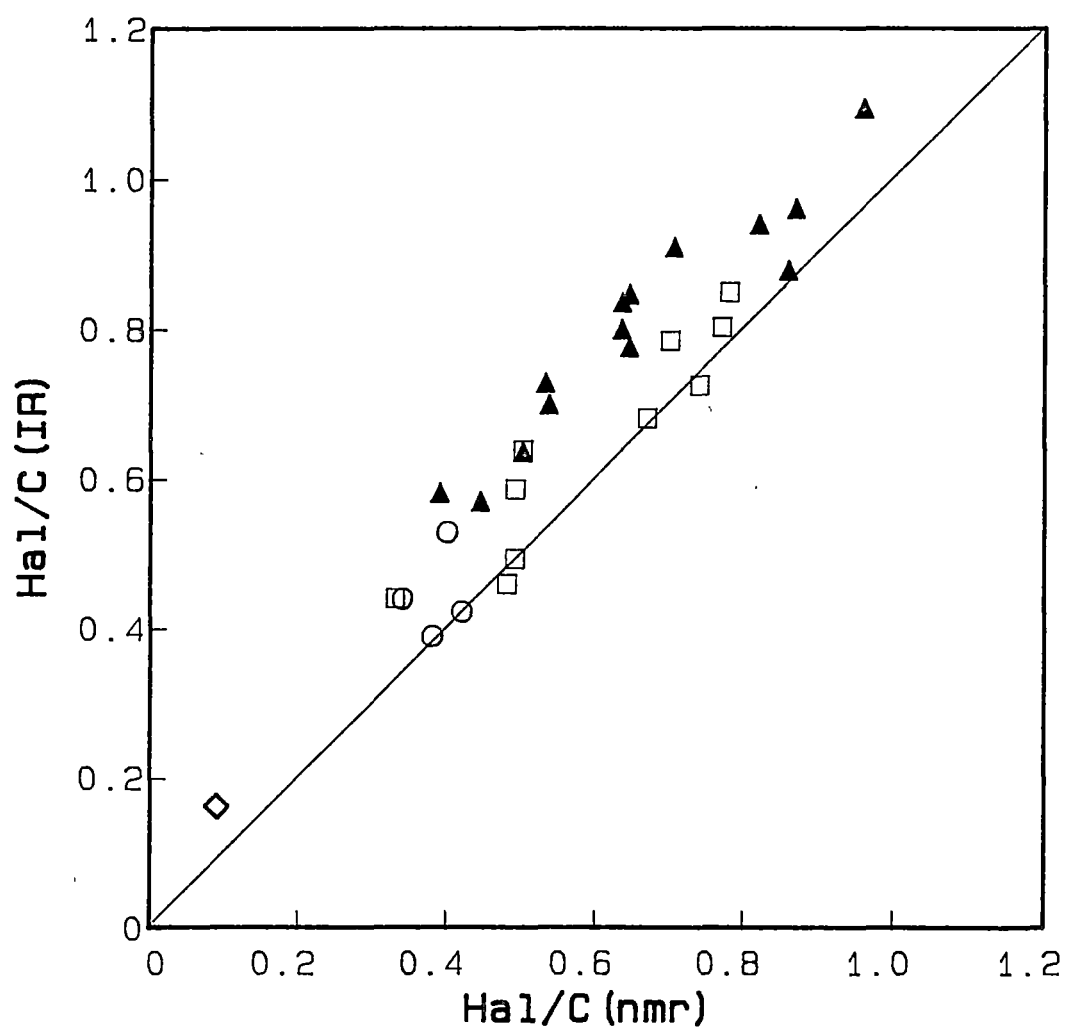
Figure 5.2 Correlation between aliphatic hydrogen to carbon ratios derived from ^{13}C nmr and FTIR data (see **Figure 5.1** for symbols).

b)   Carbon aromaticities.

The carbon aromaticities of the coals can be determined from the FTIR data by using the Brown-Ladner [1960] equation :

$$f_{ar}(IR) = 1 - (C_{al}/C) \qquad (5.2)$$

$$C_{al}/C = (H_{al}/H) \cdot (H/C) / (H_{al}/C_{al}) \qquad (5.3)$$

where $f_{ar}(IR)$ is the FTIR carbon aromaticity, C_{al}/C is the aliphatic-carbon fraction and H/C is an atomic hydrogen-to-carbon ratio calculated from elemental-analysis data. H_{al}/C_{al}, an atomic hydrogen-to-carbon ratio for aliphatic group, is generally taken with a value of 2 corresponding to an assumption for average aliphatic structures of methylenic groups ($-CH_2-$) and H_{al}/H is a fraction of total hydrogens present as aliphatic hydrogens. Originally the H_{al}/H values were derived from [1] H nmr analyses of coal-derived liquids. In this study, the value of H_{al}/H was determined from the FTIR data for the aliphatic-hydrogen content in the coal. Equation (5.2) assumes that all carbon atoms present are either aliphatic or aromatic in character i.e., the carbonyl carbons are assumed to be negligible.

Very few studies have been reported using the Brown-Ladner method with the IR data for solid coal samples [Painter et al., 1983b: Gerstein et al., 1982]. In most studies, the Brown-Ladner calculations were used without stating the implicit assumption that only aromatic and aliphatic carbons are present in the samples as implied by the definition of $f_{ar}(IR)$ in equation (5.2). The assumption is valid for most coal-derived materials and some coals of high rank. Results determined using this assumption

are plotted against the $f_{ar}(NMR)$ values in **Figure 5.3**. It is evident that there are significant deviations from the expected correlation especially at low f_{ar} values corresponding to the brown coals. Previous work by Painter et al. [1983b] and Gerstein et al. [1982] was for higher-rank coals where the deviations were not as apparent. For our coal sample, in particular the brown coals, there is a considerable amount of carbonyl groups that have to be taken into account. Therefore, instead of **equation (5.2)** the $f_{ar}(IR)$ is more correctly expressed as:

$$f_{ar}(IR) = 1 - (C_{al}/C)_{IR} - (C_{C=O}/C)_{IR} \qquad (5.4)$$

where $(C_{al}/C)_{IR}$ is the term defined in **equation (5.3)**, $(C_{C=O}/C)_{IR}$ is the carbonyl carbon fraction. Since this fraction cannot be easily estimated from IR spectra due to contributions from other functional groups, for this work its value has been set equal to the ^{13}C nmr value from **Table 4.7** in **Chapter 4**. The significance of the carbonyl carbon fraction is seen when the $f_{ar}(IR)$ values determined according to the definition in **equation (5.4)** are compared with the $f_{ar}(NMR)$ values as shown in **Figure 5.4**. The values of $f_{ar}(IR)$ for the coals are also reported in **Table 5.1**. With a correlation coefficient of 0.93 and the ratio $f_{ar}(NMR)/f_{ar}(IR)$ ranging from 0.91 to 1.16, the correspondence between the two sets of data can be considered to be good. The discrepancies observed may be related to the parameter H_{al}/C_{al} used in **equation (5.3)** for the determination of C_{al}/C values [Retcofsky et al., 1977; Painter et al., 1983b]. In practice, one would expect the H_{al}/C_{al} to vary according to the variability in the aliphatic structures of coals. The parameter H_{al}/C_{al} can be estimated from **equation (5.3)** by using the C_{al}/C value taken from solid state ^{13}C nmr spectrum and using the values for the other parameters as previously.
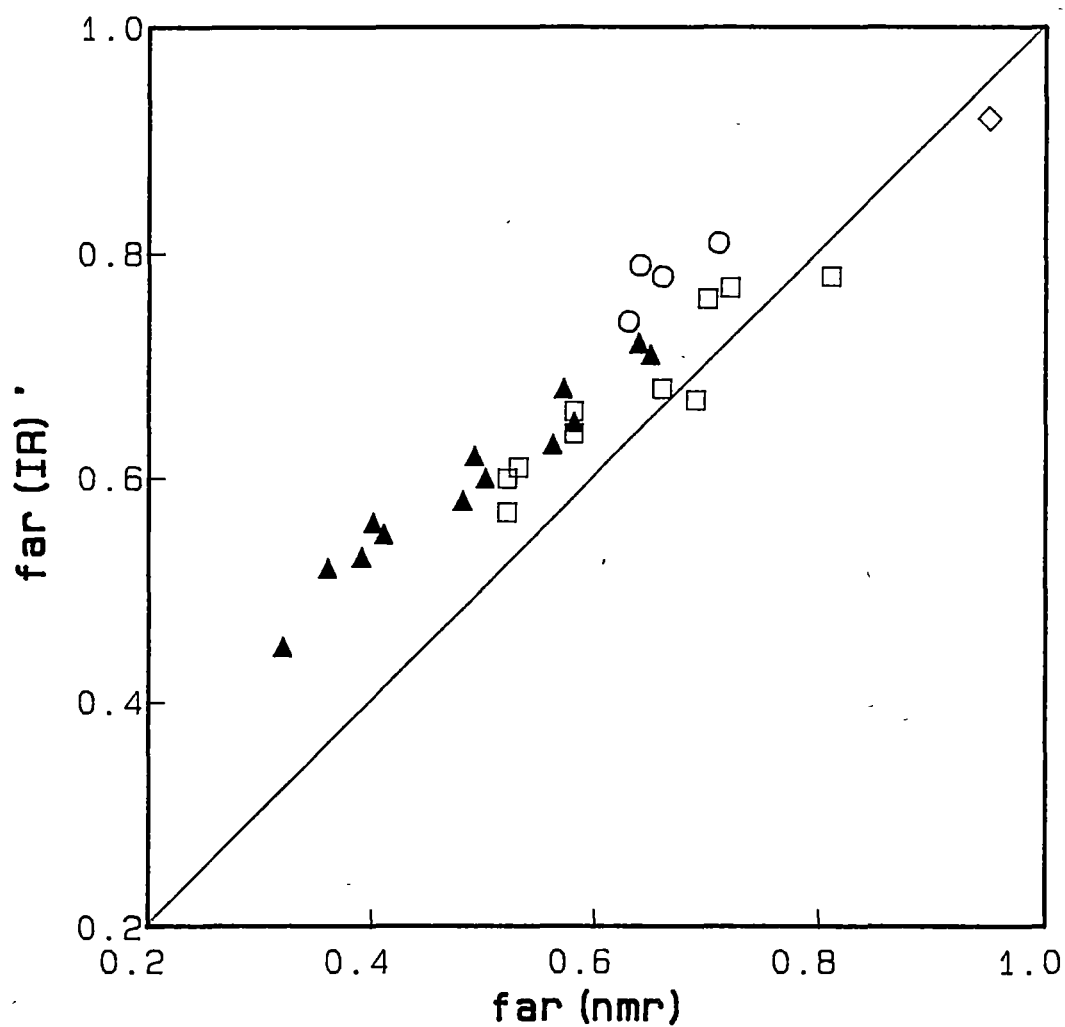
Figure 5.3 Comparison of carbon aromaticity obtained from ^{13}C nmr, $f_{ar}(nmr)$, and that calculated from FTIR data without a correction for carbonyl-carbon fraction, $f_{ar}(IR)'$ (see **Figure 5.1** for symbols).
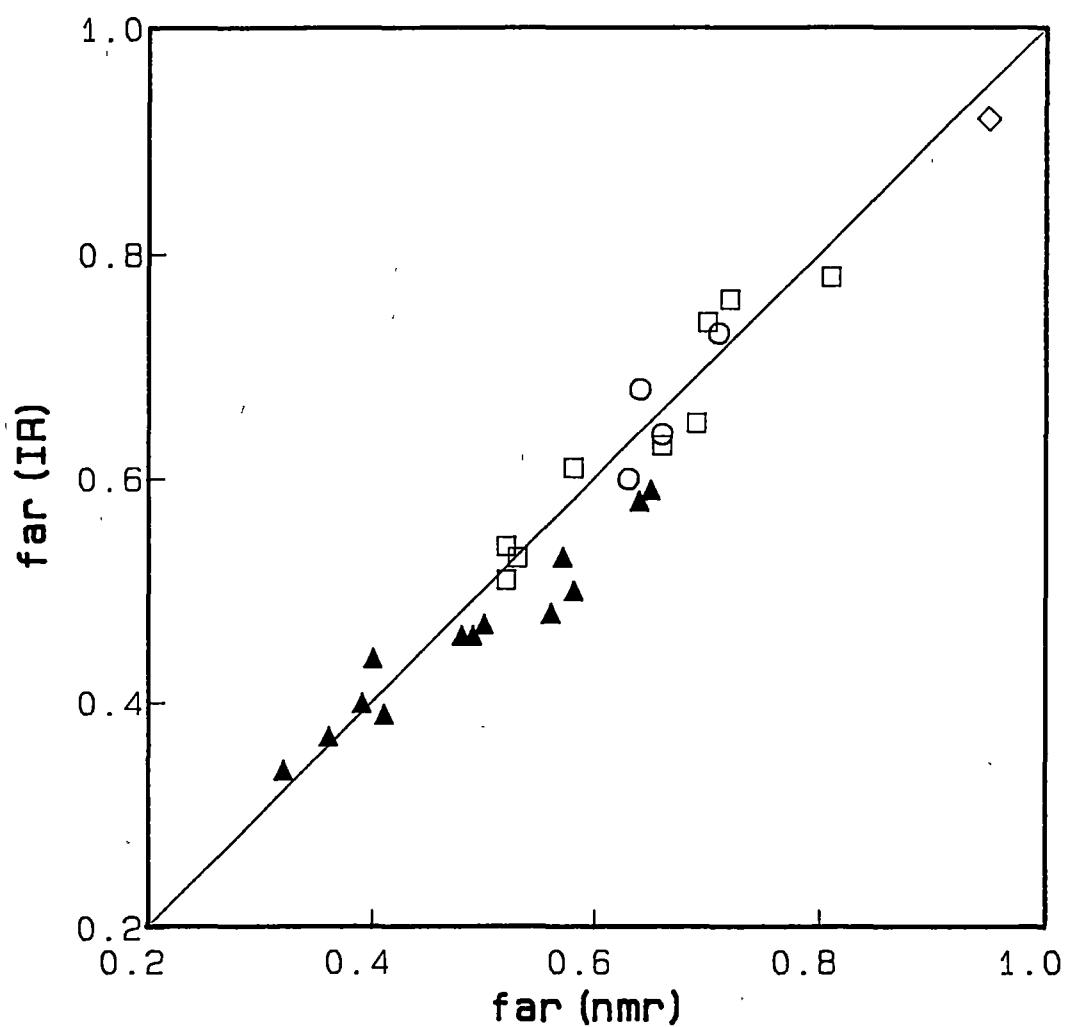
Figure 5.4 Comparison of carbon aromaticity obtained from ^{13}C nmr, f_{ar}(nmr) , and that calculated from FTIR data with a correction for carbonyl-carbon fraction, f_{ar}(IR) (see **Figure 5.1** for symbols).

The results are given in **Table 5.1.** For the whole suite of coals, there is no simple trend in the variation of H_{al}/C_{al} with **H/C** ratios or carbon contents. Values are in the ranges of 3.21 to 1.69 and 2.59 to 1.83 for the higher-rank coals and brown coals respectively. In order to illustrate the range of the H_{al}/C_{al} values for coals studied, the ^{13}C nmr data for C_{al}/C are plotted against the FTIR values of H_{al}/C as shown in **Figure 5.5.** The lines represent the H_{al}/C_{al} value ranging from 2.50 to 1.75 are indicated in the Figure. The average values of H_{al}/C_{al} for the higher-rank coals and the brown coals are 2.1 and 2.2 respectively. It is concluded that the value of 2.0 used previously as a first estimate for H_{al}/C_{al} is not unreasonable. Painter et al. [1983b] reported the H_{al}/C_{al} value, varying from 2.58 to 1.66 for U.S. vitrinite concentrates, while the range 2.42 to 1.32 was reported by Gerstein et al. [1982] for U.S. coal samples, ranging in rank from anthracite to lignite . It should be noted that when the sample contains a significant concentration of carbonyl groups the value of H_{al}/C_{al} can be underestimated with a large error if the carbon aromaticity, $f_{ar}(NMR)$, is used for C_{al}/C in the calculation without taking into account the carbonyl carbon fraction i.e., by using :

$$C_{al}/C = 1 - f_{ar}(NMR) \qquad (5.5)$$

In both previous studies [Painter et al., 1983b; Gerstein et al., 1982], no details regarding the calculation of H_{al}/C_{al} were given.

The H_{al}/C_{al} values can be also estimated from the solid-state ^{13}C nmr data alone. They are also given in **Table 5.1.** The ^{13}C nmr H_{al}/C_{al} values, however, may be underestimated, as being due to the error associated with the ^{13}C nmr H_{al}/C as noted earlier.
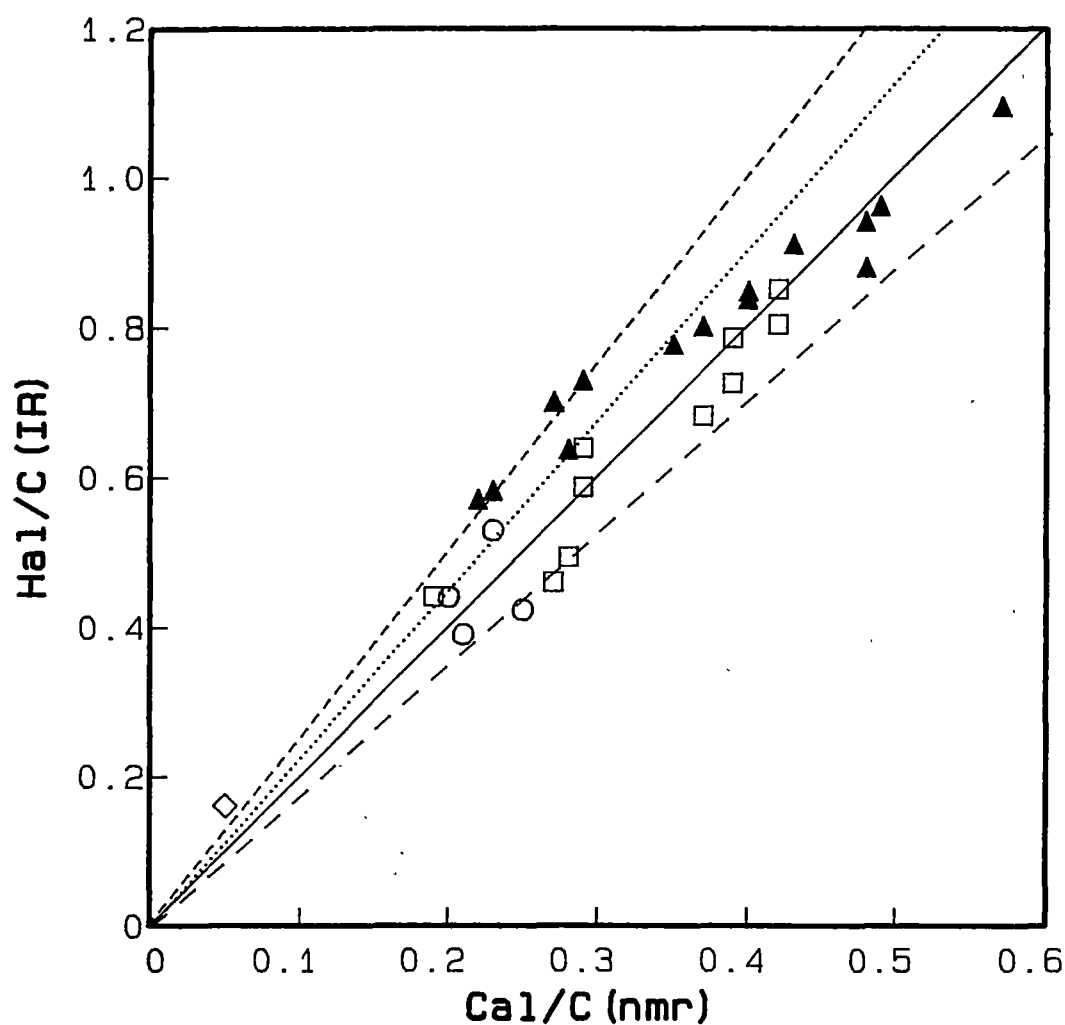
Figure 5.5 Plot of ^{13}C nmr aliphatic-carbon fraction , C_{al}/C , versus aliphatic hydrogen to carbon ratio, H_{al}/C , calculated from FTIR data: lines represent H_{al}/C_{al} values of 2.50 (------) , 2.25 (·········), 2.00 (————) and 1.75 (— — —) (see **Figure 5.1** for symbols).

5.2.1 Comparisons of parameters related to oxygen-functional groups

a) Hydroxyl groups

In this study, the intensity at 3200 cm⁻¹ of the coal FTIR spectrum was used as a measure of the hydroxyl concentration in the coal. The measurement is for both the alcoholic-type and carboxyl **OH** groups. The content of these **OH** groups, however, cannot be readily obtained from the solid-state ^{13}C nmr measurement because the ^{13}C nmr method cannot differentiate the **OH** bearing carbons from other oxygenated carbons, namely, the carbons associated with ether or ester groups. In order to be able to compare with the FTIR data, a ratio of hydroxyl oxygen to carbon, **O$_{OH}$/C** , is determined from the ^{13}C nmr data by using the equation :

$$O_{OH}/C = [f_{car}^{CO} + (2 . f_{car}^{COO}) + f_{ar}^{O} + (0.5. f_{al}^{O})] - [O/C]_{non} \qquad (5.6)$$

where the first term is the total oxygen to carbon ratio derived from ^{13}C nmr parameters defined in **Table 4.6 , Chapter 4** (see also **equation (4.10)**) and **[O/C]$_{non}$** is a non-acidic oxygen to carbon ratio which can be estimated from non-aqueous titration data [Redlich et al.,1989a].

The value of **O$_{OH}$/C** is plotted against the intensity at 3200 cm⁻¹ of the coal FTIR spectra in **Figure 5.6.** Regarding the uncertainties associated with the two parameters, the overall correlation observed is considered to be reasonable. However, there is a considerable scatter in the brown coal data. The data points of three oxygen-rich subbituminous coals, ABL4, ABL7 and ABL8, also deviate from the general trend of the correlation. The scatter of the data of these coals is probably related to the errors in the

non-aqueous titration data used in **equation (5.6)**. As noted in **Chapter 3,** **section 3.3.1,** the phenolic esters in these coals can be hydrolysed by the titration solvent, giving a titratable phenol [Redlich et al., 1989a]. Therefore, the value of $[O/C]_{non}$ may be underestimated, giving rise to an overestimated value of O_{OH}/C.

b)   Carbonyl groups

The integrated area of the carbonyl C=O stretching band in the FTIR spectrum of coal has been used as a measure of carbonyl content in the coal. A comparison between the total area of the IR carbonyl C=O band and the total carbonyl-carbon fraction, f_{car}, determined by ^{13}C nmr is made as shown in **Figure 5.7.** The comparison indicates that while there is a broad correlation for the data of the higher-rank coals (correlation coeff. = 0.90), no correlation is observed for the data of the brown coals (correlation coeff. = 0.02). As reported in **Chapter 3 , section 3.3.2 ,** the IR absorption in the carbonyl region can arise from many types of carbonyl structures. In view of the complexity in the structure of the coal, any type of carbonyl structures outlined in **Table 3.2** is possibly present in the brown coals. The comparison of the ^{13}C nmr f_{car} data and the carbonyl-band area for the brown coals, illustrated in **Figure 5.7,** reflects such a variability in the carbonyl structures of the brown coals.   FTIR measurements of three model compounds, **stearic acid, stearyl benzoate** and **cetyl behenate** have revealed that extinction coeffifients of the carbonyl bands for the three compounds are significantly different, as indicated by their band areas (see **Figure 5.8**). The FTIR spectra of the three compounds were recorded by using the same procedure as for the coal sample.
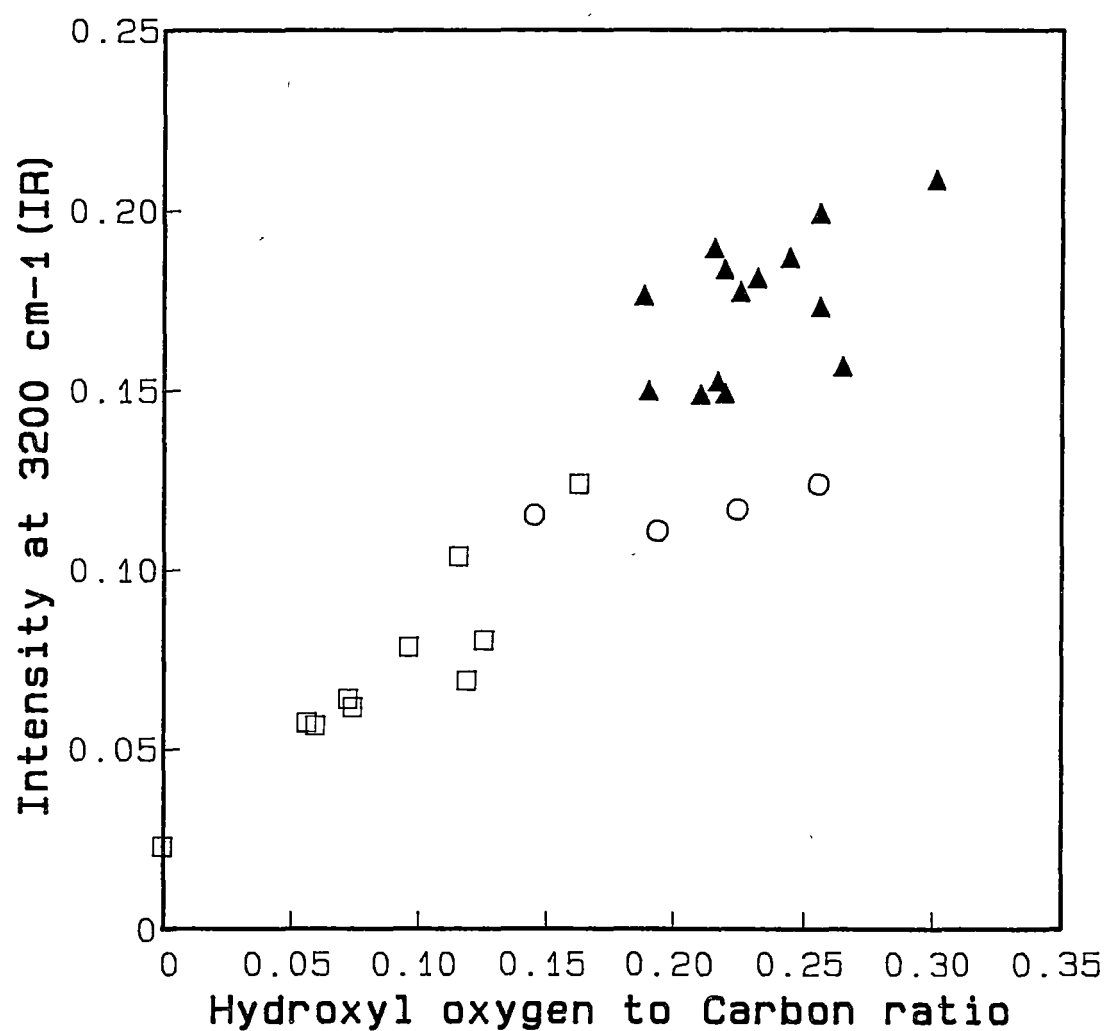
Figure 5.6 Correlation between intensities at 3200 cm⁻¹ in coal IR spectra
and the values of hydroxyl oxygen to carbon ratio, O_{OH}/C (see **Figure 5.1**
for symbols).

It is probable that for the brown coals, the extinction coefficients of the carbonyl bands may be also variable. Therefore, the variation in the areas of the carbonyl bands in the brown coal spectra may not represent the variation in the carbonyl contents in the coals, but it rather indicates the variability in the carbonyl structures of the coals.

It is also anticipated that for some coals having a high proportion of phenolic carbons, the ^{13}C nmr f_{car} values can be overestimated as being due to the overlapping tail of the phenolic resonances.
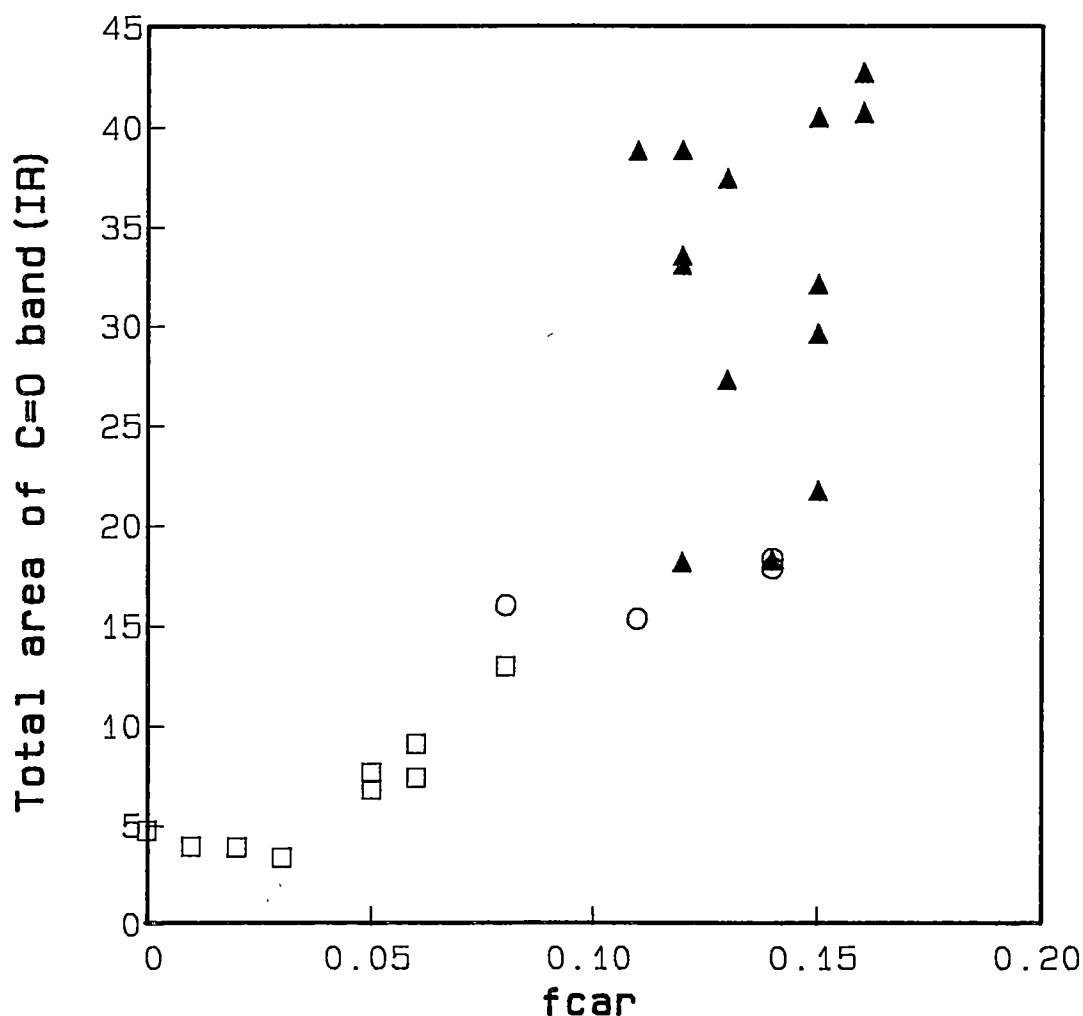
Figure 5.7 Comparison between the total areas of carbonyl band in the IR spectra of coals and the total carbonyl-carbon fraction, f_{car} , estimated by ^{13}C nmr method (see **Figure 5.1** for symbols).
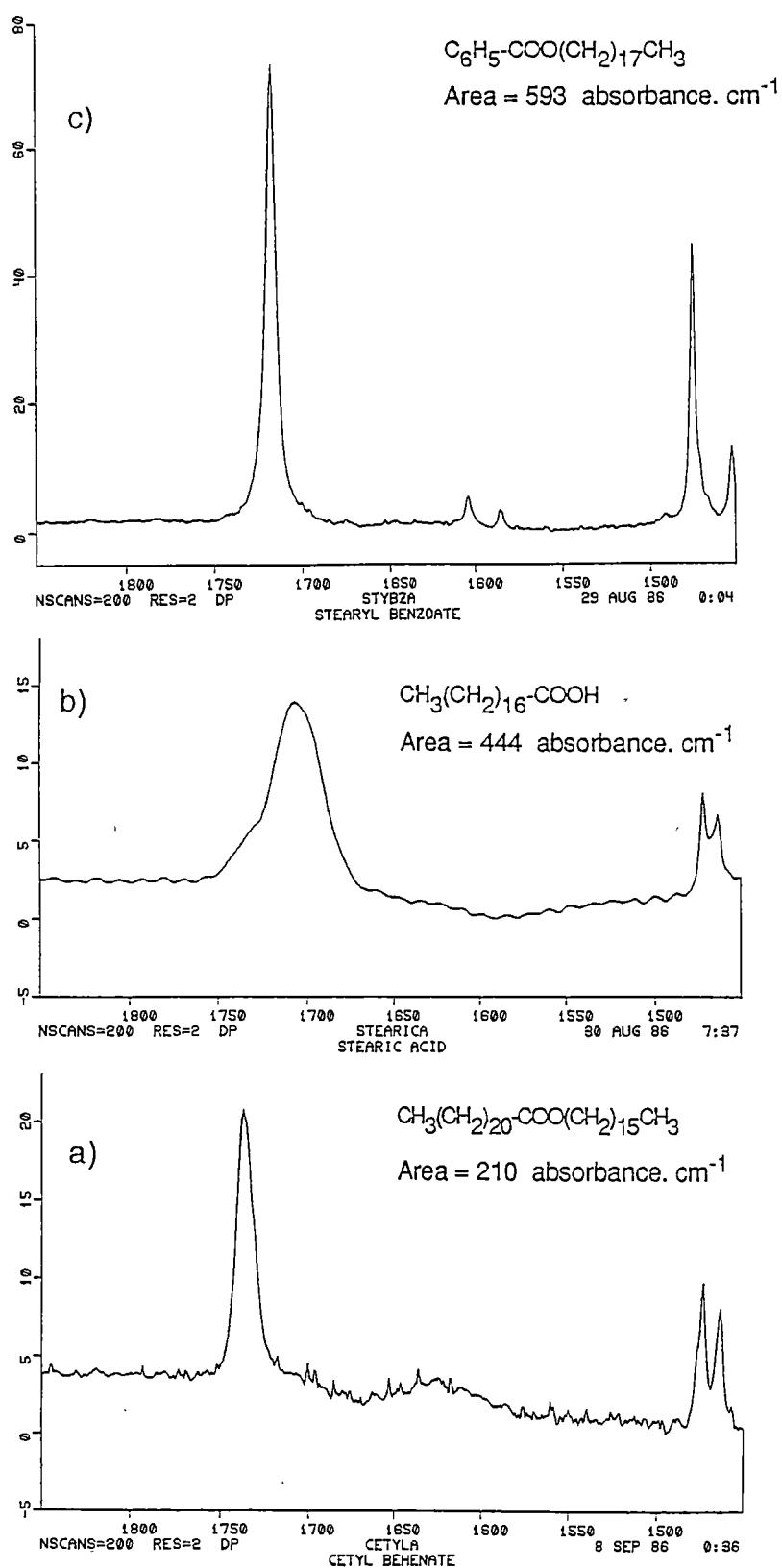
Figure 5.8 Carbonyl absorption bands in the FTIR spectra of model compounds a) **cetyl behenate**, b) **stearic acid** and c) **stearyl benzoate**.

5.3 CONCLUSIONS

The FTIR and solid-state ^{13}C nmr data related to the aromatic and aliphatic contents in Australian coals have been compared. The parameters are the aromatic hydrogen to carbon ratio, H_{ar}/C, the aliphatic hydrogen to carbon ratio, H_{al}/C and carbon aromaticity, f_{ar}. The results show general correlations between the FTIR and solid-state ^{13}C nmr values of the three parameters. However, a substantial difference between the FTIR and solid-state ^{13}C nmr H_{ar}/C values is observed, in particular, for the data of brown coals. It is suggested that the FTIR H_{ar}/C value may not be reliable according to the problem of the aromatic CH band area measurement and the uncertainty in the band absorptivity used in the calculation of aromatic hydrogen content. Since the "true" absolute value of the aromatic hydrogen content in the coal is generally small, at least as indicated by the ^{13}C nmr data, the relative error associated with the value seems to be fairly large compared to that of the aliphatic hydrogen content. However, for a relative measurement of the aromatic or aliphatic content in the coals studied, the correlations between the FTIR and solid-state ^{13}C nmr data indicate the reliability of the two techniques. The comparison study also demonstrates that a good correspondence between the aromaticities derived from IR and ^{13}C nmr data can be observed only when the IR values are corrected for carbonyl carbons.

The intensities at 3200 cm^{-1} in the coal IR spectra are well correlated with the value of hydroxyl oxygen to carbon ratio, derived from the combined ^{13}C nmr and non-aqueous titration data. The deviations of the data for the brown coals and the oxygen-rich subbituminous coals are noted as being related to the uncertainty in the non-aqueous titration data.

The total areas of the carbonyl band in the IR spectra of coals have been compared with the total carbonyl-carbon fraction estimated by ^{13}C nmr. The lack of correlation between the two sets of data for the brown coals suggests that the extinction coefficient for the carbonyl species may be variable in different coals. Hence, for the suite of brown coals, it may not be appropriate to use the area of the IR carbonyl band as a direct measure of the carbonyl content in the coal.

CHAPTER SIX

CONCLUSIONS

6.1   THE STRUCTURE OF AUSTRALIAN COALS

The studies presented in this thesis have demonstrated the capabilities of the FTIR and solid-state ^{13}C nmr techniques to unravel the structural complexity of the Australian coals. In particular, the solid-state ^{13}C nmr studies can provide detailed structural data for the coals. In spite of the fact that the coals studied are quite diverse, as they cover a wide range of rank, general structural features of the coals can be observed as rank characteristics. In this final Chapter, conclusions on the structural characteristics of the coals studied will be given. For each rank, the average structural data, based on the solid-state ^{13}C nmr studies, are taken to illustrate the general features of the coals in that rank. For the semianthracite, ABL1, and the low volatile bituminous coal, ABL3, their structural data are presented together as the average values, since they have a similar characteristic,

6.1.1   The aromatic structure

Based on a model of pericondensed aromatic clusters, the average
aromatic cluster size of the coals/was found to increase with coal rank.
, as defined in equation (4.9), p.137

The number of aromatic rings significantly increases from 2 to 3 units for
the brown coals and subbituminous coals to 4-7 units for the bituminous
coals and the semianthracite.   Accompanying the increase in aromatic
cluster size is the decrease in the aromatic substitution.   The main
aromatic substituents that diminish as the rank increases, are those
related to oxygen-functional groups, namely, the phenolic, methoxyl and
carbonyl groups.   In view of the coalification process, it is proposed that
during the early stage the loss of oxygenated substituents was the
predominant process in coal metamorphism whereas the aromatization
would occur at much later stage of coalification. **Figure 6.1** demonstrates
the trend of a decrease in the degree of aromatic substitution/ with
, as defined in equation (4.8), p.133

increase in coal rank.   The values of carbon content and the degree of
aromatic substitution are taken from the average data for each group of
coals. **Figure 6.2** summarizes the average distribution of aromatic carbons
on the basis of average value of wt. % coal for the coals in each rank.

6.1.2   The aliphatic structure

For the entire suite of coals, both aliphatic hydrogen and aliphatic carbon
contents were found to increase with coal **H/C** value.   It was also found
that the main contributor to the variation in coal **H/C** ratio is the
methylenic groups, especially for the brown coals and the subbituminous
coals.
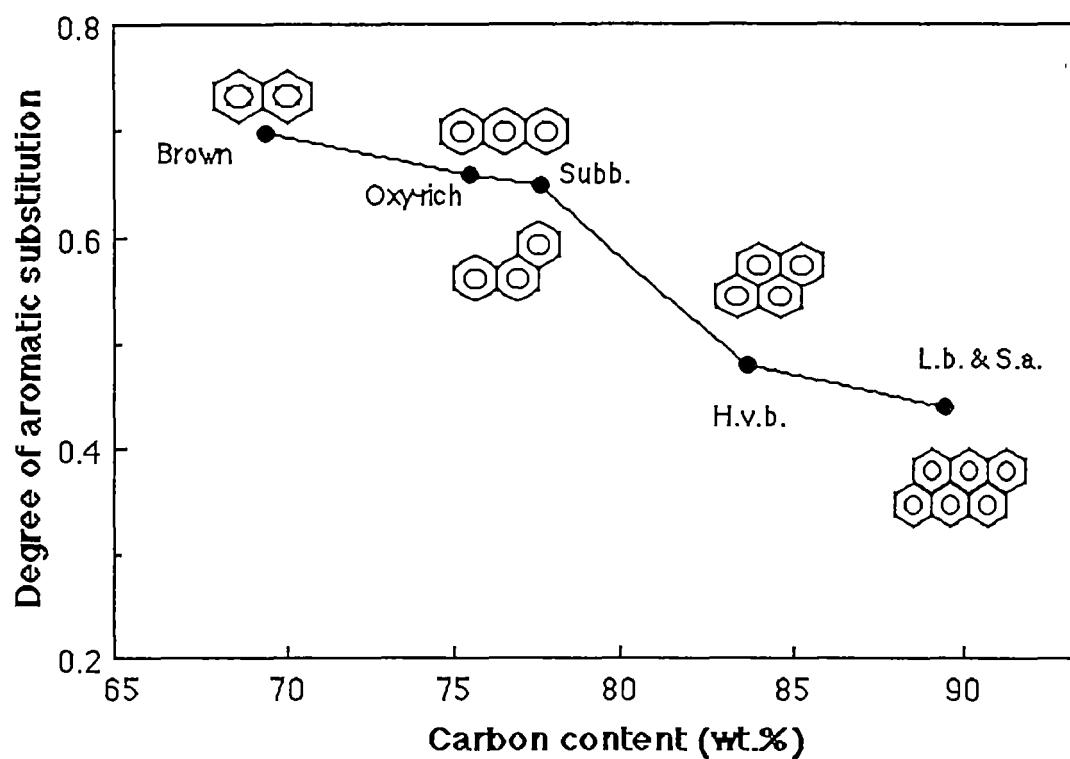
Figure 6.1 Average values of degree of aromatic substitution and average aromatic cluster sizes for Australian coals.(Brown = Brown coals;Oxy-rich = Oxygen-rich subbituminous; Subb. = Subbituminous coals; H.v.b. = High volatile bituminous coals; L.b.& S.a. = Low volatile bituminous and Semianthracite)
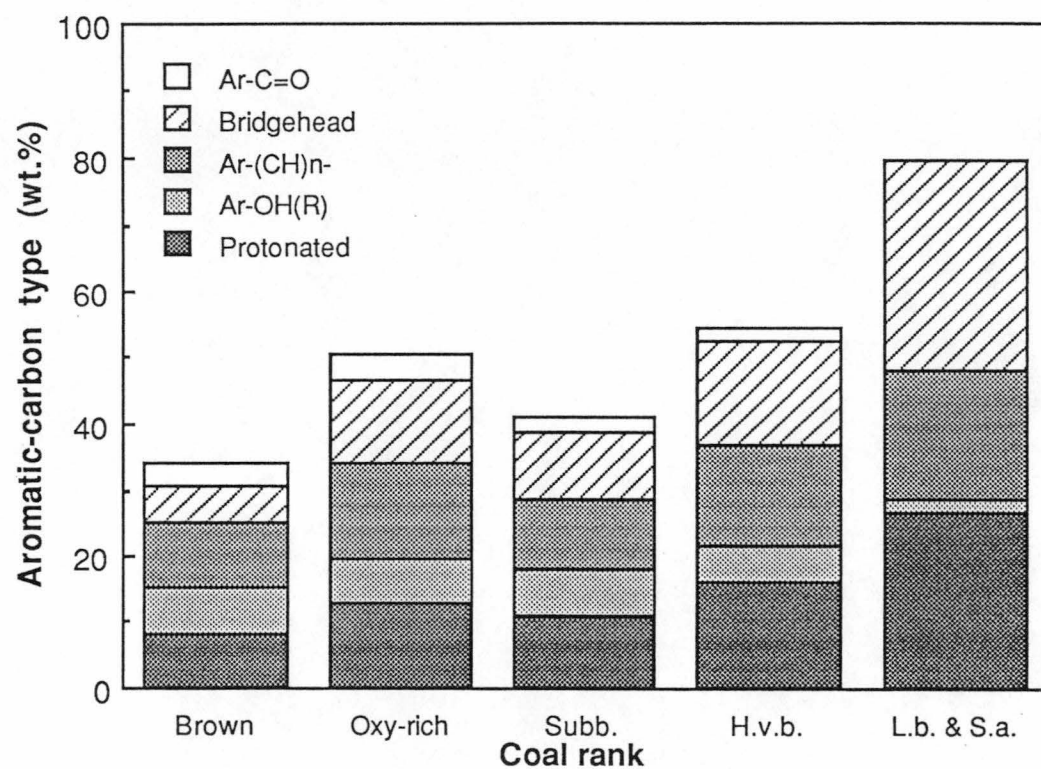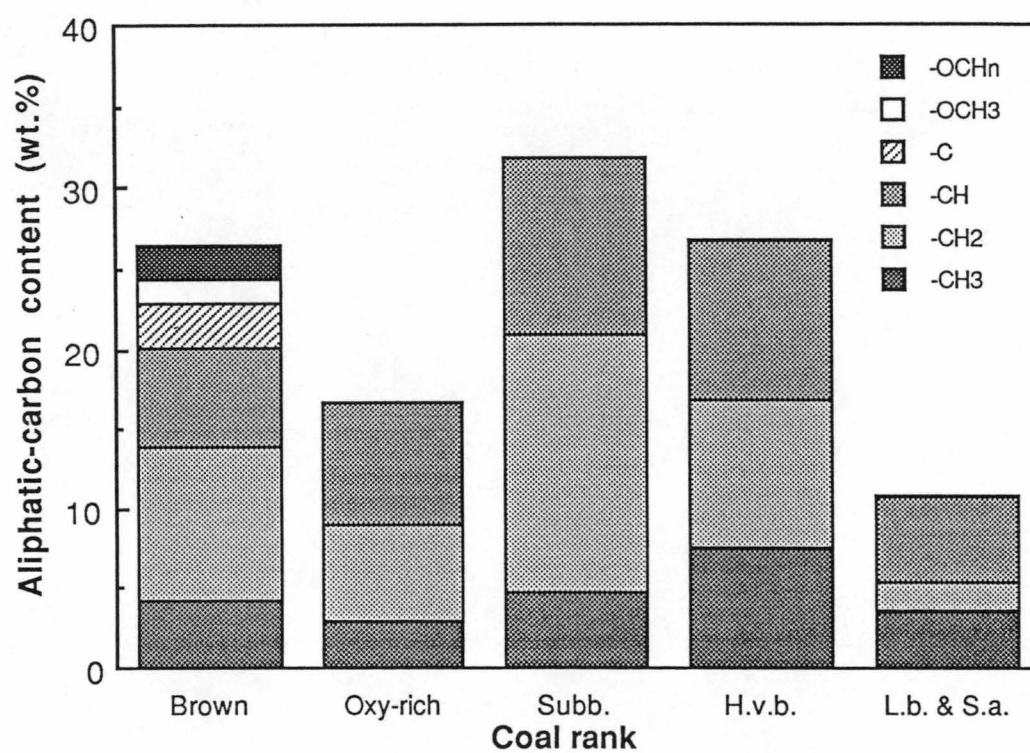
Figure 6.2 Average contents of various aromatic carbons in Australian coals. (see abbreviations for coal rank in **Figure 6.1**)

A good relationship between the aliphatic content in the coals and the liquefaction reactivity has been observed, in particular, the oil yields and total hydrocarbon products. Comparison studies of the aliphatic hydrogen contents in the asphaltenes and residues with those in the parent coals have been made. The results support the "guest-host" model for the structure of brown coals as proposed by the liquefaction studies [Redlich, 1987; Redlich et al.,1985; Redlich et al., 1989b]. In this model, the major proportion of aliphatic content in the brown coals is considered to be present in the "guest" component and this "guest" material is responsible to the liquefaction reactivities of these brown coals. The major types of the aliphatic groups in the "guest" component are long chain hydrocarbons, including some terpenoid compounds. For the higher-rank coals, the results are also consistent with the interpretation that the aliphatic portions of the coals are strongly bound to the coal macromolecular structures, therefore, the "guest-host" model may not be appropriate for describing their structures. **Figure 6.3** illustrates the average contents of the aliphatic carbons observed in the Australian coals.

6.1.3   The oxygen-functional groups.

As a young coal, Australian brown coals contain many types of oxygen-functional groups in varying amounts. The major oxygen-containing groups in these brown coals are carboxyl groups which are probably present as esters and carboxylic acids. The methoxyl and other oxygenated aliphatic groups were also found in the brown coals but in a minor quantity. These methoxyl and oxygenated aliphatics, including the esters, are the first oxygen-containing groups that were eliminated during the early stage of coalification.

Figure 6.3   Average contents of various aliphatic carbons in Australian coals.(see abbreviations for coal rank in **Figure 6.1**)

In the brown coals, a large proportion of the esters and carboxylic acids are present in the aliphatic moieties and probably are related to the "guest" component. Further loss of oxygen-containing groups in the coalification process is principally of the carboxylic acid and ketonic-type structures. As a consequence, the phenolic groups, both as phenols and ethers, are the main oxygen-functional groups present in the coals of higher-rank than the subbituminous coals. The general trend of the variations in oxygen-functional groups summarized above is clearly illustrated in **Figure 6.4** where the average contents of the groups in the coals are given on the wt. % coal basis.
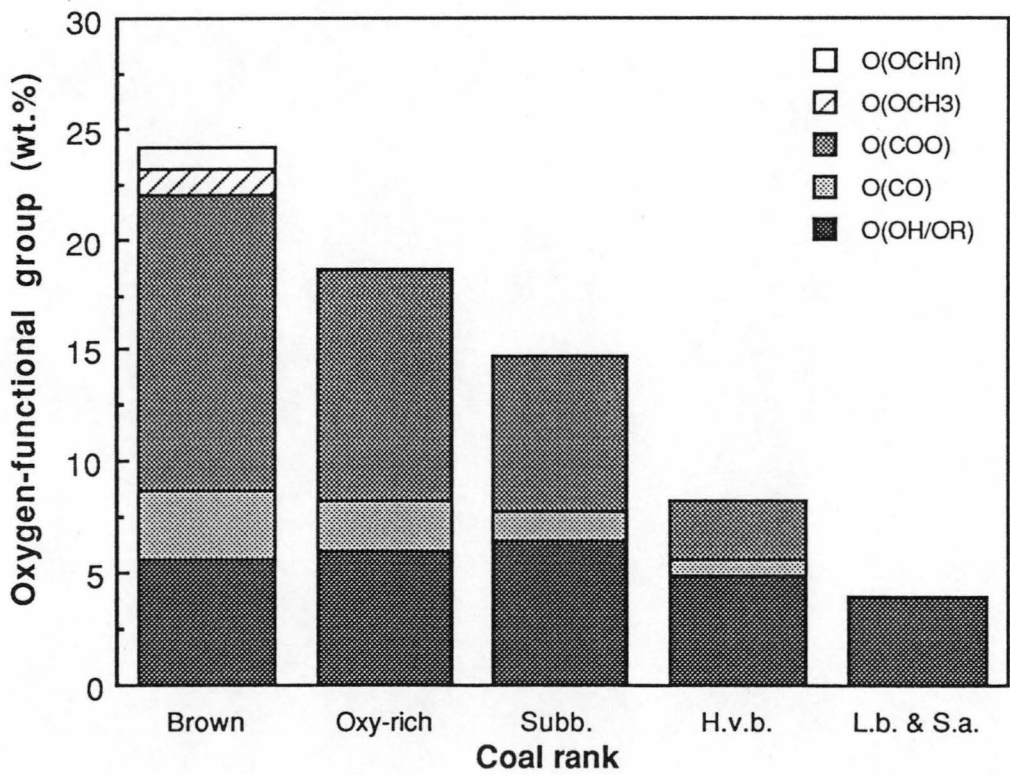
Figure 6.4 Average contents of various oxygen-functional groups in Australian coals.(see abbreviations for coal rank in **Figure 6.1**)

6.2   RECOMMENDATIONS FOR FURTHER STUDY

As a final conclusion for this thesis, three research areas are recommended for future studies.

1. Since the quantities of several oxygen-functional groups such as ethers and esters groups in the coals cannot be directly determined by the techniques used, further study for the method of analysing these functional groups is required. The combined procedure of chemical methods such as alkylation reaction [Choi, C. et al.,1989 and references therein] with the spectroscopic techniques of FTIR and solid-state ^{13}C nmr, is the probable method for future work.

2. As discussed in **Chapter 5,** the quantitative reliability of both the FTIR and solid-state ^{13}C nmr techniques, in terms of absolute measurements, are still uncertain. Studies of the coal products, asphaltenes, by using solution-state ^{1}H and ^{13}C nmr techniques, in comparison with the solid-state ^{13}C nmr and FTIR data, may provide a useful insight into the quantitative accuracies of the solid-state ^{13}C nmr and FTIR data.

3. In spite of the limitations noted above, the combined method of FTIR and solid-state ^{13}C nmr has been shown to be capable of obtaining considerable details of the structural characteristics of the coals studied. The techniques may be used to investigate other coals or coal-related materials such as oil shales. The methods will be also useful in studying coal processing or other coal properties such as coal weathering or coal oxidation.

REFERENCES

Alemany, L.B., Grant, D.M., Alger, T.D. and Pugmire, R.J. (1983) Cross Polarization and Magic Angle Sample Spinning NMR Spectra of Model Organic Compounds. 3. Effect of the ^{13}C-^{1}H Dipolar Interaction on Cross Polarization and Carbon-Proton Dephasing *J. Am. Chem. Soc.* **105**, 6697-6704.

Alla, M. and Lippmaa, E. (1976) High Resolution Broad Line ^{13}C NMR and Relaxation in Solid Norbornadiene *Chem. Phys. Lett.* **37**, 260-264.

Attar, A. and Hendrickson, G.G. (1982) Functional Groups and Heteroatoms in Coals In *Coal Structure* (Edited by Meyer, R.A.), pp. 132-198. Academic Press, New York.

Axelson, D.E. (1987a) Solid State Carbon-13 Nuclear Magnetic Resonance Study of Canadian Coals *Fuel Process. Technol.* **16**, 257-278.

Axelson, D.E. (1987b) Spinning sideband suppression and quantitative analysis in solid state ^{13}C n.m.r. of fossil fuels *Fuel* **66**, 195-199.

Bellamy, L.J. (1975) The Infra-red Spectra of Complex Molecules Vol. 1, 3rd ed., Chapman and Hall, London.

Berkowitz, N. (1985) The Chemistry of Coal In *Coal Science and Technology Ser.* (Edited by Anderson, L.L.), Elsevier, Amsterdam.

Berkowitz, N. (1985a), *ibid.*,pp. 49-55

Botto, R.E., Wilson, R. and Winans, R.E. (1987) Evaluation of the Reliability of Solid ^{13}C NMR Spectroscopy for the Quantitative Analysis of Coals: Study of Whole Coals and Maceral Concentrates *Energy Fuels* **1**, 173-181.

Breitmaier, E. and Voelter, W. (1974) ^{13}C NMR Spectroscopy In *Monographs in Modern Chemistry* (Edited by Ebel, H.F.), Verlag Chemie, Weinheim.

Brookes, N. (1984) FTIR Characterization of Australian Coals and Coal Derived Hydrogenation Products, Honours Thesis, University of Tasmania.

Brown, J.K. (1955) The infrared spectra of coals *J. Chem. Soc. (London)*, 744-752.

Brown, J.K. and Ladner, W.R. (1960) A study of the hydrogen distribution in coal-like materials by high resolution NMR spectroscopy II - a comparison with infrared measurement and the conversion to carbon structure *Fuel* 39, 87-96.

Brown, R,F,C. (1980) Pyrolytic Methods in Organic Chemistry In *Organic Chemistry. A series of Monographs* (Edited by Wasserman, H.H.),. Academic Press, New York.

Burgar, M.I., Kalman, J.R. and Stephens, J.F. (1985) A New Method for estimating Aromatic ring condensation in coals *Proc.,Int., Conf. on Coal Science*, Sydney , pp. 780-783.

Cannon, C.G., and Sutherland, G.B.B. (1945) The infrared absorption spectra of coals and coal extracts *Trans. Faraday Soc.* 41, 279-288.

Chaffee, A.L., Liepa, I., Redlich, P.J., Jackson, W.R. and Larkins, F.P. (1986) The Molecular Nature of Oil from Coal GC-MS Analysis of Oils Produced Using SnO_2/H_2. *Proc. Australian Coal Science Conf.*, Newcastle, pp. 369-374.

Chien, P.-L., Markuszewski, R. and McClelland, J.F. (1985) Comparison of fourier transform infrared-photoacaustic spectroscopy (FTIR-PAS) and conventional methods for analysis of coal oxidation *Proc. Int. Conf. Coal Science* ,Sydney , pp. 818-821.

Choi, C., Muntran, J.V., Thompson, A.R. and Botto, R.E. (1989) Characterization of Coal Macerals Using Combined Chemical and NMR Spectroscopic Methods *Energy Fuels* 3, 528-533.

Davidson, R.M. (1980) *Molecular structure of coal*, IEA Coal Research, London.

Davidson, R.M. (1986) *Nuclear magnetic resonance studies of coal* IEA Coal Research, London.

Davidson, R.M. (1986a), *ibid.*, p. 22.

Davidson, R.M. (1986b), *ibid.*, p. 51-59.

Davidson, R.M. (1986c), *ibid.*, p. 33-39.

Demco, D.E., Tegenfeldt, J. and Waugh, J.S. (1975) Dynamics of cross relaxation in nuclear magnetic double resonance *Phys. Rev. B* **11**, 4133-4151.

Dixon, W.T. (1982) Spinning-sideband-free and spinning-sideband-only NMR spectra in spinning samples *J. Chem. Phys.* **77**, 1800-1809.

Dixon, W.T., Schaefer, J., Sefcik, M.D., Stejskal, E.O. and Mckay, R.A. (1982) Total Suppression of Sidebands in CPMAS C-13 NMR *J. Magn. Reson.* **49**, 341-345.

Dudley, R.L and Fyfe, C.A. (1982) Evaluation of quantitative reliability of the ^{13}C CP/MAS techniques for the analysis of coals and related materials *Fuel* **61**, 651-657.

Durie, R.A., Shewchyk, Y. and Sternhell, S. (1966) Spectroscopic studies of the hydrogen distribution in vitrains and their solvent extracts from some Australian bituminous coals *Fuel* **45**, 99-113.

Fraser, R.D.B. and Suzuki, E. (1969) Resolution of Overlapping Bands: Functions for Simulating Band Shapes *Anal. Chem.* **41**, 37-39.

Fujii, S. (1963) Infrared spectra of coal - absorption band at 1600 cm-1 *Fuel* **42**, 341-343

Fuller, M.P., Hamadeh, I.M., Griffiths, P.R. and Lowenhaupt, D.E. (1982) Diffuse Reflectance infrared spectrometry of powdered coals *Fuel* **61**, 529-536.

Furimsky, E. and Ripmeester, J. (1983) Characterization of Canadian coals by nuclear magnetic resonance spectroscopy *Fuel Process. Technol.* **7**, 191-202.

Gerstein, B.C., Murphy, P.D. and Ryan, L.M. (1982) Aromaticity in Coal In *Coal Structure* (Edited by Meyer, R.A.), pp. 87-129. Academic Press, New York.

Gerstein, B.C. and Dybowski, C.R. (1985) *Transient Techniques in NMR of Solids*, Academic Press, Orlando.

Given, P.H. (1984) An Essay on the Organic Geochemistry of Coal In *Coal Science* (Edited by Gorbaty, M.L., Larsen, J.W. and Wender, I.) , pp. 63-252. Academic Press, New York.

Given, P.H. and Marzec, A. (1988) Protons of differing rotational mobility in coals *Fuel* **67**, 242-244.

Hagaman, E.W. and Woody, M.C. (1982) Structure analysis of coals by resolution enhanced solid state ^{13}C nmr spectrosopy *Fuel* **61**, 53-57.

Havens, J.R., Koenig, J.L., Kuehn, D., Rhoads, C., Davis, A. and Painter, P.C. (1983) Characterization of coals and coal oxidation by magic-angle C-13 n.m.r. spectroscopy *Fuel* **62**, 936-941

Herzfeld, J. and Berger, A.E. (1980) Sideband intensities in NMR spectra of samples spinning at the magic angle *J. Chem. Phys.* **73**, 6021-6030.

Hippo, E.J., Neavel, R.C., Smith, S.E. and Lang, R.J. (1987) The Measurement of Water Tightly Bound by Low Rank Coals *Am. Chem. Soc., Div. Fuel Chem., Prepr.* **32**, 179-184.

Hirsch, P.B. (1954) X-ray scattering from coals *Proc. Roy. Soc. Lond.* **226A**, 143-169.

Hooper, R.J. and Evans, D.G. (1978) Reaction of a coal liquid with a hydrogen-donor solvent to form a carbon-rich solid *Fuel* **57**, 799-801.

Jacobsen, H.J., Daugaard, P. and Langer, V. (1988) CP/MAS NMR at High speeds and High Fields *J. Magn. Reson.* **76**, 162-168.

Jelinski, L.W. and Meichior, M.T. (1987) High-Resolution NMR of Solids In *NMR Spectroscopy techniques* (Edited by Dybowski, C. and Lichter, R.L.), pp. 253-329. Marcel Dekker, New York.

Kuehn, D.W., Snyder, R.W., Davis, A. and Painter, P.C. (1982) Characterization of vitrinite concentrates. 1. Fourier Transform infrared studies *Fuel* **61**, 682-694.

Kuehn, D.W., Davis, A. and Painter, P.C. (1984) Relationships Between the Organic Structure of Vitrinite and Selected Parameters of Coalification as indicated by Fourier Transform IR Spectra *Am. Chem. Soc. Symp. Series* **252**, pp. 99-119.

Maciel, G.E. and Sullivan, M.J. (1982) ^{13}C NMR Characterization of Solid Fossil Fuels Using Cross-Polarization and Magic-Angle Spinning *Am. Chem. Soc. Symp. Series* **191**, 319-343.

Maddams, W.F. (1980) The Scope and Limitations of Curve Fitting *Appl. Spectrosc.* **34**, 245-267.

Maricq, M.M., and Waugh, J.S. (1979) NMR in rotating solids *J. Chem. Phys.* **70**, 3300-3316.

Marquardt, D.W. (1963) An Algorithm for Least-Squares Estimation of Non-Linear Parameters *J. of Siam.* **11**, 431-441.

Mayne, C.L., Alderman, D.W. and Grant, D.M. (1975) Nuclear relaxation in coupled spin systems. A heteronuclear two pulse experiment and general numerical method for analyzing spin dynamics *J. Chem. Phys.* **63**, 2514-2523.

Mehring, M. (1983) *Principles of High Resolution NMR in Solids* , Springer-Verlag, Heidelberg.

Muntean, J.V., Stock, L.M. and Botto, R.E. (1988) Improving the reliability of quantitative solid-state ^{13}C NMR analysis of coal *Energy Fuels* **2**, 108-110.

Murphy, P.D., Cassidy, T.J. and Gerstein, B.C. (1982) Determination of the apparent ratio of quarternary to tertiary aromatic carbon atoms in an anthracite coal by ^{13}C-^{1}H dipolar dephasing n.m.r. *Fuel* **61**, 1233-1239.

Neavel, R.C., Smith, S.E., Hippo, E.J. and Miller, R.N. (1986) Interrelationships between coal compositional parameters *Fuel* **65**, 312-320.

Netzel, D.A. (1987) Quantitation of Carbon Types Using DEPT/QUAT NMR Pulse Sequences: Application to Fossil-Fuel-Derived Oils *Anal. Chem.* **59**, 1775-1779.

Newman, R.H. and Davenport, S.J. (1986) Comparison of Australasian tertiary coals based on resolution-enhanced solid-state ^{13}C n.m.r. spectra *Fuel* **65**, 533-540.

Ohtsuka, Y., Nozawa, T., Tomita, A., Tamai, Y., and Hatano, M. (1984) Application of high-field, high-resolution ^{13}C CP/MAS n.m.r. spectroscopy to the structural analysis of Yallourn coal *Fuel* **63**, 1363-1366.

Olejniczak, E.T. and Griffin, R.G. (1984) Multiple pulse NMR in rotating solids *J. Chem. Phys.* **81**, 4804-4817.

Opella, S.J. and Frey, M.H. (1979) Selection of Nonprotonated Carbon Resonances in Solid-State Nuclear Magnetic Resonance *J. Am. Chem. Soc.* **101**, 5854-5856.

Osawa,Y. and Shih, J.W.(1971) Infrared spectra of Japanese coal: the absorption bands at 3450 and 1260 cm^{-1} *Fuel* **50**, 53-57.

Painter, P.C., Snyder, R.W., Starsinic, M., Coleman, M.M., Kuehn, D.W. and Davis, A. (1981) Concerning the Application of FT-IR to the Study of Coal: A Critical Assessment of Band Assigmments and The Application of Spectral Analysis Programs *Appl. Spectrosc.* **35**, 475-485.

Painter, P.C., Starsinic, M., Squires, E. and Davis, A.A. (1983a) Concerning the 1600 cm^{-1} region in the i.r. spectrum of coal *Fuel* **62**, 742-744.

Painter, P.C., Kuehn, D.W., Starsinic, M., Davis, A., Havens, J.R. and Koenig, J.L. (1983b) Characterization of vitrinite concentrates. 2. Magic-angle ^{13}C nuclear magnetic resonance studies *Fuel* **62**, 103-111.

Painter, P.C., Sobkowiak, M. and Youtcheff, J. (1987) FT-ir study of hydrogen bonding in coal *Fuel* **66**, 973-978.

Pines, A., Gibby, M.G. and Waugh, J.S. (1973) Proton-enhanced NMR of dilute spins in solids *J. Chem. Phys.* **59**, 569-590.

Pretch, E., Seibl,J. Simon, W. and Clerk, T. (1983) *Tables of Spectral Data for Structure Determination of Organic Compounds* , Springer-Verlag, Berlin.

Pugmire, R.J., Zilm, K.W., Grant, D.M., Larter, S.R., Allen, J., Senftle, J.T., Davis, A. and Spackman, W. (1981) Carbon-13 CP/MAS Study of Coal Macerals of Varying Rank *Am. Chem. Soc. Symp. Series* **169**, pp.23-42.

Pugmire, R.J., Woolfenden, W.R., Mayne, C,L., Karas, J. and Grant, D.M. (1984) Structural Variations in Coal Macerals: Application of Two-Dimensional and Dipolar Dephasing ^{13}C-NMR Techniques *Am. Chem. Soc. Symp. Series* **252**, pp. 79-97.

Raleigh, D.P., Olejniczak, E.T., Vega, S. and Griffin, R.G. (1987) An Analysis of Sideband Suppression Techniques in Magic-Angle Sample Spinning NMR *J. Magn. Reson.* **72**, 238-250.

Rao, C.N.R. (1963) *Chemical Applications of Infrared Spectroscopy*, Academic Press, New York , .

Redlich, P., Jackson, W.R. and Larkins, F.P. (1985) Hydrogenation of Brown Coal. 9. Physical Characterisation and Liquefaction Potential of Australian Coals *Fuel* **64**, 1383-1390.

Redlich, P.J. (1987) *The Chemical and Structural Characteristics of Coals and their Relationship to Liquefaction* Ph.D. Thesis, Monash University.

Redlich, P.J., Jackson, W.R., Larkins, F.P. and Rash, D. (1989a) Studies related to the structure and reactivity of coals.14. Chemical characterization of a suite of Australian coals *Fuel* **68**, 222-230.

Redlich, P.J., Jackson, W.R., Larkins, F.P. (1989b) Studies related to the structure and reactivity of coals. 15 Conversion characteristics of a suite of Australian coals *Fuel* **68**, 231-237.

Retcofsky, H.L. (1977) Investigation of the Chemical Structure of Coal by Nuclear Magnetic Resonance and Infrared Spectrometry *Appl.spectros.* **31**, 116-121.

Retcofsky, H.L., Schweighardt, F.K. and Hough, M. (1977) Determination of Aromaticities of Coal Derivatives by Nuclear Magnetic Resonances Spectrometry and the Brown-Ladner Equation *Anal. Chem.* **49**, 585-588

Retcofsky, H.L. and Van der Hart, D.L. (1978) ^{13}C-^{1}H cross polarization nuclear magnetic resonance spectra of macerals from coal. *Fuel* **57**, 421-423.

Riesser, B., Starsinic, M., Davis, A. and Painter, P.C. (1984) Determination of aromatic and aliphatic CH groups in coal by FT-i.r. *Fuel* **63**, 1253-1261.

Russell, N.J., Wilson, M.A., Pugmire, R.J. and Grant, D.M. (1983) Preliminary studies on the aromaticity of Australian coals *Fuel* **62**, 601-605.

Sardashti, M. and Maciel, G.E. (1987) Effects of Sample Spinning on Cross Polarization *J. Magn. Reson.* **72**, 467-474.

Schaefer, J. and Stejskal, E.O. (1976) Carbon-13 Nuclear Magnetic Resonance of Polymers Spinning at the Magic Angle *J. Am. Chem. Soc.* **98**, 1031-1032.

Schafer, H.N.S. (1970) Carboxyl groups and ion exchange in low-rank coals *Fuel* **49**, 197-213.

Schmitt, K.D. and Sheppard, E.W. (1984) Determination of carbon centre types in solid fuel materials by CP/MAS n.m.r. *Fuel* **63**, 1241-1244.

Senftle, J.T., Kuehn, D., Davis, A., Brozoski, B., Rhoads, C. and Painter, P.C. (1984) Characterization of vitrinite concentrates 3. Correlation of FT-i.r. measurements to thermoplastic and liquefaction behaviour *Fuel* **63**, 245-250.

Sfihi, H., Quinton, M.F., Legrand, A., Pregermain, S., Carson, D. and Chiche, P. (1986) Evalution of aromaticity in French coals by ^{13}C-^{1}H cross polarization, magic angle spinning and dipolar dephasing nuclear magnetic resonance spectroscopy *Fuel* **65**, 1006-1011.

Snape, C.E. and Ladner, W.R. and Bartle, K.D. (1979) Survey of Carbon- 13 Chemical Shifts in Aromatic Hydrocarbons and its Application to Coal-Derived Materials *Anal. Chem.* **51**, 2189-2198.

Snape, C.E., Ladner, W.R. and Bartle, K.D. (1985) Fate of aliphatic groups in low-rank coals during extraction and pyrolysis procedures *Fuel* **64**, 1394-1400.

Snape, C.E., Axelson, D.E., Botto, R.E., Delpuech, P.T., Gerstein, B.C., Pruski, M., Maciel, G.E. and Wilson, M.A. (1989) Quantitative re liability of aromaticity and related measurements on coals by ^{13}C n.m.r. A debate *Fuel* **68**, 547-560.

Snyder, R.W., Painter, P.C., Havens, J.R. and Koenig, J.L. (1983) The Determination of Hydroxyl Groups in Coal by Fourier Transform Infrared and C-13 NMR Spectroscopy *Appl.spectros.* **37**, 497-502.

Sobkowiak, M., Reisser, E., Given, P. and Painter, P. (1984) Determination of aromatic and aliphatic CH groups in coal by FT-i.r. 2. Studies of coals extracts *Fuel* **63**, 1245-1252.

Soderquist, A., Burton, D.J., Pugmire, R.J., Beeler, A.J., Grant, D.M., Durand, B. and Huk, A.Y. (1987) Structural Variations and Evidence of Segmental Motion in The Aliphatic Region in Coals Observed with Dipolar-Dephasing NMR *Energy Fuels* **1**, 50-55.

Solomon, P.R. (1979) Relation between coal structure and thermal decomposition products *Am. Chem. Soc., Div. Fuel Chem., Prepr.* **24**, 184-195.

Solomon, P.R. and Carangelo, R.M. (1981) *Characterization of Wyoming Subbituminous Coals and Liquefaction Products by Fourier Transform Infrared Spectrometry* Final Report, EPRI AP 2115 ,.

Solomon, P.R. and Carangelo, R.M. (1982) FTIR analysis of coal. 1. Techniques and determination of hydroxyl concentrations *Fuel* **61**, 663-669.

Solomon, P.R. and Carangelo, R.M. (1988) FT-i.r. analysis of coal 2. Aliphatic and aromatic hydrogen concentration *Fuel* **67**, 949-959.

Solum, M.S., Pugmire, R.J. and Grant, D.M. (1989) ^{13}C Solid-State NMR of Argonne Premium Coals *Energy Fuels* **3**, 187-193.

Speight, J.G. (1978) Assessment of Structures in Coal by Spectroscopic Techniques In *Analytical methods for coal and coal products*, Vol II (Edited by Karr, C.), pp.75-101. Academic Press, New York.

Starsinic, M., Otake, Y., Walker Jr., P.L. and Painter, P.C. (1984) Application of FT-i.r. spectroscopy to the determination of COOH groups in coal *Fuel* **63**, 1002-1007.

Stejskal, E.O., Schaefer, J. and Waugh, J.S. (1977) Magic-Angle Spinning and Polarization Transfer in Proton-Enhanced NMR *J. Magn. Reson.* **28**, 105-112.

Stray, G., Cassidy, P.J., Jackson, W.R., Larkins, F.P. and Sutton, J.F. (1986) Studies Related to the Structure and Reactivity of Coals: (11) The hydrogenation of lignin *Fuel* **65**, 1524-1530.

Sullivan, M.J. and Maciel, G.E. (1982a) Structural Resolution in the Carbon- 13 Nuclear Magnetic Resonance Spectrometric Analysis of Coals by Cross Polarization and Magic-Angle Spinning *Anal. Chem.* **54**, 1606-1615.

Sullivan, M.J. and Maciel, G.E. (1982b) Spin Dynamics in the Carbon- 13 Nuclear Magnetic Resonance Spectroscopic Analysis of Coal by Cross Polarization and Magic-Angle Spinning *Anal. Chem.* **54**, 1615-1623.

Teichmuller, M. and Teichmuller, R. (1982) Fundamentals of coal petrology In *Stach's Textbook of Coal Petrology* 3rd edn. (Edited by Stach, E., Mackowsky, M.-TH, Teichmuller, M., Taylor, G.H., Chandra, D. and Teichmuller, R.), pp. 5-86. Gebruder Borntraeger, Berlin.

Theriault, Y. and Axelson, D.E. (1988) Solid state ^{13}C n.m.r. dipolar dephasing study of Canadian coals *Fuel* **67**, 62-66.

Van der Hart, D.L. and Retcofsky, H.L. (1976) Estimation of coal aromaticities by proton-decoupled carbon-13 magnetic resonance spectra of whole coals*Fuel* **55**, 202-204.

van Krevelen, D.W. and Schuyer, J. (1957a) *Coal Science* ,pp. 182-188, Elsevier, Amsterdam.

van Krevelen, D.W. and Schuyer, J. (1957b), *ibid.*, p.97.

van Krevelen, D.W. and Schuyer, J. (1957c), *ibid.*, p.98.

Wenkert, E. and Gottlieb, H.E. (1977) Carbon-13 Nuclear Magnetic Resonance Spectroscopy of Flavanoid and Isoflavanoid Compounds *Phytochemistry* **16**, 1811-.

Wilson, M.A., Pugmire, R.J., Karas, J., Alemany, L.B., Woolfenden, W.R. , Grant, D.M. and Given, P.H. (1984) Carbon Distribution in Coals and Coal Macerals by Cross Polarozation Magic Angle Spinning Carbon- 13 Nuclear Magnetic Resonance Spectrometry *Anal. Chem.* **56**, 933-943.

Wilson, M.A. (1987a) N.M.R. *Techniques and Applications in Geochemistry and Soil Chemistry* , pp. 248-277, Pergomon Press, Oxford.

Wilson, M.A. (1987b), *ibid.*,pp. 266-270.

Wilson, M.A. (1987c), *ibid.*,pp. 252-260.

Wilson, M.A. (1987d), *ibid.*,p. 257

Wilson, M.A., Batts, B.D. and Hatcher, P.G. (1988) Molecular Composition and Mobility of Torbanite Precursors: Implications for the Structure of Coal *Energy Fuels* 2, 668-672.

Yannoni, C.S. (1982) High-Resolution NMR in Solids: The CPMAS Experiment *Acc. Chem. Res.* 15, 201-208.

Yarzabs, R. F., Baset, Z. A. and Given, P. H. (1979) Hydroxyl contents of coals: new data and statistical analyses *Geochim. Cosmochim. Acta.* 43, 281-287.

Yoshida, T., Nakata, Y., Yoshida, R., Shigeru, U. Nobuyasu, K. and Maekawa, Y. (1982) Elucidation of structural and hydroliquefaction characteristics of Yalloum brown coal by carbon-13 CP/MAS n.m.r. spectrometry *Fuel* 61, 824-830.

Yoshida, T. and Maekawa, Y. (1987) Characterization of Coal Structure by CP/MAS Carbon-13 NMR Spectrometry *Fuel Process. Technol.* 15, 385-395.

Yost, R.S. (1985) *The role of oxygen-containing functional groups in Hydrogenation of brown coals* University of Melbourne.

Youtcheff, J., Painter, P. and Given, P. (1986) FTIR Spectroscopic Studies of Coal Liquefaction products *Am. Chem. Soc., Div. Fuel Chem., Prepr.* 31, 318-322.

Zhou, P., Dermer, O.C. and Crynes, B.L. (1984) Oxygen in Coals and Coal-Derived Liquids In *Coal Science* (Edited by Gorbaty, M.L., Larsen, J.W. and Wender, I.), pp. 253-300. Academic Press, New York.

APPENDICES

APPENDIX A GENERAL INFORMATION ON AUSTRALIAN COALS
(from Redlich,1987)

APPENDIX A1 Sources and Characteristics of brown coal samples

Code	Open cut[a]	Sample #	Depth(m)	Lithotype[b]	Bed Moisture wt. % as received
ABR1	LY1276	102	83.0	dark	65.7
ABR2	R327	29	199.9	dark	62.5
ABR3	R326	7	93.0	med.light	64.7
ABR4	R327	18	58.7	med.light	64.6
ABR5	R327	30	214.6	med.dark	58.0
ABR6	R327	17	44.7	light	61.7
ABR7	R327	25	138.1	light	58.0
ABR8	MOC46	6	-	pale	56.2
ABR9	R327	22	110.9	light	61.0
ABR10	H1317	53	66.5	pale	58.9
ABR11	R327	28	186.6	pale	53.3
ABR12	LY1279	121	66.7	pale	61.4
ABR13	R326	5	69.1	pale	57.5
ABR14	BM	-	-	pale	-

[a]LY = Loy Yang Bore (La trobe Valley, Gippsland, Victoria)

R = Rosedale Bore (La trobe Valley, Gippsland, Victoria)

BM = Bacchus March coalfield (West of Melbourne)

[b]med.= medium

Continue over..../

APPENDIX A1 (continue)

Coal	Volatile matter	Specific energy	Maceral contents		
			Huminite	Liptinite	Inertinite
	wt. %dmif	MJ/kg(daf)	(vol. % dmif)		
ABR1	45.7	26.1	98.8	1.2	0
ABR2	46.6	26.7	97.4	2.4	0.2
ABR3	51.1	26.2	93.2	6.4	0.4
ABR4	53.4	26.0	90.8	9.2	0
ABR5	55.2	27.8	85.8	13.2	0.8
ABR6	55.6	26.6	80.2	18.8	1.0
ABR7	56.0	27.5	80.6	19.2	0.2
ABR8	54.6	30.1	78.4	19.1	2.3
ABR9	57.3	28.1	80.6	18.6	0.8
ABR10	57.7	28.5	76.2	22.0	1.8
ABR11	59.6	29.1	67.2	30.6	2.2
ABR12	62.9	29.6	68.8	29.2	2.0
ABR13	62.4	29.8	61.0	38.2	0.8
ABR14	70.0	29.5	65.4	32.8	1.8

APPENDIX A2 Sources and Characteristics of Higher-rank coal samples

Code	Rank	Coal Seam/Colliery
ABL1	S.A.	Yarrabee mine, Blackwater district, Bowen Basin, Queensland (Q'ld)
2	m.v.s.b.	(Theiss Mine), Callide Basin, Biloela (Q'ld)
3	l.v.b.	Appin Colliery, Bulli seam, Southern Coalfield, Sydney Basin, New South Wales (N.S.W.)
4	m.v.s.b.	Oaklands Basin, Southern N.S.W.
5	h.v.b.	Pike's Gully seam, Lower N.W. District, Sydney Basin, N.S.W.
6	h.v.b.	Certified Reference Material ASCRM-001, Wongawilli Seam, Burragorang Valley District, Sydney Basin, N.S.W.
7	m.v.s.b.	Collie Basin, Western Australia
8	m.v.s.b.	Q. seam, Leigh Creek basin, South Australia.
9	h.v.b.	Young Wallsend seam, Central Newcastle District, N.S.W.
10	h.v.b.	As for ABL5
11	h.v.b.	Liddell, B seam, N.W. Singleton District, Sydney Basin
12	h.v.b.	Greta 2, Adadane East, Hunter Valley, Sydney Basin, N.S.W.
13	h.v.s.b.	A seam, Austinvale Mine, Surat Basin, Q'ld.
14	h.v.s.b.	Taroom Deposit, core sample. Drill Hole L191. Sample depth 16.6 m. Surat Basin, Q'ld.
15	h.v.s.b.	Box cut in Commodore 1 deposit, Millmerran, Moreton Basin, Q'ld.

(Continue over/)

APPENDIX A2   (continue)

Coal	Volatile matter	Specific energy	Maceral contents Vitrinite	Exinite	Inertinite
	wt. %dmif	MJ/kg(daf)	(vol. % dmif)		
ABL1	11.0	35.8	68.0	0	23.0
ABL2	29.8	28.8	26.0	4.0	59.0
ABL3	21.3	35.7	44.0	4.0	48.0
ABL4	34.2	28.6	17.0	19.0	53.0
ABL5	30.1	-	18.8	9.6	67.6
ABL6	37.2	35.6	73.6	1.2	19.5
ABL7	37.3	26.4	42.0	4.0	52.0
ABL8	36.8	27.6	35.8/54.8	8.3/7.4	52.4/33.6
ABL9	35.4	34.0	87.4	2.7	6.2
ABL10	34.2	-	77.4	9.8	7.4
ABL11	37.2	34.5	80.7	5.3	10.6
ABL12	40.8	34.9	62.2	16.3	20.0
ABL13	48.0	31.9	-	-	-
ABL14	47.4	31.0	77.0	15.5	1.0
ABL15	49.1	38.0	47.8	36.0	0

PUBLICATIONS

Supaluknari, S., Larkins, F.P., Redlich, P. and Jackson W.R. (1988) An FTIR Study of Australian Coals: A Comparison of Structural and Hydroliquefaction Data *Fuel Processing Technol.* **18**, 147-160.

Supaluknari, S., Larkins, F.P., Redlich, P. and Jackson W.R. (1988) An FTIR Study of Australian Coals: Characterization of Oxygen-Functional Groups *Fuel Processing Technol.* **19**, 123-140

Supaluknari, S., Larkins, F.P., Redlich, P. and Jackson W.R. (1989) Determination of Aromaticities and other Structural Features of Australian Coals using Solid State ^{13}C NMR AND FTIR Spectroscopies *Fuel Processing Technol.* **23**, 47-61.

Supaluknari, S., Burgar M.I. and Larkins, F.P. (1989) High-resolution Solid-state ^{13}C nmr studies of Australian Coals *Org. Geochem.*, submitted.